



**HAL**  
open science

## Link between medium and long-range order to macroscopic properties of silicate glasses and melts

Daniel R. Neuville, Charles Le Losq

► **To cite this version:**

Daniel R. Neuville, Charles Le Losq. Link between medium and long-range order to macroscopic properties of silicate glasses and melts. *Reviews in Mineralogy and Geochemistry*, 2022, 87 (1), pp.105-162. 10.2138/rmg.2022.87.03 . hal-03857133

**HAL Id: hal-03857133**

**<https://hal.science/hal-03857133v1>**

Submitted on 17 Nov 2022

**HAL** is a multi-disciplinary open access archive for the deposit and dissemination of scientific research documents, whether they are published or not. The documents may come from teaching and research institutions in France or abroad, or from public or private research centers.

L'archive ouverte pluridisciplinaire **HAL**, est destinée au dépôt et à la diffusion de documents scientifiques de niveau recherche, publiés ou non, émanant des établissements d'enseignement et de recherche français ou étrangers, des laboratoires publics ou privés.

1  
2  
3  
4 **Link between medium and long-range order to macroscopic properties of**  
5 **silicate glasses and melts**  
6

7 Daniel R. Neuville and Charles Le Losq  
8

9 *Géomatériaux, Institut de physique du globe de Paris, CNRS, Université de Paris*  
10 *[neuville@ipgp.fr](mailto:neuville@ipgp.fr) - [lelosq@ipgp.fr](mailto:lelosq@ipgp.fr)*  
11  
12  
13  
14

15 **Abstract:** Understanding the cationic network and the medium range order of glasses and melts allows  
16 rationalization of each elements role in terms of the network former, charge compensator or network  
17 modifier concepts. Such knowledge can be combined with further details, e.g. regarding the role of highly  
18 coordinated network former elements, to model the macroscopic properties of glasses and melts, like  
19 their molar volume, density, configurational entropy and viscosity. In this chapter, we present recent  
20 advances on such work, which open new avenues for the production of useful and precise models of  
21 geologic and industrial glasses and melts.  
22  
23

24 *1. Introduction*

25 The two first chapters of this volume focus on the structure of magmas at different scales: short and  
26 medium range order. A quick review of the glass literature, from the 90's or older, reveals that most  
27 published papers focused on the structure of glasses, or on properties of glasses or melts. Depending on  
28 their original discipline, the work of the scientific community in those areas are different. Physicists  
29 published papers on glass structure, including the structure of SiO<sub>2</sub>, GeO<sub>2</sub>, B<sub>2</sub>O<sub>3</sub> as seen by X-Ray or  
30 neutron diffraction and Raman spectroscopy for example ([Wright 1990](#), [Gaskell et al., 1991](#), [Galeener et  
31 al., 1983](#)). Chemists worked on more complex glass compositions, like chalcogenide ([Poulain and Lucas,  
32 1970](#), [Poulain 1983](#)), or focused their work on specific properties of glasses like refractive index, density  
33 or the oxidation state of multivalent elements ([Schreiber, 1986](#)). Earth scientists worked on properties of

34 melts involved in geologic phenomena, like diffusivity, heat capacity, density or viscosity (Ryan and  
35 Blevins, 1987, Carmichael et al. 1977, Bacon 1977; Robie et al., 1979, Bottinga and Weill 1970, 1972).  
36 This has changed over time. Since the 2000's, it is easier to simultaneously investigate the structure and  
37 properties of glasses. Industrial and technological needs evolved, and the interest of the Earth sciences  
38 community became more and more focused on the acquisition and interpretation of *in situ* data to address  
39 problems requiring insights about silicate melts at high temperature and high pressure. As a result, the  
40 scientific community became more unified, performing more and more studies that simultaneously  
41 investigated the structure and properties of glasses and melts. Presently, we have reached a point where  
42 it is possible to link together experimental and structural/thermodynamic data to build models for solving  
43 industrial or Earth sciences problems. The aim of this chapter is to show how this is possible.

#### 44 45 *1.1 Glass structure versus macroscopic properties*

46 Among the most important questions about glasses and melts, one is critical for many applications  
47 and studies: how the melt/glass structure affects macroscopic properties? For Doremus (1973), a glass is  
48 an amorphous solid. The term solid implies a high viscosity, usually greater than  $10^{10}$  Pa.s. This viscosity  
49 therefore limits the flow of the body. The amorphous term implies the absence of long-range order (see  
50 Figure 5A in the previous chapter, Drewitt et al., 2021), which reveals an analogy with the liquid state.  
51 So, a glass is a solid whose properties are similar to those of liquids. Parks and Huffman (1926) even talk  
52 about "a fourth state of matter". However, no consensus exists regarding glass, and the nature of glass  
53 and the glass transition are two fundamental questions that remain open in condensed matter physics  
54 (e.g., see the different definitions in and debate between Zanotto and Mauro, (2017), Popov (2018),  
55 Schmelzer and Tropin, (2018)).

56  
57 An important point is that glasses can exhibit very different chemical compositions and can be  
58 prepared by different means. Mineral (i.e. silicate), oxide, non-oxide, metal and organic glasses exist (see  
59 for an exhaustive description in Musgraves et al. (2019)). In fact, glasses are found regardless of the type  
60 of chemical bonds that link the atoms they contain: covalent, ionic, metallic, Van der Waals or hydrogen  
61 bonding. The glassy state is a characteristic of condensed matter. Glasses can be obtained by the rapid  
62 quench of liquids, or of a gas by solid condensation, by amorphization of a crystalline phase or by sol-  
63 gel methods (Descamps 2017). The most common method for obtaining a glass is by the rapid quench of  
64 a liquid<sup>1</sup>. During the quench, viscosity continuously increases up to a value so high that the final state  
65 can be considered as solid. One can therefore imagine the structure of the glass as being similar to that

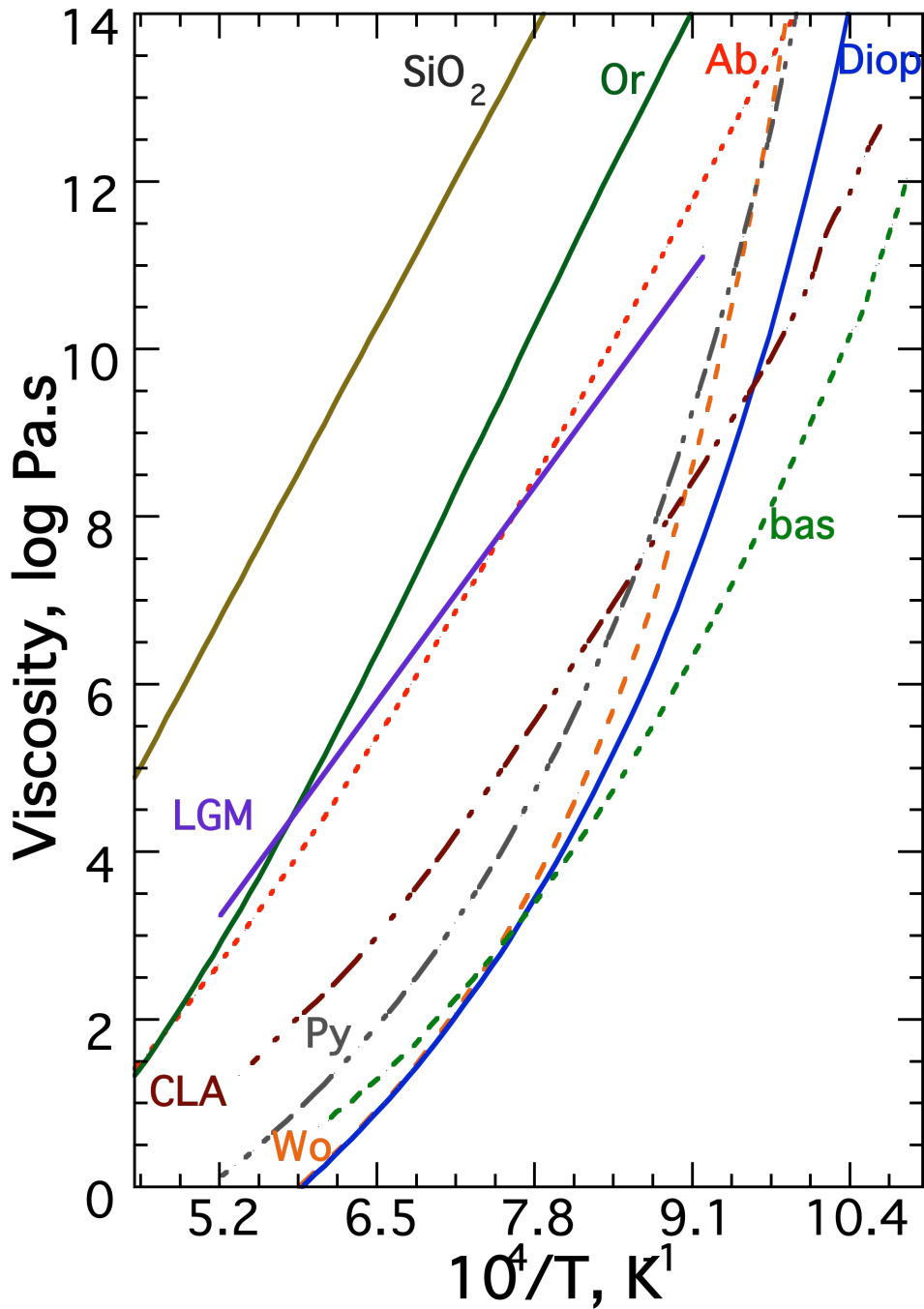
<sup>1</sup> rapid cooling rate means 15°/min, the term classic cooling rate is also used.

66 of a liquid whose movements are hindered. Glasses, like undercooled liquids, have a disordered structure  
67 that was frozen in at the glass transition temperature.

68

69 A fundamental question is *what happens when a liquid crosses the glass transition temperature?* The  
70 latter is the temperature (often abbreviated  $T_g$ , and more realistically it is a small temperature interval) at  
71 which second order thermodynamic properties like heat capacity show a transition, revealing the locking-  
72 in of the atoms in fixed (but undetermined) positions. In essence,  $T_g$  is the temperature at which a number  
73 of thermodynamic properties go from liquid-like to solid-like values.

74 Unlike a crystallized solid, it is not possible to introduce the term of melting temperature for the glassy  
75 state. The solidification of a liquid into glass is accompanied, in fact, by a continuous and gradual increase  
76 in viscosity upon cooling, without the appearance of a crystalline structure (Figure 1). This behavior  
77 remains true regardless of the glass/melt chemical composition (silicate, aluminosilicate, borate,  
78 borosilicate, germanate, chalcogenate, tellurate, metallic, organic... see for details regarding each glass  
79 family the [Musgraves et al., 2019](#)). This shows the continuous transition from glass to liquid for a  
80 property such as viscosity ([Tamman, 1925](#); see Figure 1). The glass transition is a dynamic phenomenon  
81 that characterizes the loss of internal thermodynamic equilibrium. Indeed, the properties of a glass no  
82 longer depend solely on pressure and temperature, but also on the temperature at which the glass  
83 transition occurs. Finally, Tamman ([1925](#)) sums the concept as “*The viscosity of a liquid increases with  
84 increasing undercooling, and in a rather narrow temperature interval it increases very rapidly to values  
85 characteristic of solid crystals. A brittle glass is thus formed from an easily mobile liquid. This change  
86 in viscosity does not correspond to the behavior of the other properties, which in this temperature interval  
87 change relatively only slightly. The change in viscosity is a continuous one and no temperature can be  
88 chosen as the freezing-point, the point at which the liquid becomes solid. Glasses are undercooled  
89 liquids.*”



90

91 *Figure 1: Viscosity versus  $1/T$  curves for different melt compositions. LGM and CLA are rhyolite and*  
 92 *andesite melts from [Neville et al. \(1993\)](#), bas is a basalt melt from [Villeneuve et al. \(2008\)](#),  $\text{SiO}_2$  is silica*  
 93 *melt from [Heterington et al. \(1964\)](#) and [Urbain et al., \(1982\)](#), Ab and Or are albite,  $\text{NaAlSi}_3\text{O}_8$ , and*  
 94 *orthoclase,  $\text{KAlSi}_3\text{O}_8$  melts from ([Le Losq and Neville, 2013](#); [Le Losq et al., 2017](#)); Py, Wo, Diop, are*  
 95 *Pyrope,  $\text{Mg}_3\text{Al}_2\text{Si}_3\text{O}_{12}$ , Wollastonite,  $\text{CaSiO}_3$ , and Diopside,  $(\text{CaMg})\text{SiO}_3$ , melt compositions ([Neville](#)*  
 96 *and [Richet, 1991](#)).*

97

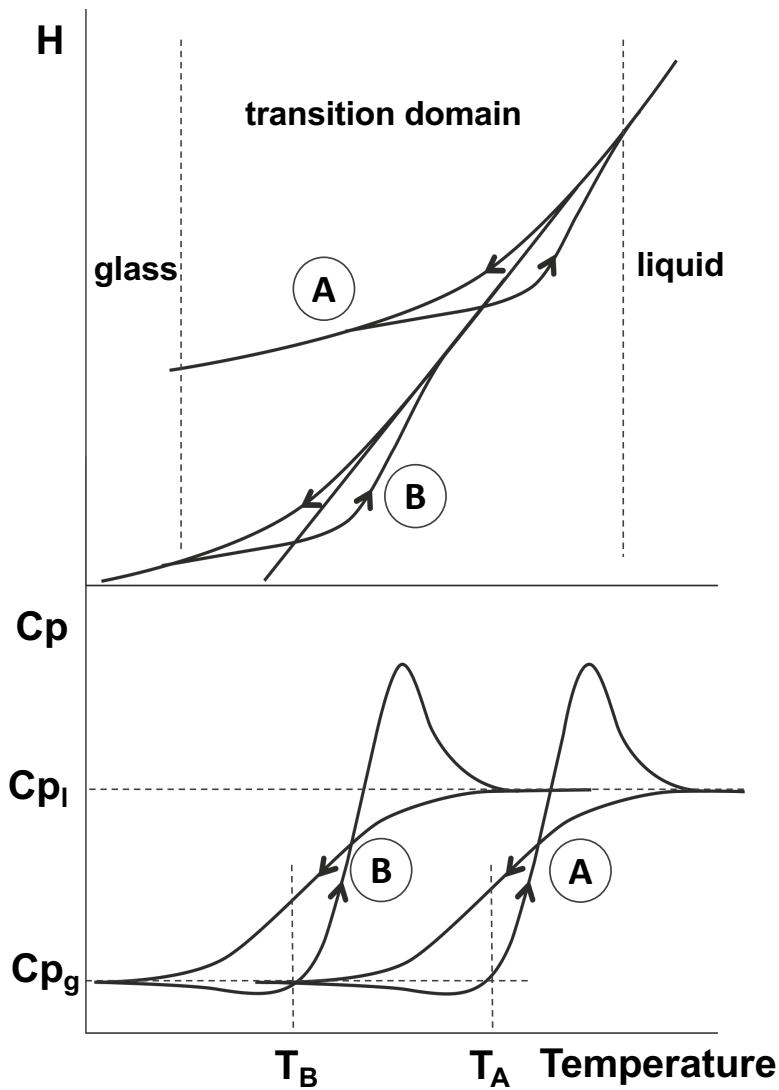
98 The simplest and earliest characterization of the glass transition is due to Parks and Huffmann  
99 (1927), who investigated organic liquids. They note Nernst (1911), has stated that heating a glass  
100 “externally it has the properties of a solid, owing to great viscosity and considerable rigidity, produced  
101 by strong mutual action of the molecules. An amorphous body differs from a crystal, however, in its  
102 complete isotropy and absence of a melting point; on heating, it passes continuously from the amorphous  
103 to the usual liquid state, as its properties show steady change with rise of temperature, and no breaks  
104 anywhere.”

105 In fact, Parks and Huffmann (1927) stated “While there is no definite temperature, comparable  
106 to the melting point of a crystal, at which all properties undergo a sharp change, there is nevertheless a  
107 temperature interval, definite and reproducible, in which a number of properties change with a rapidity  
108 approaching that observed in the case of the melting process of a crystal. In brief, there is a softening  
109 region instead of a melting point. The glass as it exists below this softening region differs so markedly  
110 from the liquid existing above that it might well be considered as a different state of the substance.”

111 From an energetic point of view, Moynihan et al. (1974) showed that the variations in relative  
112 enthalpy and heat capacity with temperature for two different cooling or heating speeds exhibit a sudden  
113 change in temperature and corresponds to a dampened variation of these two properties. They showed  
114 that for the same liquid, the glass transition temperature varies with the cooling or heating rate. The higher  
115 the cooling rate, the higher relative enthalpy or heat capacity (Figure 2). The glass transition thus  
116 corresponds to a small temperature and pressure interval upon which properties such as heat capacity  
117 undergo a second order transition (Moynihan et al., 1974). This interval is at higher temperatures at high  
118 cooling rates (situation A in Figure 2), and moves to lower temperatures at slower cooling rates (situation  
119 B in Figure 2).

120 It is theoretically possible to obtain identical variations for all properties as a function of time at the  
121 same temperature (thermal expansion, viscosity for example) but it is not necessary (Moynihan, et al.,  
122 1974). With sudden changes in temperature, variations of the liquid properties linked to atomic mobility  
123 require some time to reach a new equilibrium. This time is called the relaxation time,  $\tau$ . A liquid has a  
124 large number of different configurational states (Goldstein 1969; 1976). Each state corresponds to a  
125 minimum in potential energy and when temperature decreases, the number of possible configurations  
126 decreases as the domains for structural rearrangement become larger and larger. As a result, the time for  
127 structural relaxation,  $\tau$ , of the liquid increases. Crossing the glass transition leads to the atoms trapped  
128 in given but disorganised positions. This results in quenching the liquid into a glass. The configuration  
129 state of the glass does not change from  $T_g$  to 0 K, as shown by the fact that the residual entropy of glass  
130 remains constant below  $T_g$  (e.g., see Tequi et al., 1993; Richet et al., 1991; Richet and Neuville, 1992;  
131 Richet et al., 1986; Goldstein, 2011; Schmelzer et al. 2018 and references cited therein). It should be

132 noted that Raman and infrared vibrational spectroscopy data suggest that the structure of a glass is an  
 133 image of the instantaneous configuration of the liquid at  $T_g$  (Kashio et al, 1980; Kusabiraki and Shiraishi,  
 134 1981; Kusabiraki 1986; Sharma et al., 1978; Shevyakov et al., 1978, Neuville and Mysen, 1996).  
 135



136  
 137 *Figure 2: relative enthalpy and heat capacity versus temperature for 2 different cooling rates, A and*  
 138 *B correspond respectively to fast and low temperature change (redrafted from Moynihan et al., 1974).*  
 139  *$C_{p_l}$  and  $C_{p_g}$  correspond to the heat capacities of the liquid and the glass, respectively.  $T_B$  and  $T_A$*   
 140 *correspond to the glass transition at the two different rates A and B, respectively.*  
 141

142

143 The uniform cooling of a liquid at a rate  $q=dT/dt$  can be likened to a series of instant temperature  
144 jumps  $\Delta T = T_{fi} - T_i$ , where  $T_{fi}$  and  $T_i$  are the final and initial temperatures, each jump being followed by  
145 a  $\Delta t$  period during which the temperature remains constant and equal to  $T_{fi}$ . Just after each jump, the  
146 viscosity of the liquid,  $\eta_l$ , is still worth  $\eta_{Ti}$  and differs from  $\eta_{Tfi} - \eta_{Ti}$  from the new balance value,  $\eta_{Tfi}$ .  
147 This is called relaxation, the process by which the liquid tends to reach the state of equilibrium associated  
148 with the final temperature  $T_{fi}$ . To characterize the kinetics of this evolution, we can define a viscous  
149 relaxation time  $\tau_\eta$  as equal to:

$$150 \quad \tau_\eta = \eta_l - \eta_{Tfi} / (\delta\eta / \tau_\eta). \quad (1)$$

151 Experimentally,  $\tau_\eta$  increases when  $T$  decreases. Three cases can be distinguished:

152  $\Delta\tau \gg \tau_\eta$ , the substance has a relatively long time to equilibrate its structure at the new  
153 temperature. We are in the liquid state or in a glass state at the thermodynamic equilibrium for which the  
154 equilibrium viscosity is reached almost instantaneously. During cooling, the viscosity increases to its  
155 equilibrium value.

156  $\Delta\tau \sim \tau_\eta$ , this corresponds to the glass transition domain. Viscosity depends on both the time and  
157 temperature to which the glass was previously subjected.

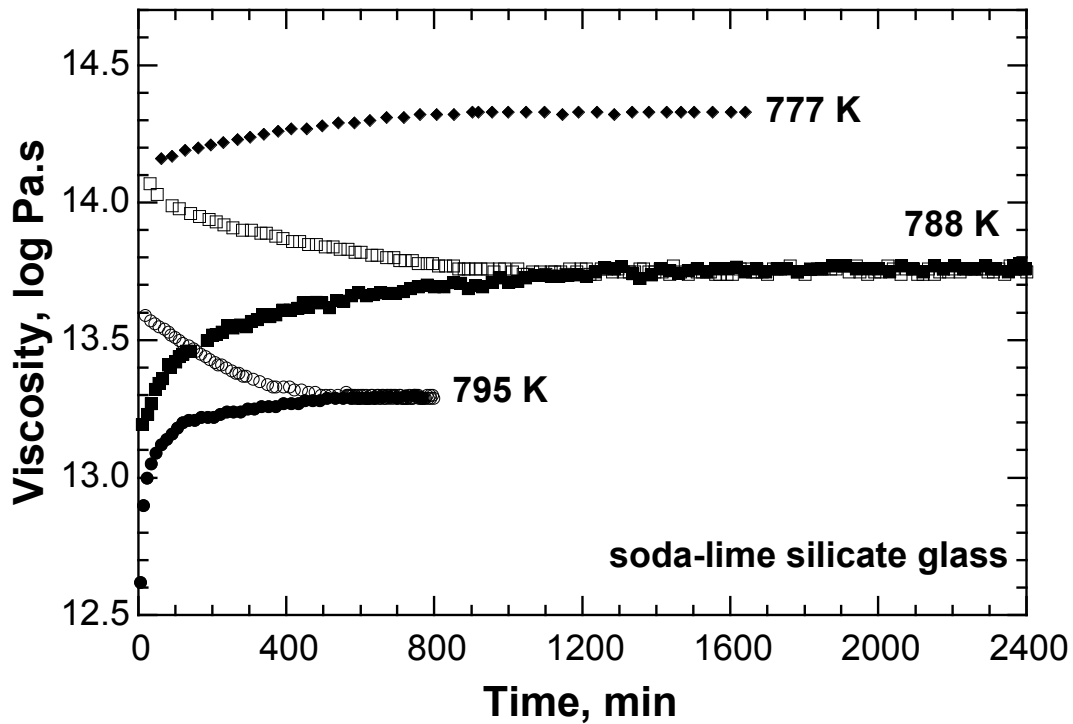
158  $\Delta\tau \ll \tau_\eta$ , the relaxation time is much higher than the measurement time. No configurational  
159 rearrangement is then possible. The liquid freezes. Only the vibrational part of the heat capacity remains,  
160 which is close to the heat capacity of the crystal.

161

162 Relaxation times depend heavily on temperature (Rehson, 1975; 1989, Simmons et al., 1970; 1974,  
163 Dingwell and Webb, 1990), as well as on the structure and therefore glass composition; e.g. borosilicate  
164 glasses have higher relaxation times than silicate or aluminosilicate glass compositions (Sipp et al., 1997).  
165 Figure 3 shows, for a soda-lime silicate glass, that relaxation time increases with decreasing temperature:  
166 e.g. equilibrium is reached after 500, 1200, 1600 min respectively at 795, 788 and 777 K.

167





168

169 *Figure 3: Viscosity versus time for a soda-lime silicate glass at different temperatures (redrafted from*  
 170 *Sipp et al., 1997). We can note that increasing viscosities represent relaxation after previous*  
 171 *measurements performed at higher temperatures, whereas decreasing viscosities indicate relaxation*  
 172 *after annealing at lower temperatures.*

173

174 However, it is important to note that there is no reason why the relaxation times of the various  
 175 properties should be identical at equal cooling speeds. Moynihan et al. (1976a) indicate that “for example,  
 176 the enthalpy changes occurring during the approach to equilibrium of a network glass following a change  
 177 in temperature could be considered to arise from the breaking of some of the network bonds, while the  
 178 volume changes are due to rearrangement of the structure into less densely packed configurations. One  
 179 cannot say a priori, however, which of these two processes should on the average occur earlier in time.  
 180 That is, bond breaking might be a necessary precursor to volume-changing rearrangements of the  
 181 structure, so that one would expect  $H$  to relax faster than  $V$ . On the other hand, configurational  
 182 rearrangements leading to large volume changes might occur early in time, stressing the network and  
 183 leading to subsequent bond breaking, so that one would expect  $V$  to relax faster than  $H$ .” In practice, it  
 184 appears that the differences in relaxation time between volumetric and calorimetric relaxation times are  
 185 relatively small, if not almost non-existent, and are essentially due to differences in cooling or heating

186 rates (Sasabe et al., 1977; Moynihan and Gupta, 1978; Dingwell and Webb, 1990). Differences between  
187 relaxation times for the same material but determined with methods sensitive to different properties are  
188 clearly visible when comparing data from dilatometry, calorimetry and viscosimetry. For example, in the  
189 case of alkaline-earth aluminosilicate glass compositions, drop calorimetry  $T_g$  are generally found at  
190 temperatures at which viscosities are of  $10.7 \pm 0.5 \log \text{ Pa}\cdot\text{s}$ , a value lower than that of  $\sim 12 \log \text{ Pa}\cdot\text{s}$  that  
191 is known to be the reference for the determination of the viscous  $T_g$  (Neuville and Richet 1991; Tequi et  
192 al., 1991).

### 194 *1.2 Thermodynamic approach to glass transition*

195 We have seen that temperature and pressure are not sufficient parameters to characterize the state of  
196 glass. Tool and Eichlin (1931) introduced the concept of fictive temperature,  $T_{fic}$ , to characterize a glass  
197 at constant pressure. It can be defined as the temperature at which the glass would be in an equilibrium  
198 state (as a melt) if it could be heated and measured instantly. The fictive temperature can be defined  
199 during cooling in dilatometry or calorimetry, as the glassy transition temperature.

200  
201 It is possible to give a formal thermodynamic definition of the fictive temperature, considering it as  
202 an order parameter. Moynihan et al. (1974, 1976a,b) discussed fictive temperatures, their influence on  
203 enthalpy properties and order parameters. It can be recalled, that the glass transition looks like a second-  
204 order transition for which volume, enthalpy and viscosity are continuous functions of T but not heat  
205 capacity, dilatation and compressibility coefficients. For the latter parameters, a steep transition is  
206 observed when temperature crosses the glass transition.

207  
208 In reality, fictive temperature is a critical parameter as it reflects how viscosity, hence relaxation time,  
209 can show non-equilibrium behavior and can depend on time in the supercooled domain. In Figure 3, the  
210 effect of fictive temperature is clearly visible. The downward curve is obtained from a sample that has a  
211 fictive temperature below the measurement temperature. Similar behaviors are visible for density, or  
212 refractive index (Winter, 1943, Ritland, 1954). When the fictive temperature of the glass is higher than  
213 the measurement temperature, the glass has a more disordered configurational state than the state it should  
214 have if the glass were in thermodynamic equilibrium, i.e. its "fictive" configuration entropy is too high.  
215 It has a lower viscosity than its equilibrium viscosity, so its viscosity increases over time until the fictive  
216 temperature equals the measurement temperature. For a fictive temperature lower than that of  
217 measurement, the viscosity decreases until the establishment of the thermal equilibrium characterized by  
218 the equality of the two temperatures. In Figure 2, the relaxation curves over time for the cases of cooling

219 or heating are asymmetrical. This is because a liquid increases its entropy faster with an increase in  
 220 temperature (Rehson, 1980, Dingwell and Webb, 1990; Sipp et al., 1997)<sup>2</sup>.

221  
 222 *1.3 Viscosity and glass transition*

223 The glass transition is closely related to transport phenomena and more specifically to viscosity (Adam  
 224 and Gibbs 1965; Gibbs and Dimarzio, 1958; Goldstein, 1969; Grest and Cohen, 1980; Scherer 1984,  
 225 Richet, 1984), one of the fundamental properties of liquids that intervenes in transport processes. For the  
 226 experimentalist, liquid viscosity also can be considered as a structural probe. Many models attempt to  
 227 describe the variation of viscosity with temperature. Among them, we can cite the empirical Arrhenius and  
 228 Tamman-Vogel-Flucher (TVF) equations, or the thermodynamic Adam-Gibbs (AG) model (see also  
 229 section 2) allows linking melt mobility to its thermodynamic properties such as heat capacity and  
 230 configurational entropy, and can be used for viscosity predictions and extrapolations (Neuville and  
 231 Richet, 1990). Le Losq and Neuville (2017) further showed that the AG model allows linking melt  
 232 structural knowledge to thermodynamic properties and viscosity, in order to build complete, extensive  
 233 models for property predictions.

234  
 235 *1.4 Configurational properties and glass structure*

236 Configuration properties are the key to understand the difference between liquids and glasses. To  
 237 illustrate the importance of such configurational aspects, consider the second order thermodynamic  
 238 properties of crystal, glass and liquid pyrope ( $\text{Mg}_3\text{Al}_2\text{Si}_3\text{O}_{12}$ ).

239  
 240 TABLE 1: Heat capacity of pyrope and  $\text{Mg}_3\text{Al}_2\text{Si}_3\text{O}_{12}$ , glass and liquid in  $\text{J mol}^{-1} \text{K}^{-1}$ . Data are from  
 241 Tequi et al. (1991).

T(K)	Crystal	Glass	Liquid
298	325,6	327,8	
1020	492,2	504,4	665,7
1700	522,6		689,5

242  
 243 Above room temperature, the glass and crystalline phase have similar heat capacities,  $C_p$ . On the  
 244 contrary, the  $C_p$  of the liquid is 25% higher than that of solids (crystal or glass). Moreover, it should also  
 245 be noted that the  $C_p$  of the liquid usually increases with temperature of the liquid and cannot be  
 246 considered as a constant. These differences can have a significant impact when you integrate with

<sup>2</sup> A fictive pressure,  $P_{fic}$ , can be defined as the pressure at which the glass would be in an equilibrium state if it were subjected instantly to pressure equal to  $P_{fic}$ , at constant temperature.

247 temperature or pressure, as shown by the example of pyrope and  $\text{Mg}_3\text{Al}_2\text{Si}_3\text{O}_{12}$  liquid. For instance, a  
 248 simple extrapolation of the heat capacity of the  $\text{Mg}_3\text{Al}_2\text{Si}_3\text{O}_{12}$  liquid to low temperatures would produce  
 249 a liquid with a lower entropy than that of its crystalline form below 694 K (Figure 4A). This temperature  
 250 actually corresponds to the Kauzmann temperature, a temperature below which the liquid entropy would  
 251 become lower than that of a crystal with the same composition. Such a system does not exist because a  
 252 property of a liquid like the entropy should always remain higher than that of its crystalline form at a  
 253 given temperature. The violation of this idea is known as the Kauzmann paradox (Kauzmann, 1948)<sup>3</sup>.  
 254 The pyrope example shows that configuration terms play an important role on the properties of liquids.  
 255 It is therefore necessary to understand how configurational properties vary, and their link to melt and  
 256 glass structure. Figure 4A shows the variation of the entropy of a crystal, glass and liquid for the  
 257  $\text{Mg}_3\text{Al}_2\text{Si}_3\text{O}_{12}$  composition as a function of temperature. It is clear that the residual entropy corresponds  
 258 to the difference between the entropy of the glass and that of the crystal at 0 K. This residual entropy is  
 259 very small compared to the entropy of glass, crystal and liquid. This residual entropy is called  
 260 configurational entropy,  $S^{conf}$ , and it is the key to understanding glasses and liquids. To determine  $S^{conf}$ ,  
 261 it is necessary to solve the entropic cycle represented in Figure 4A. However, this is only possible for  
 262 minerals that melt congruently, and with a composition that can exist in a stable form as crystal, liquid  
 263 and glass. Measuring the heat capacity of the crystal,  $C_{pc}$ , from 0 K to the melting temperature,  $T_m$ , allows  
 264 determining its absolute entropy  $S_c$  at  $T_m$ :

$$265 \quad S_c = \int_0^{T_m} \frac{C_{pc}}{T} dt. \quad (2)$$

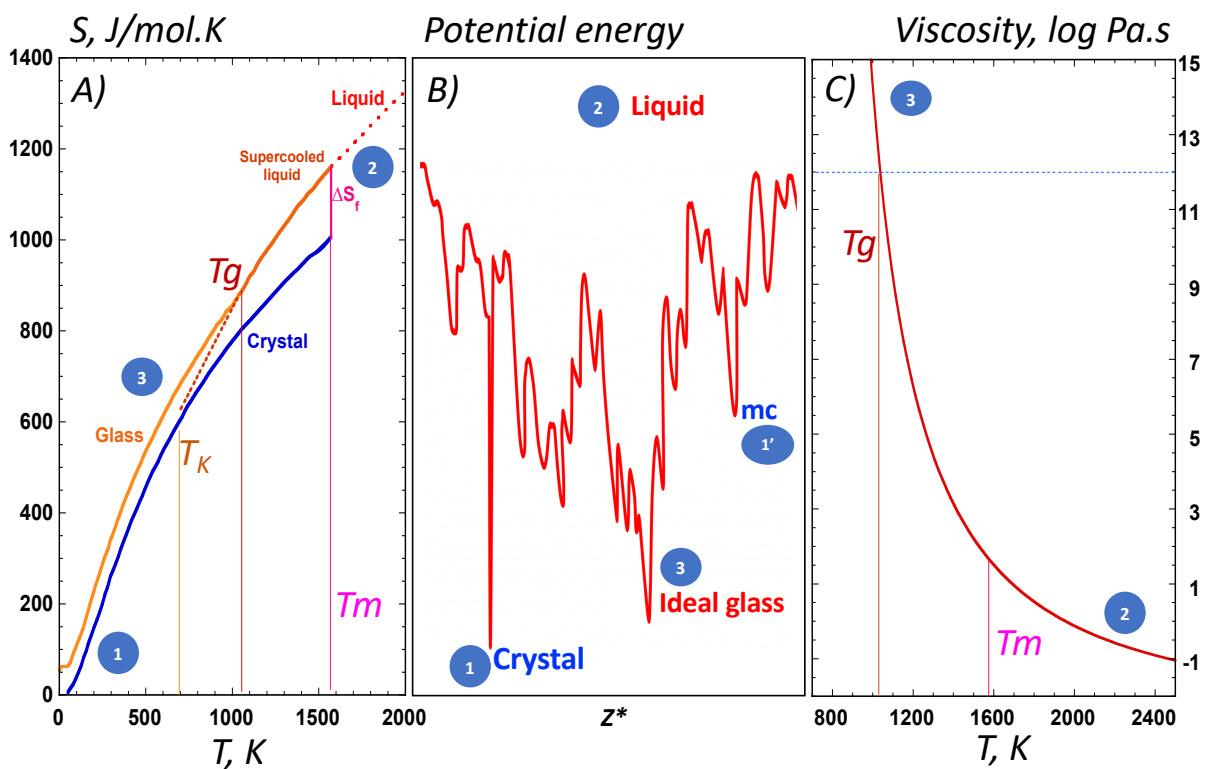
266 By adding the entropy of fusion of the crystal,  $\Delta S_f$ , to  $S_c$ , the entropy of the liquid  $S_l$  is then obtained  
 267 at  $T_m$ . Measuring the heat capacity between the melting temperature,  $T_m$ , and the glass transition  
 268 temperature,  $T_g$ , allows determining the heat capacity of the liquid and the supercooled liquid,  $C_{pl}$ . The  
 269 measurement of the heat capacity of the glass between  $T_g$  and 0 K provides  $C_{pg}$ . Finally, the residual  
 270 entropy, also known as the so-called configurational entropy  $S^{conf}$ , is obtained at 0 K via:

$$271 \quad S^{conf}(0\text{ K}) = \int_0^{T_m} \frac{C_{pc}}{T} dt + \Delta S_f + \int_{T_m}^{T_g} \frac{C_{pl}}{T} dt + \int_{T_g}^0 \frac{C_{pg}}{T} dt. \quad (3)$$

272 This calculation is illustrated in Figure 4A for a composition of  $\text{Mg}_3\text{Al}_2\text{Si}_3\text{O}_{12}$  (Tequi et al.,  
 273 1991). As this Figure shows,  $S^{conf}$  represents a small difference between large numbers, and its value will  
 274 be affected by a very large error if calorimetric measurements are not made with the highest possible  
 275 accuracy. For this purpose, the studies focused on determining  $S^{conf}$  from calorimetry measurements  
 276 require high-precision measurements of thermal capacity: heat capacities need to be determined better

<sup>3</sup> this well-known paradox in temperature is recently proposed via pressure, but without any  
 experimental basis see papers of Schmelzer et al., (2016) and Mauro (2011).

277 than 0.2 % by adiabatic calorimetry between 0 K and ambient, and better than 0.5 % by high-temperature  
 278 drop calorimetry (e.g. Tequi et al., 1991). Aside from the time and the difficulty of performing such high  
 279 precision heat capacity measurements, one of the main drawbacks of the calculation of the  
 280 configurational entropy through the thermodynamic cycle is the necessity to study minerals that melt  
 281 congruently, with compositions existing as glass, liquid and crystal as stated previously. Only a few  
 282 chemical compositions can be studied in this way. Fortunately, as we shall see later,  $S^{conf}$  can be  
 283 determined through the use of the Adam and Gibbs model combined with viscosity measurements.



284  
 285 *Figure 4: A) entropy versus temperature (Tequi et al., 1991), B) schematic representation of the com-*  
 286 *plex higher dimensional potential energy hypersurface of an  $N$ -particle system in terms of a two-dimen-*  
 287 *sional diagram of chemical potential versus some collective configuration coordinate  $Z^*$ , which defies*  
 288 *precise definition, but the width of the funnel represents entropy (Angell, 1991; Mossa et al. 2002),*  
 289 *and C) viscosity versus temperature for the  $Mg_3Al_2Si_3O_{12}$  composition (Neuville and Richet, 1991). The*  
 290 *same numbers are all connected together in the three figures. 1 is the Pyrope crystal that presents the*  
 291 *minimum potential energy. 1' is a metastable crystal, mc, that can have a potential energy higher than*  
 292 *that observed for the glass. 2 is the liquid with a low viscosity, high entropy and high potential energy,*  
 293 *in which atoms can move rapidly from one position to one other. 3 is the glass, in which atoms can*  
 294 *move very slowly, there is a relaxation time, viscosity increase and entropy decrease, and the atom can*  
 295 *fall in different potential energy minima and stay inside or jump to another with a lower potential en-*  
 296 *ergy.  $T_m$  is melting temperature,  $T_g$ , glass transition temperature,  $T_K$  Kauzmann temperature,  $\Delta S_f$  en-*  
 297 *tropy of melting at the melting temperature. Supercooled liquids are liquids between melting tempera-*  
 298 *ture and glass transition temperature.*

299  
300  
301

302 Figure 4B schematically illustrates the positions of atoms in a crystal as a function of the collective  
303 configuration coordinate, as determined by local minima of interatomic potentials that are at specific  
304 positions, allowing the building of a repetitive pattern characterized by long range order. In a glass, the  
305 bond angles and interatomic distances are not constant but extend over a range of relatively close values.  
306 Long-range order does not exist, and one can represent the interatomic potentials as a plane showing  
307 minima separated by barriers with varying shapes and heights. As a result, glass entropy is higher than  
308 that of crystal at given temperature (point 3, Figure 4). The ideal glass with the minimum potential exists,  
309 but also other minima can exist with higher potential for the glass state or even the metastable crystal  
310 (point 1'). Now suppose that a certain amount of heat is brought instantly to the glass. Below the glass  
311 transition, the thermal energy brought upon increasing temperature is accommodated as vibrations, via  
312 an increase in average vibration amplitudes. The specific heat is vibrational in nature and the material  
313 behaves like a solid. At and above  $T_g$ , the thermal energy becomes important enough to allow the atoms  
314 to cross the energy barriers that separate the different configurational states (Richet and Neuville, 1992).  
315 This configurational contribution is necessarily positive, and the liquid or glass states can be defined by  
316 the existence or absence of this contribution (Davis and Jones, 1953). In a way, the glass transition can  
317 be seen as the beginning of the exploration by atoms of positions corresponding to the highest values of  
318 interatomic potential (Goldstein, 1969). This distribution of configurations over increasingly high  
319 potential energy states is the main characteristic of atomic mobility and low viscosity or relaxation time  
320 (point 2, Figure 4).

321 If we now look at the changes in volume in an amorphous material, we notice that a general  
322 characteristic of interatomic potentials is their anharmonic nature, i.e. that the forces applied to the  
323 vibrational atoms are not exactly proportional to the movements in relation to the equilibrium positions  
324 of these atoms (Richet and Neuville, 1992). An increase in vibration amplitudes therefore leads to an  
325 increase in interatomic distances. Like solids, liquids also have such anharmonic vibrational expansion,  
326 but higher-energy patterns that begin to be explored over the glass transition are generally associated  
327 with increased interatomic distances. This is why the thermal expansion coefficient generally increases  
328 significantly at the glass transition (Richet and Neuville 1992).

329

### 330 *1.5 pressure-temperature space*

331 As we have mentioned before, there is a glassy transition pressure (Rosenhauer et al., 1979), which  
332 allows one to place the glass transition in a pressure-temperature plane for a given cooling or heating

333 rate. However, the effects of pressure and temperature on the properties of glasses are actually different.  
334 High pressure can produce irreversible configurational changes. So, for given experimental quench rates  
335 or measurement time scales, the kinetics of configurational changes are markedly different depending on  
336 whether they are caused by pressure or temperature. The main reason for this difference is that the shape  
337 of potential energy wells varies little with temperature but significantly with pressure. If high kinetic  
338 energy is required to cross the potential barriers at constant pressure, changes in these barriers with  
339 pressure can lead to new configurational states at lower temperatures, if the pressure is high enough. The  
340 processes occurring at high pressure in glasses are likely similar to those that occur in liquids. Since the  
341 2000's, many papers have shown significant changes in the glass structure with increasing pressure, more  
342 or less linked to changes in their properties (e.g. [Poe et al., 2001](#), [Suzuki et al., 2002](#), [Wang et al., 2014](#)).  
343 In this volume, an exhaustive chapter can be found on the effect of pressure on the structure and properties  
344 of melts and glasses by Sakamaki and Ohtani (2021).

## 346 2. Silicate glasses and melts

### 347 2.1 Alkali or earth alkaline silicate glasses and melts

348 As depicted in the previous two chapters, silica glass is a material well-connected at the molecular scale,  
349 built from a three-dimensional network of tetrahedral units composed of covalently bonded central Si  
350 and apical O atoms (a.k.a. Bridging Oxygens or BO). However, contrary to  $\alpha$ -quartz that forms perfect  
351 trigonal crystals,  $\text{SiO}_2$  glass is built by  $\text{SiO}_4$  tetrahedra distributed disorderly yet not totally randomly  
352 (e.g. see Figure 5A in chapter 3, this volume). The relative density  $d$  of silica glass equals 2.20 (molar  
353 volume  $V_m = 27.311 \text{ cm}^3$ ), a value lower than that observed for  $\alpha$ -quartz ( $d = 2.65$ ,  $V_m = 22.673 \text{ cm}^3$ ) that  
354 presents a compact and well-ordered structure. This implies that silica glass presents a rather porous  
355 structure, with possibly a minor amount of Non-Bridging Oxygen (NBO, see Chapter 2, this volume)  
356 atoms not connected to 2 Si atoms ([Brückner 1970](#); [Fanderlik, 1990](#)). The fraction of NBO in silica is  
357 usually considered as negligible, making the silica structure a very strong one.

358 As an alkali oxide is added,  $\text{Na}_2\text{O}$  for example, more and more NBO are created until reaching the  
359 possibility to create isolated  $\text{SiO}_4$  tetrahedra linked together by only ionic Na-O bonds. For alkali  
360 silicates, this corresponds to a theoretical view because  $\text{Na}_4\text{SiO}_4$  glasses do not exist. However, in the  
361 Ba-silicate system, it is possible to obtain glasses with 33% and 37% silica with classic cooling rate  
362 ([Bender et al., 2002](#)), while in the Mg-silicate system it is possible to obtain glasses up to 62 MgO in  
363 mole percent (38% $\text{SiO}_2$ ) but below 50 percent of silica, it is necessary to use a fast cooling rate as shown  
364 in Raman spectra ([Neuville et al., 2014](#)). Glass formation in the  $\text{SiO}_2$ - $\text{Na}_2\text{O}$  system is actually not possible  
365 for amounts of  $\text{Na}_2\text{O}$  lower than that of the metasilicate composition  $\text{Na}_2\text{SiO}_3$  ([Schairer and Bowen,](#)  
366 [1956](#)). At higher  $\text{Na}_2\text{O}$  contents, up to 58 mole percent, it is possible to obtain Na silicate glasses only

367 via high-speed quenching of a small quantity of melt (a few grams; [Imaoka and Yamazaki, 1963](#)). Stable,  
368 large pieces of glass cannot be formed below 60 mol% of SiO<sub>2</sub> in this system ([Neuvillle, 2006](#)). For other  
369 alkali-silicate glasses, it is possible to make glasses up to 35 and 55 mole % of Li<sub>2</sub>O and K<sub>2</sub>O, respectively  
370 ([Imaoka and Yamazaki, 1963](#), [Levin et al., 1964](#)).

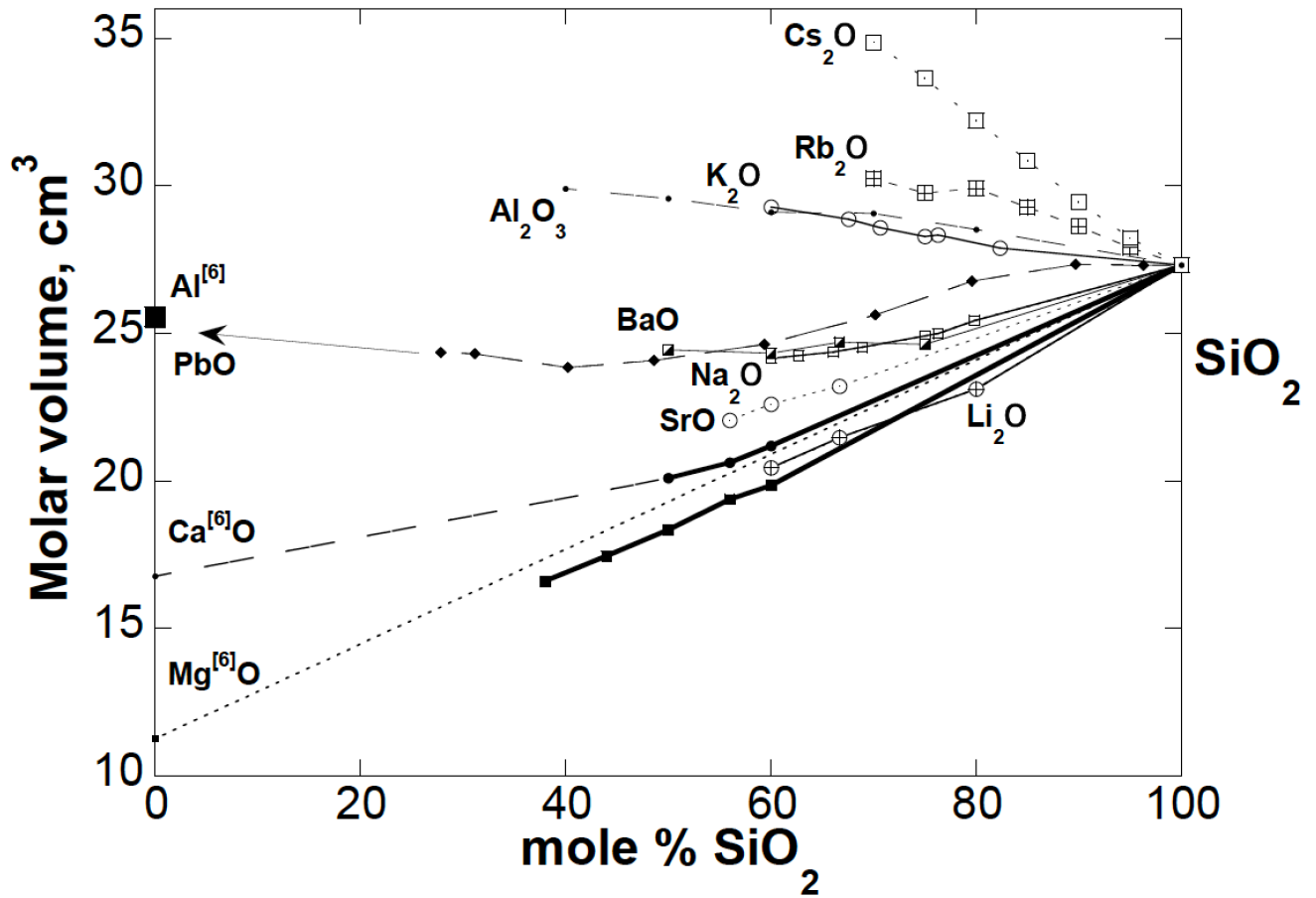
371  
372 To summarize, alkali silicate glasses can be easily obtained at normal cooling rates in the 60 to 99  
373 mole % SiO<sub>2</sub> range (see Raman spectra of silicate glasses in [Neuvillle et al., \(2014\)](#)), and alkaline-earth  
374 silicate glasses between 33 and 75 mol% SiO<sub>2</sub>, particularly with heavy alkaline-earth elements like Ba.  
375 For Mg, the glass forming domain is smaller, and ranges between 37 and 55 mole % SiO<sub>2</sub> ([Imaoka and  
376 Yamazaki, 1963](#), [Richet et al., 2009](#)). In the CaO-SiO<sub>2</sub> system between 1 and 62 mole % SiO<sub>2</sub>, the melts  
377 at temperatures just above the liquidus consists of two immiscible phases ([Imaoka and Yamazaki, 1963](#),  
378 [Levin et al., 1964](#), [Hudon and Baker 2002ab](#); [Neuvillle 2006](#)).

379  
380 Alkali or alkaline-earth silicate glasses show almost linear variations in molar volume with addition  
381 of M<sub>2</sub>O or M<sup>2+</sup>O in silica glasses (Figure 5). Molar volumes obtained from density measurements for  
382 CaO-Al<sub>2</sub>O<sub>3</sub>-SiO<sub>2</sub> and Na<sub>2</sub>O-Al<sub>2</sub>O<sub>3</sub>-SiO<sub>2</sub> are also available in the literature ([Seifert et al., 1982](#), [Doweidar  
383 1998, 1999](#)) but we have chosen not to report them on the figures for two reasons: -i) they show similar  
384 trends to ours, - ii) they are made with different cooling rate than ours (not mentioned in the articles).  
385 The molar volume ( $V_m$ ) of silicate glasses increases or decreases as a function of the cation size<sup>4</sup>. In the  
386 case of cations presenting an ionic radius larger than O<sup>2-</sup> (132 pm), like Cs<sup>+</sup>, Rb<sup>+</sup> or K<sup>+</sup>, the glass molar  
387 volume increases with cation addition. For cations presenting an ionic radius lower than that of O<sup>2-</sup>, like  
388 Na<sup>+</sup> and Li<sup>+</sup>,  $V_m$  of silicate glasses decreases both with the cation size and its amount. A similar behavior  
389 is observed in alkaline-earth silicate glasses. In Ca and Mg silicate glasses,  $V_m$  varies almost linearly with  
390 the glass SiO<sub>2</sub> (Figure 5). In Figure 5, a dotted straight line is drawn between SiO<sub>2</sub> and MgO with MgO  
391 with Mg in 6-fold coordination, and it is clearly observed that the  $V_m$  of Mg-silicate glasses are below  
392 this line, which suggests that the CN of Mg is significantly less than 6 in amorphous magnesium silicates.  
393 Such an interpretation agrees with <sup>25</sup>Mg Nuclear Magnetic Resonance (NMR) spectroscopy that shows  
394 that Mg is essentially in four-fold coordination in silicate glasses ([Fiske and Stebbins, 1994](#); [Georges and  
395 Stebbins, 1998](#), [Kroeker and Stebbins, 2000](#), [Shimoda et al., 2007a,b](#)), as well as with XANES at the Mg  
396 *K*-edge ([Trcera et al., 2009](#)) while Ca is essentially in six fold coordination in silicate glasses as shown  
397 by XANES at the Ca *K*-edge ([Neuvillle et al., 2004b](#), [Cormier and Neuvillle, 2004](#); [Ispa et al., 2010](#);  
398 [Cicconi et al., 2016](#)). These gentle variations may indicate that Ca and Mg remain almost in the same

<sup>4</sup>Cation size are given in [Whittaker and Muntus \(1970\)](#) and molar volumes are from [Robie et al. \(1979\)](#).



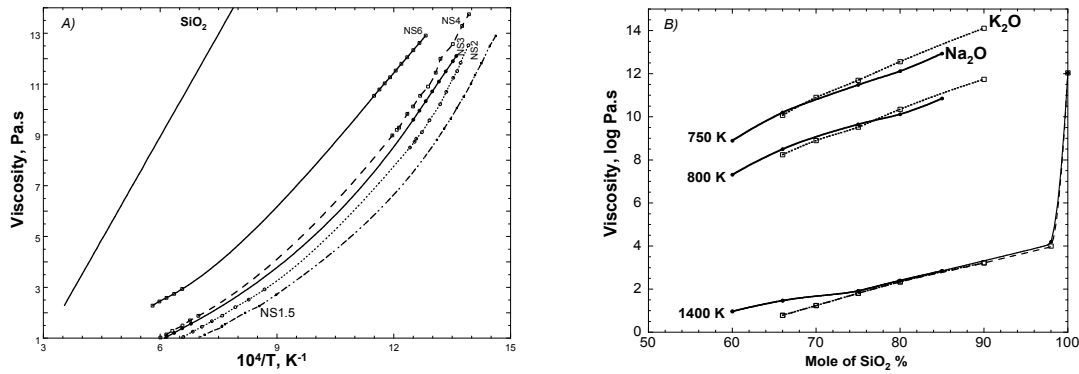
399 coordination number, CN, in silicate glasses, this CN being slowly affected by the SiO<sub>2</sub> content or by the  
 400 variation in the number of bridging oxygens around Si.  
 401



402  
 403  
 404 **Figure 5:** Molar volume of glasses at room temperature: data for Ca, Mg, Na, K, Li silicate glasses  
 405 are original data from Neuville, Sr and Ba Novikov (2017) Rb, Cs O'Shaughnessy et al., (2017, 2020);  
 406 Pb-silicate (Ben Kacem et al., 2017) and Al-silicate glasses (Wang et al., 2020). Molar volume of <sup>[6]</sup>Al  
 407 corresponds to Al<sub>2</sub>O<sub>3</sub>, and MgO and CaO are from Robie et al. (1979). Density of MA44.00 and MA38.00  
 408 glasses are respectively 2,807 and 2,881, Raman spectra of these two glasses are given by Neuville et al.  
 409 (2014).

410  
 411  
 412 *Viscosity of silicate melts*

413 In Figure 6A, the viscosity of SiO<sub>2</sub> and soda silicate melts are plotted as a function of reciprocal  
 414 temperature. Silica shows the highest viscosity of all glass compositions, as well as a strongly linear  
 415 behavior indicating an Arrhenian behavior (slope is equal to an activation energy).



416

417 **Figure 6:** A) viscosity versus reciprocal temperature (SiO<sub>2</sub> NS6, NS4, NS3, NS2, NS1.5, data from  
 418 [Neville, 2006](#), and [Le Losq et al., 2014](#)). NSx: x corresponds to the ratio of SiO<sub>2</sub>/Na<sub>2</sub>O in mole percent  
 419 (e.g. NS4: x = 4 = 80/20 - 80 % SiO<sub>2</sub> and 20 % Na<sub>2</sub>O); B) viscosity versus SiO<sub>2</sub> content for Na- and K-  
 420 silicate glasses (data from [Poole, 1948](#), [Bockris et al., 1955](#), [Neville, 1992](#), [2006](#)).

421

422 The fact that silica easily forms a glass, albeit a strong one with a very high viscosity, directly indicates  
 423 that Si is a network former cation. Other elements, presenting lower valence and larger ionic radius, can  
 424 play different roles in the glass structure. For instance, the introduction of Na<sub>2</sub>O in silica glass yields to  
 425 breaking the covalent Si-O-Si bridges, and, hence, to the formation of Non-Bridging Oxygens, NBO. Na  
 426 is considered, in this case, as a network modifier cation. Na fits into the glass structure as cations linked  
 427 to the surrounding oxygens by bonds that are much more ionic and thus weaker than Si-O covalent bonds.  
 428 Thus, the structure of sodium silicate glasses is weaker than that of vitreous silica. This translates into a  
 429 lowering of the viscosity at given temperature when adding Na<sub>2</sub>O in SiO<sub>2</sub> (Figure 6A). Furthermore, the  
 430 introduction of Na<sub>2</sub>O in silica glass produces a non-Arrhenian behavior that increases with x for the NSx  
 431 glass; x corresponds to the ratio of SiO<sub>2</sub>/Na<sub>2</sub>O in mole percent (Figure 5A). When viscosity varies with  
 432 1/T following an Arrhenian behavior, it follows this equation:

433

$$434 \quad \text{Log } \eta = A + B/T, \quad (4)$$

435

436 with A the viscosity at infinite temperature and B an activation energy. This equation can only be used  
 437 for a few chemical compositions like SiO<sub>2</sub>, GeO<sub>2</sub>, NaAlSi<sub>3</sub>O<sub>8</sub> or KAlSi<sub>3</sub>O<sub>8</sub>. An Arrhenian behavior  
 438 implies that the activation energy, B, is independent of temperature, and, hence, that the process  
 439 underlying melt viscous flow remains the same regardless of temperature. For melts showing a strong  
 440 non-Arrhenian behavior like NS3, the activation energy term, B, decreases from 2000 kJ mol<sup>-1</sup> at 1000  
 441 K down to 300 kJ mol<sup>-1</sup> at 1800 K. In such conditions, it is no longer possible to use the Arrhenian

442 equation. For this reason, Tamman, Vogel and Fulcher proposed the so-called TVF equation (Vogel,  
443 1921; Fulcher, 1925, Tamman and Hesse, 1926) to link viscosity and temperature:

444  
445 
$$\text{Log } \eta = A + B/(T-T_1), \quad (5)$$

446  
447  $A$ ,  $B$  and  $T_1$  are just fitting parameters without physical meaning. The TVF equation is very useful to  
448 fit and interpolate viscosity data at low and/or at high temperature (Neuville and Richet, 1990). This  
449 equation has been used in many different papers and is at the basis of several viscosity models (Bottinga  
450 and Weill, 1971; Shaw, 1972; Persikov 1991; Giordano et al., 2008; Giordano et Russell, 2018). The  
451 empirical parameters  $A$ ,  $B$ ,  $T_1$  can be linked to glass structure (Giordano and Russell, 2018). However,  
452 while finding very practical applications, this equation remains purely empirical.

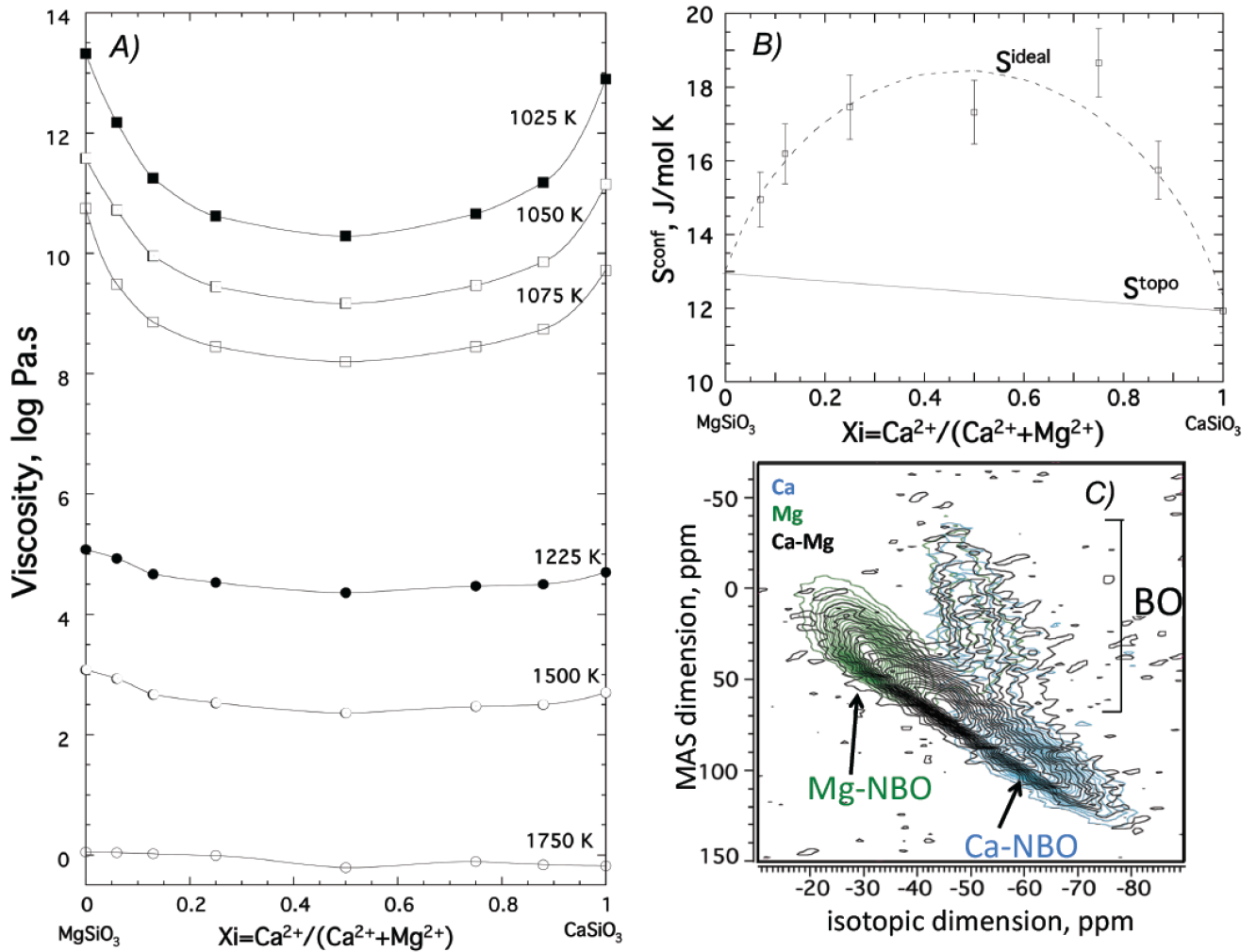
453  
454 Aside from the empirical Arrhenius or TVF equations, the Adam-Gibbs equation, derived from the  
455 theory of Adam and Gibbs (1965), is one of the best candidates to fit and extrapolate viscosity  
456 measurements for silicate melts (Urbain, 1972, Wong and Angel, 1976; Scherer, 1984, Richet 1984,  
457 Neuville and Richet, 1990; 1991, Mauro et al., 2009). The strength of this equation is that it allows  
458 relating viscosity measurements to heat capacity and configurational entropy data (Urbain, 1972; Wong  
459 and Angell, 1976; Scherer, 1984, Richet, 1984). The Adam-Gibbs theory and equation will be discussed  
460 in more details in the next section. No other equation allows relating thermodynamic to dynamic variables  
461 in a simple way.

462  
463 The variations observed and described previously for sodium silicate glasses are similar for all alkali  
464 oxides, as for instance visible for  $K_2O$  in Figure 6B. Generally, the addition of a few percent of alkali in  
465 silica glass produces an important viscosity decrease of a few orders of magnitude (Lecko et al., 1977).  
466 Ten mole percent of alkali oxides decreases the viscosity by  $\sim 10$  orders of magnitude at 1400 K, this  
467 decrease being larger at low temperature near the glass transition temperature. After 10 mol% of added  
468 alkali oxides, the decrease in viscosity with increasing alkali content becomes less pronounced and the  
469 viscosity varies almost linearly at high temperature. These viscosity variations for more than 10% of  
470 added alkali are well correlated with increases in thermal expansion and heat capacity of the liquid which  
471 vary almost linearly as a function of chemical change at high temperature (Bockris et al., 1955; Lange  
472 and Carmichael, 1987; Lange and Navrotsky 1992).

474 *2.2 ideal mixing: mixing alkali or alkaline-earth in silicate glasses and melts*

475 In section 2.1, we observed that molar volumes, as well as viscosity and glass transition temperature  
476 of alkali and alkaline-earth silicate glasses all changes with the addition of network modifiers. Mixing  
477 different metal cations (like Ca and Mg, or Na and K) in silicate glasses results in large variations in their  
478 properties, such as large decreases of their glass transition temperatures or large increases in their  
479 electrical conductivity (Day, 1976). This is the so-called mixed alkali effect, MAE, reviewed many times  
480 (Richet, 1984, Neuvillle and Richet, 1991, Allward and Stebbins, 2004; Cormier and Cuello, 2013, Le  
481 Losq and Neuvillle, 2013, Le Losq et al., 2017, Bødker et al., 2020) in the literature for alkali silicate  
482 glasses since the work of Day (1976).

483  
484 In this section, we show and introduce some terminology about mixing elements and their effect on  
485 the structure and macroscopic properties of melts and glasses. Ca and Mg are very important elements in  
486 Earth and material sciences, and it thus it is particularly important to understand how they mix in silicate  
487 melts. To understand this, we can look at how viscosity varies along the  $\text{CaSiO}_3$ - $\text{MgSiO}_3$  binary. Neuvillle  
488 and Richet (1991) have shown that at constant temperature, the viscosity of  $(\text{Ca},\text{Mg})\text{SiO}_3$  composition is  
489 always lower than the viscosity of the end-member,  $\text{CaSiO}_3$  or  $\text{MgSiO}_3$  (Figure 7A).



491  
 492 **Figure 7:** A) Viscosity versus  $x_i = Ca^{2+}/(Ca^{2+} + Mg^{2+})$  at constant temperature and B) configurational  
 493 entropy for Ca/Mg mixing data from dashed line correspond to the total configurational entropy and  
 494 full line to the topological variation of the entropy see text (Neville and Richet, 1991) C)  $^{17}O$  triple-  
 495 quantum NMR spectrum redrafted from Allwardt and Stebbins (2004).  
 496

497 By using the Adam-Gibbs equation, it is possible to determine the configurational entropy,  $S^{conf}$ .  
 498 Adam and Gibbs (1965) theory of relaxation processes is based on the idea that transporting matter in a  
 499 viscous liquid requires a cooperative change in the fluid configuration. A liquid with zero configuration  
 500 entropy would be analogous to a perfect crystal, and no material displacement could occur since a single  
 501 configuration would be available. The viscosity would then be infinite. If only two configurations were  
 502 possible, a movement of matter could only occur if all the atoms of the liquid changed position  
 503 simultaneously. The probability of such a cooperative movement would be very low and viscosity  
 504 extremely high, but no longer infinite. More generally, as  $S^{conf}$  grows, cooperative configurational  
 505 changes can occur independently of each other in increasingly smaller volumes of the liquid. At the same  
 506 time, viscosity decreases and is predicted by:

$$\log \eta = A_e - B_e/TS^{conf}(T), \quad (6)$$

where  $A_e$  is a pre-exponential term and  $B_e$  a measure of the Gibbs-free energy barriers hindering configurational rearrangements in the liquid.  $S^{conf}(T)$  can be written as:

$$S^{conf}(T) = S^{conf}(T_g) + \int_{T_g}^T \frac{C_p^{conf}(T)}{T} dt, \quad (7)$$

And

$$C_p^{conf}(T) = C_{pl}(T) - C_{pg}(T_g), \quad (8)$$

where  $C_{pl}$  and  $C_{pg}$  are the heat capacity of the liquid and the glass.

$C_p^{Conf}$  is the melt configurational heat capacity, equal to the difference between the heat capacity of the liquid  $C_{pl}$  and the heat capacity of the glass at  $T_g$ ,  $C_{pg}(T_g)$  (Richet et al., 1986). Those values can be measured or modelled with the existing parametric equations (Stebbins et al., 1984; Richet and Bottinga 1984; Richet 1987; Tangeman and Lange 1998; Russell and Giordano 2017), see for examples and details Neuville (2005, 2006), Le Losq et al. (2014) and Le Losq and Neuville (2017). One may also note that  $C_{pg}(T_g) \sim 3R$ , the Dulong and Petit limit (Petit and Dulong, 1819), such that it can be easily estimated from this simple calculation (Richet, 1987). The configurational heat capacity is a very important term, in particular, the higher  $C_p^{conf}$  is, the faster  $S^{conf}$  increases with T, and the lower the  $B_e/S^{conf}$  ratio.

The importance of these differences between configurational  $C_p$  is illustrated in Figure 1, where in the case of  $\text{NaAlSi}_3\text{O}_8$ , the liquid  $C_p^{conf}$  represents less than 10% of that of the glass, and deviations from Arrhenius behavior are small. On the contrary,  $\text{CaSiO}_3$  or  $\text{Mg}_3\text{Al}_2\text{Si}_3\text{O}_{12}$  have a  $C_p^{conf}$  representing 30% of the  $C_p$  of the glass, and the viscosity versus  $1/T$  curves depart significantly from a straight line. Because of the importance of  $C_p^{conf}$ , it is therefore imperative to know the heat capacity of liquids and glasses for a given temperature and chemical composition. We can note that the configurational heat capacity  $C_p^{conf}(T)$  depends essentially on the heat capacity of the liquid,  $C_{pl}$ , and in the case of alkaline-earth silicate melts,  $C_{pl}$  is independent of T and varies mostly linearly with melt composition (Stebbins et al., 1984, Richet and Bottinga, 1985, Lange and Navrotsky, 1992). This explains the pseudo-linear variations of viscosity observed at high temperature (1750 K, Figure 7A).

However, near  $T_g$ , the melt viscosity depends strongly on  $S^{conf}(T_g)$ , which shows large non-linear variations with melt composition. This explains the large, non-linear viscosity changes at supercooled temperature upon mixing alkaline-earth elements in silicate melts (Figure 7A). Using equation 6 in conjunction with viscosity data and heat capacity values (from data or models),  $S^{conf}$  can be calculated.  $S^{conf}$  along the  $\text{CaSiO}_3$ - $\text{MgSiO}_3$  binary is plotted in Figure 7B. To reproduce  $S^{conf}$  variations with composition, it is necessary to look at the contributions to  $S^{conf}(T_g)$  in equation 7.  $S^{conf}$  records topological contributions from the melt structure (bond angle and inter-atomic distance distributions, etc.) as well as

540 excess entropy arising from chemical mixing effects. It thus is common to express  $S^{conf}$  as the addition of  
541 those two sources (Neuville and Richet, 1991):

$$542 \quad S^{conf}(T_g) = S^{topo} + S^{mix} \quad (9)$$

543 with  $S^{mix}$  the term embedding all mixing contributions and  $S^{topo}$  the entropy arising from the topology  
544 of the glass network. The topology of the network for the two end-members is distinctly different and is  
545 also different compared to the crystalline analogues.

546  $S^{topo}$ , the topological configuration entropy can be approximated as a linear variation of the  
547 configurational entropy of the end-members and calculated as  $\sum x_i S^{conf}_i(T_g)$ , with  $S^{conf}_i(T_g)$  the  
548 configurational entropy of  $\text{CaSiO}_3$  and  $\text{MgSiO}_3$  glasses (Neuville and Richet, 1991). This  $S^{topo}$  term  
549 corresponds to a mechanical mixing between the two end-members without necessary chemical or  
550 physical interaction.  $S^{topo}$  can be expressed from the glass structure and varies linearly with composition  
551 (Le Losq and Neuville, 2017).

552  $S^{mix}$  corresponds to a chemical mixing term that can be ideal or non-ideal. In the case of Ca/Mg mixing,  
553 the simplest hypothesis that can be made is that  $S^{mix} = S^{ideal}$ , and thus can be written as:

$$554 \quad S^{ideal} = -n \sum R x_i \ln x_i, \quad (10)$$

555 where  $R$  is the perfect gas constant and  $n$  is the number of atoms exchanged per formula units, 1 in  
556 this case,  $x_i = \text{Ca}^{2+}/(\text{Ca}^{2+} + \text{Mg}^{2+})$ . From a thermodynamic point of view, the ideal solution implies that  
557 end-members components mix randomly in solution.

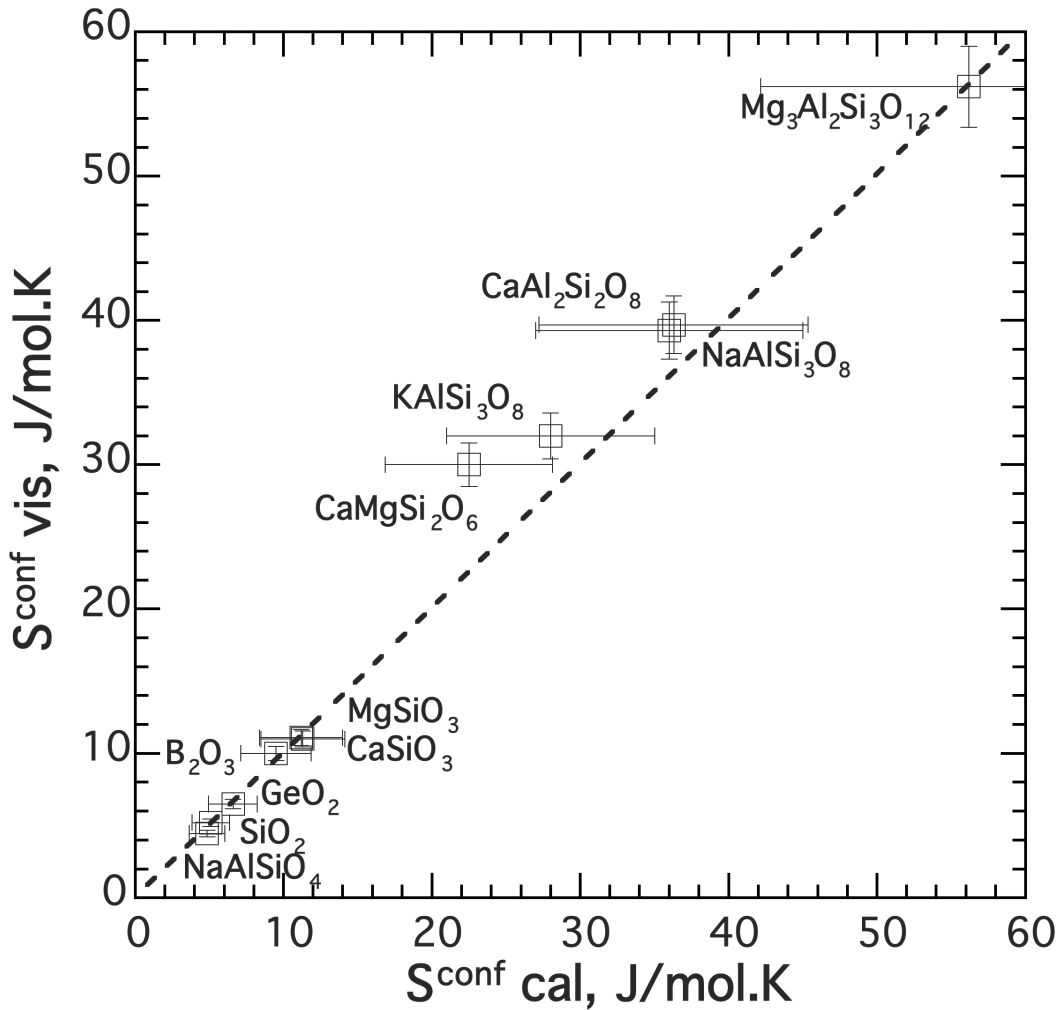
558 The excellent agreement (Figure 7B) between entropies obtained from viscosity measurements and  
559 values predicted using eqs 6 to 10 shows that the ideal mixing hypothesis for Ca/Mg is consistent with  
560 the data. It should be noted that the mixing effect is predominant near  $T_g$ . The configuration entropy of  
561 the intermediate compositions is therefore much higher than that of the end-members, explaining the  
562 minimum in viscosity observed upon Ca/Mg mixing. When temperature increases, the entropy of the  
563 end-members increases rapidly and  $S^{mix}$ , which is constant, eventually becomes small compared to  $\sum x_i$   
564  $S^{conf}_i(T_g)$  in eq. (9). Therefore, at high temperatures,  $S^{mix}$  is negligible and this results in a quasi-linear  
565 variations in viscosity, driven by the linear variation of  $C_{pl}$  upon Ca/Mg mixing.

566 These macroscopic conclusions about Ca/Mg mixing are in very good agreement with nanoscale  
567 investigations made by  $^{17}\text{O}$  NMR (Allwardt and Stebbins, 2004) and neutron diffraction and RMC  
568 (Cormier and Cuello, 2013). From neutron diffraction, the silicate network shows small but significant  
569 changes with the Mg/Ca exchange and a significant intermixing of Ca and Mg can be observed (Cormier  
570 and Cuello, 2013). From another point of view,  $^{17}\text{O}$  NMR spectra of the diopside glass  $(\text{CaMg})\text{SiO}_3$   
571 shows that only one broad non-bridging oxygen atom (NBO) peak is visible, and encompasses the entire  
572 range of chemical shifts ranging from Ca-NBO to Mg-NBO. Comparison of the isotropic projections  
573 from 3QMAS NMR to 1D spectra predicted using a random model show that Ca/Mg mixing in Ca/Mg-

574 silicate glasses is generally highly disordered (Allwardt and Stebbins, 2004), except maybe near the glass  
 575 transition temperature where a more ordered glass is possible as shown by neutron diffraction made on  
 576 CaSiO<sub>3</sub> glass by Gaskell et al. (1985).

577  
 578 *Validity of the viscosimetry approach to determine  $S^{conf}(T_g)$*

579 We have just shown that it is possible to determine configurational entropies using viscosity  
 580 measurements and the AG theory. Are those values of  $S^{conf}(T_g)$  truly representative of the glass residual  
 581 entropy? To answer this question, we can compare  $S^{conf}(T_g)$  obtained from calorimetric measurements to  
 582 those obtained from fitting viscosity data. Data from 11 very different compositions, including B<sub>2</sub>O<sub>3</sub>,  
 583 SiO<sub>2</sub> or KAlSi<sub>3</sub>O<sub>8</sub>, show very good agreement between  $S^{conf}(T_g)$  values retrieved from viscosity  
 584 measurements or calorimetric measurements (Figure 8). This thus validates the use of eq. 6 to determine  
 585  $S^{conf}(T_g)$  of melts.



586  
 587 *Figure 8: viscosimetry configurational entropy versus calorimetry configurational entropy for 10*  
 588 *different oxide glasses for which determination of calorimetric measurements are possible. Calorimetry*



589 data are from Richet (1984) for  $\text{SiO}_2$ ,  $\text{NaAlSi}_3\text{O}_8$ ,  $\text{KAlSi}_3\text{O}_8$ , de Ligny and Westrum (1996) for  $\text{GeO}_2$  and  
590  $\text{B}_2\text{O}_3$ , Richet et al. (1991) for  $\text{NaAlSiO}_4$ , Tequi et al. (1991) for  $\text{Mg}_3\text{Al}_2\text{Si}_3\text{O}_{12}$ , and Richet et al. (1986)  
591 for  $\text{MgSiO}_3$ ,  $\text{CaSiO}_3$ ,  $\text{CaMgSi}_2\text{O}_6$  and  $\text{Ca}_2\text{Al}_2\text{Si}_2\text{O}_8$ . Viscosity data are from Hetherington et al. (1964)  
592 and Urbain et al. (1982) for  $\text{SiO}_2$ , Neuville and Richet (1991) and Le Losq and Neuville (2013) and Le  
593 Losq et al. (2017) for alkali and alkaline-earth silicate and aluminosilicate compositions, from Fontana  
594 and Plummer (1966) for  $\text{GeO}_2$ , and from Eppler (1966), Macedo et Litovitz. (1965), Napolitano et al.  
595 (1965) for  $\text{B}_2\text{O}_3$ .

596

597 In the case of Na/K mixing in silicate melts, only one set of measurements is available from Poole  
598 (1948). Using those data, Richet (1984) proposed that an ideal, random Na/K mixing occurs in silicate  
599 melts, and viscosity can be modelled using the ideal mixing calculation of  $S^{conf}$ ; some differences  
600 between calculated and measured viscosity in the supercooled silicate melts are visible in Richet (1984)  
601 work, however they arise from the way the data and model are represented. The more recent study of Le  
602 Losq and Neuville (2017) resolved this, showing that it is clearly possible to model the viscosity of Na-  
603 K silicate melts while assuming a random mixing of the alkalis (see section 2.4).

604

### 605 2.3 Mixing alkali and alkaline-earth elements in silicate glasses

606 Most industrial and geologic glasses are silicate and aluminosilicate glasses containing a mixture of  
607 alkali and/or alkaline-earth elements. Igneous rocks (Morey and Bowen, 1925) as well as nearly 90 % of  
608 industrial glasses contain mixtures of alkali and alkaline-earth elements. We can cite the particular case  
609 of soda-lime silica glasses, extensively used for the construction of conventional windows and container  
610 glasses. The importance of  $\text{M}^{2+}\text{O}-\text{M}^+\text{O}-\text{SiO}_2$  glasses (with  $\text{M}^+$  an alkali and  $\text{M}^{2+}$  an alkaline-earth  
611 element) further increased recently because they also are used for the development of bioactive glasses  
612 (Hench, 1991 and Kim et al. 1995, Clupper and Hench, 2003, Hill and Brauer, 2011; Brauer, 2015).  
613 Given the importance of alkali and alkaline-earth metal cations in glasses, many studies were performed  
614 to understand the  $\text{M}^{2+}\text{O}-\text{M}^+\text{O}$  mixing in silicate glasses. They are essentially focused on the glass  
615 mechanical properties or devitrification (Morey, 1930; Frischat and Sebastian, 1985; Koike and  
616 Tomozawa, 2007, Koike et al., 2007), on glass structure (Buckerman and Müller-Warmuth, 1992, Jones  
617 et al., 2001; Lockyer et al., 1995; Lee and Stebbins, 2003; Lee et al., 2003, Neuville 2005, 2006, Hill and  
618 Brauer, 2011; Brauer, 2015; Moulton and Henderson, 2021 and reference therein) or thermodynamic  
619 properties (Natrup et al., 2005; Neuville 2005, 2006, Richet et al., 2009b; Inaba et al., 2010, Sugawara et  
620 al., 2013). Given the above-mentioned importance of  $\text{M}^{2+}\text{O}-\text{M}^+\text{O}-\text{SiO}_2$  glasses, we will in this section  
621 bring new insights to the effect of  $\text{M}^{2+}\text{O}-\text{M}^+\text{O}$  mixture on the properties of silicate glass and melt.

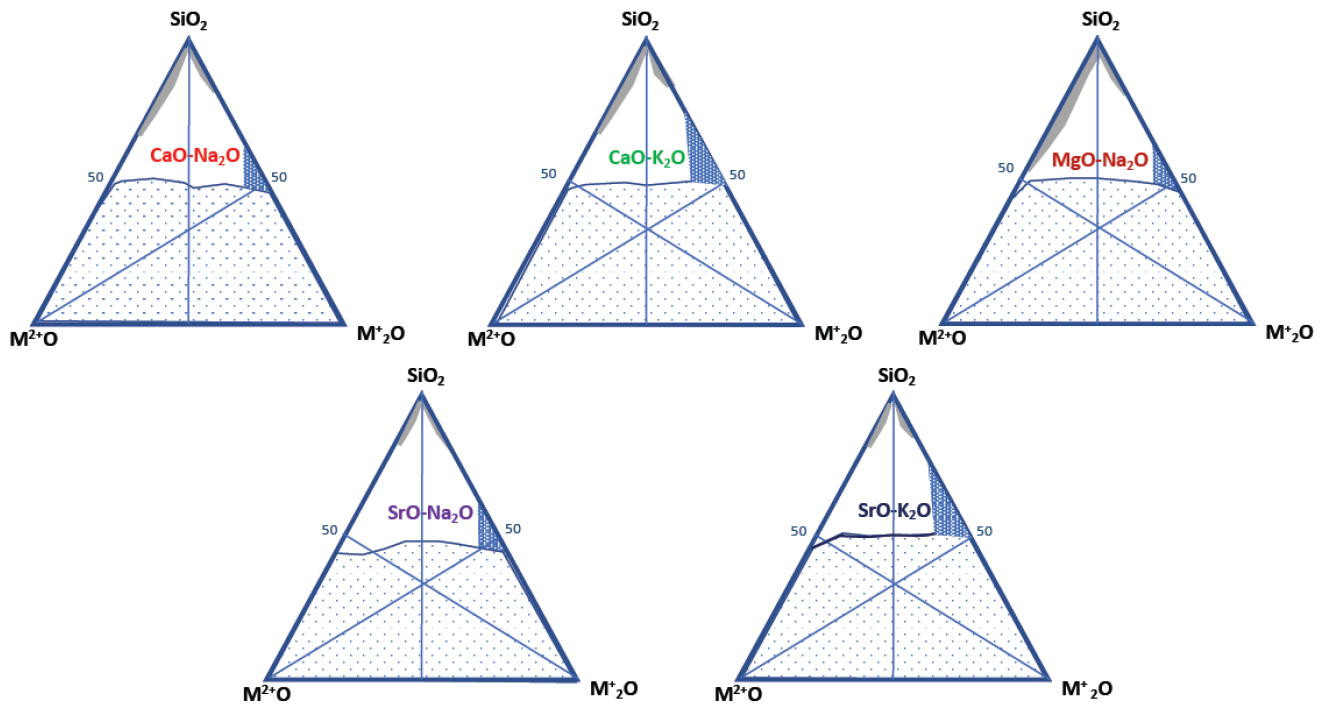
622

### 2.3.1 Glass formation domains

The substitution of alkali elements by alkaline-earth elements allows extending the glass forming domain of silica glasses to lower silica contents (Figure 9), and, more generally, it allows improving many glass properties (Moore and Carey, 1951, Imaoka and Yamazaki 1963, Tomozawa, 1978; 1999; Gahay and Tomozawa 1989, 1984, Neuville, 2005, 2006). For  $M^{2+}O$  and  $M^+O_2$  bearing silicate glasses, the vitrification domain starts near 50 mol% silica in most cases. For Mg silicates, it starts at 45.7 mol% (Moore and Carey, 1951). It was generally accepted that the presence of Mg-O bonds allows preserving somehow the continuity of the silicate network, with Mg acting to some extent as a network former (Moore and Carey, 1951), an idea in agreement with the low coordination number of Mg discussed previously. In the case of CaO-Na<sub>2</sub>O-SiO<sub>2</sub> glasses, the first phase diagram was made by Morey and Bowen (1925). It revealed the domain where glasses can be formed, but also an immiscibility domain in which phase separation is observed. This immiscibility domain is very large near the CaO-SiO<sub>2</sub> binary, extending between 62 and 100 mol% of silica. It decreases rapidly with addition of Na<sub>2</sub>O in the glass (Morey and Bowen, 1925, Greig 1927, Hudon and Baker, 2002a,b). In the immiscibility domain, different phases exist: cristobalite, SiO<sub>2</sub>, wollastonite CaSiO<sub>3</sub>, sodium disilicate Na<sub>2</sub>Si<sub>2</sub>O<sub>5</sub>, devitrite Na<sub>2</sub>Ca<sub>3</sub>Si<sub>6</sub>O<sub>16</sub>, and a non-defined compound Na<sub>2</sub>Ca<sub>2</sub>Si<sub>3</sub>O<sub>9</sub>. The proportion of these phases vary as a function of the bulk composition and the cooling rate (Morey and Bowen, 1925, Greig 1927, Tomozawa, 1978; 1999; Gahay and Tomozawa 1989; Hudon and Baker, 2002a,b; see also Schuller chapter in Neuville et al., 2017).

Similar observations can be made in the other  $M^{2+}O$ - $M^{2+}O$ -SiO<sub>2</sub> systems, with  $M^+=Li^+$ , Na<sup>+</sup>, K<sup>+</sup> and  $M^{2+}=Mg^{2+}$ , Ca<sup>2+</sup>, Sr<sup>2+</sup>, Ba<sup>2+</sup>. Generally, a pyrosilicate phase,  $M^{2+}SiO_3$ , and one or two phases  $M^+_yM^{2+}_xSi_zO_u$  crystallize at high silica contents (> 70 mol%,  $x,y,z,u$  are different proportions of each crystalline phases), except for  $M^{2+}=Ba^{2+}$  where the glass forming domain is large but mostly unconstrained. Bender et al. (2002) achieved the synthesis of Ba silicate glasses up to the BS7 (BaO/SiO<sub>2</sub>=7 in mol %) composition, and Frantz and Mysen (1995) investigated some of those glass compositions by Raman spectroscopy.

To summarize, in all of the  $M^{2+}O$ - $M^{2+}O$ -SiO<sub>2</sub> ternary diagrams, the glass forming domains are relatively small and essentially exist at silica contents higher than 50 mol%, with exception of barium silicates. In the case of sodium and potassium silicates, a large zone of high hygroscopicity exists below the glass forming domain, typically between 66 and 50 mol % of silica for sodium silicate glasses and between 70 and 50 mol % for potassium silicate glasses (Tomozawa, 1978; 1999; Gahay and Tomozawa 1989). In general, one should be careful with potassium silicate glasses that are always highly hygroscopic.



658

659

660

661

662

663

664

665

666

667

668

669

670

671

672

673

674

675

676

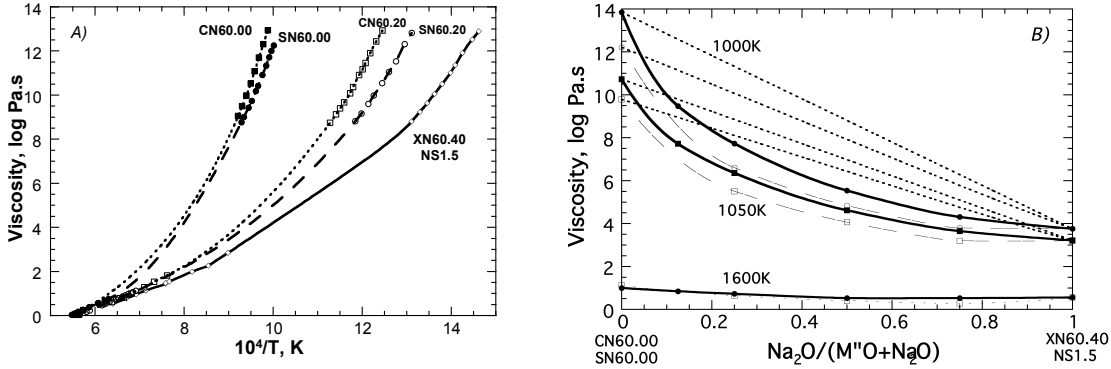
677

**Figure 9:** The upper part of the ternary diagram corresponds to the glass forming region of glass between  $M^{2+}O$  and  $M^+_2O$ , with  $M^{2+}=Mg^{2+}$ ,  $Ca^{2+}$ ,  $Sr^{2+}$  and  $M^+=Na^+$ ,  $K^+$  (redrafted from Imaoka and Yamazaki, 1963 and Levin et al., 1964). The white areas are the glass making domain, the light dotted areas are the crystallization domains, the dark dotted lines correspond to the glass making domain, but strongly hygroscopic, and the gray areas to unmixed glass.

### 2.3.2 Viscosity variations

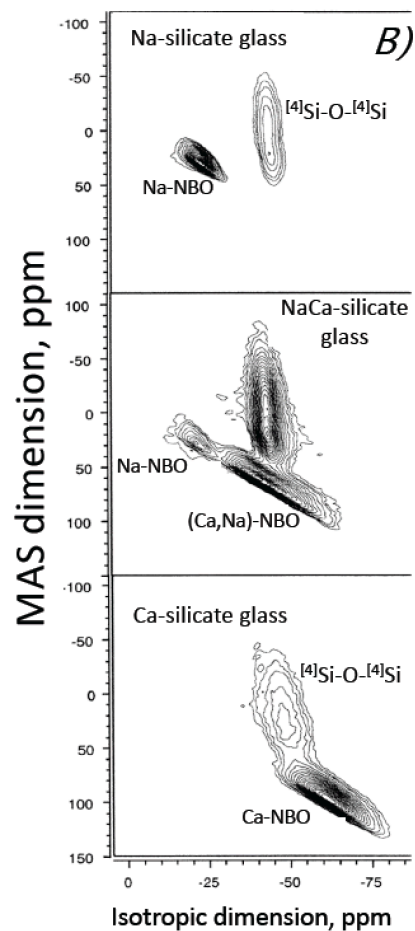
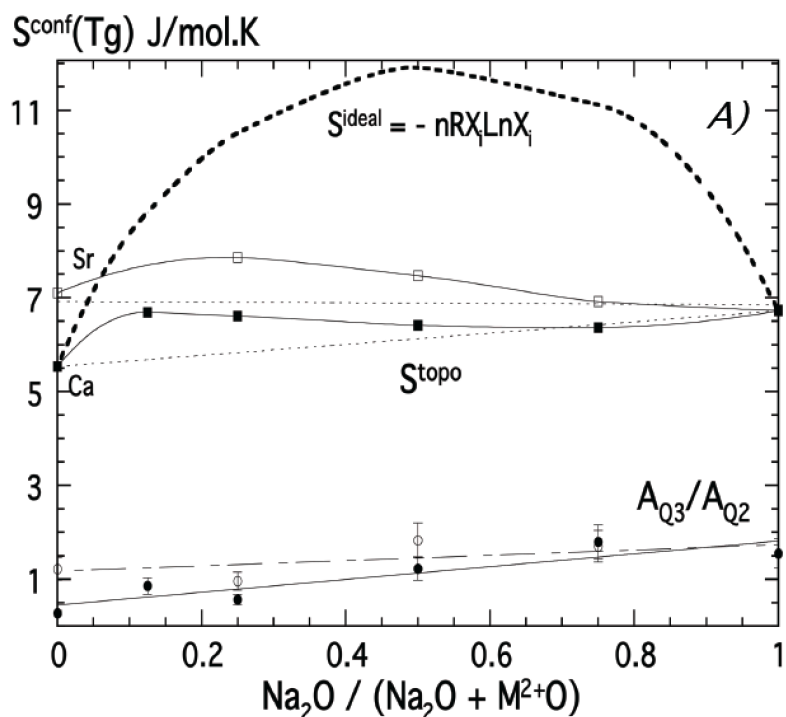
Figure 10A shows viscosity measurements of silicate melts for  $M^{2+}$ -Na mixing with  $M^{2+} = Ca^{2+}$ ,  $Sr^{2+}$ . Ca- and Sr-silicate melts show similar behavior. The addition of those elements produces a large increase in melt viscosity at constant temperature, in agreement with previous measurements (English, 1923). The lack of measurement between  $10^2$  and  $10^9$  Pa·s results from the very rapid rate of crystallization in this viscosity-temperature range for mixed alkali and alkaline-earth silicate glasses (Meiling and Uhlmann, 1977; Mastelaro et al. 2000, Neuville, 2005, 2006). In the Figure 10B, we clearly observe that addition of 10 mole %  $Na_2O$  in an alkaline-earth silicate melt has a stronger effect on melt viscosity than addition of 10 mole %  $M^{2+}O$  to a soda-silicate melt composition. This indicates that a sodium silicate glass network can incorporate alkaline-earth elements more easily than the opposite. A striking difference exists in the behavior of the viscosity between pure Na-silicate melts and pure alkaline-earth silicate melts (CN60.00 or SN60.00). Indeed, at constant viscosity and near  $T_g$  (Figure 10B), i.e. near 1000 K, the viscosity of the end-member compounds differ by 10 orders of magnitude. This difference decreases

678 with temperature: it is less than 0.5 order of magnitude at 1600 K. Furthermore, at 1600 K, the viscosity  
 679 of the  $\text{Na}_2\text{O}-\text{M}^{2+}\text{O}-\text{SiO}_2$  melts decreases almost linearly with  $\text{Na}_2\text{O}/(\text{Na}_2\text{O}+\text{M}^{2+}\text{O})$ . Similar behaviors  
 680 were already observed by English (1923) in the same system with 75 mole %  $\text{SiO}_2$  and 25 mole %  $\text{Na}_2\text{O}$ ,  
 681 and with a substitution of  $\text{Na}_2\text{O}$  by up to 12 mole %  $\text{CaO}$ .



682  
 683 **Figure 10:** A) Viscosity versus  $1/T$  for silicate melts ranging from the pure alkaline-earth silicate  
 684 melt) to pure soda silicate (XN60.40) composition names are: XN60.Y, X=C or S for the Ca or Sr system,  
 685 Y correspond to  $\text{Na}_2\text{O}$  content, 60 to  $\text{SiO}_2$  in mole percent, and  $X=100-(60+Y)$  all in mole percent. B)  
 686 Viscosities of  $\text{Na}/\text{M}^{2+}$  silicate melts versus  $\text{Na}_2\text{O}/(\text{Na}_2\text{O}+\text{M}^{2+}\text{O})$  at constant temperature,  $\text{M}^{2+}=\text{Ca}, \text{Sr}$ ,  
 687 dashed lines correspond to the linear viscosity variation at 1000 K, 1050 K and 1600 K, solid and open  
 688 symbols correspond to the  $\text{CaO}-\text{Na}_2\text{O}-\text{SiO}_2$  and  $\text{SrO}-\text{Na}_2\text{O}-\text{SiO}_2$  systems, respectively compiled from  
 689 Neuville (2006, 2005).

690  
 691 The viscosity variations observed in Figure 10 can be understood using equations 6 to 9. It is possible  
 692 to determine how configurational entropy varies upon the mixing of  $\text{Na}_2\text{O}$  with  $\text{M}^{2+}$  in the glasses (Figure  
 693 11A).  $S^{conf}$  can be decomposed in  $S^{topo}$  and  $S^{mix}$  (eq. 9).  $S^{topo}$  is equal to the sum of endmembers.  $S^{mix}$ , in  
 694 the case of  $\text{M}^+/\text{M}^{2+}$  mixing, has a complex expression that depends on the way the cations mix into the  
 695 glass structure.



696  
 697 **Figure 11:** A)  $\text{Na}_2\text{O}/(\text{Na}_2\text{O}+\text{M}^{2+}\text{O})$  dependence of configurational entropy,  $S^{\text{conf}}(T_g)$ ,  $A_{Q3}/A_{Q2}$  ratio for  
 698 in black symbol CaO and in open symbol for SrO (entropy are in J/mol.K and  $A_{Q3}/A_{Q2}$  without units and  
 699 are calculated from the  $Q^3$  and  $Q^2$  areas of the Raman spectra, see Neuvill (2005, 2006) for more detail).  
 700 B)  $^{17}\text{O}$  3QMAS MAS spectra for Ca-Na silicate glasses at 9.4 T redrafted from Lee and Stebbins, (2003).  
 701

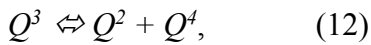
702 Between the calcium and sodium silicate glasses,  $S^{\text{conf}}(T_g)$  varies non-linearly with  $\text{Na}_2\text{O}/(\text{Na}_2\text{O}$   
 703  $+\text{CaO})$ . It increases rapidly with increasing  $\text{Na}_2\text{O}/(\text{Na}_2\text{O}+\text{CaO})$  to 0.2, then it slightly decreases with  
 704 further substitution  $\text{Ca}^{2+}$  by  $\text{Na}^+$ . Similar observations are made in the SrO- $\text{Na}_2\text{O}$ - $\text{SiO}_2$  system (Neuvill,  
 705 2005). The observed variations strongly depart from the predictions made by the ideal model given in  
 706 equation 10 (Figure 11A). In the case of  $\text{Na}^+$  and  $\text{Ca}^{2+}$ , or of  $\text{Na}^+$  and  $\text{Sr}^{2+}$ , it is clear that, as their  $S^{\text{conf}}(T_g)$   
 707 variations are close to linear trends, those atoms do not mix randomly in the silicate melts. The fits of  
 708  $S^{\text{conf}}(T_g)$  presented in Figure 11A thus require the use of a non-ideal mixing model. To model  $S^{\text{mix}}$  in the  
 709 case of a non-ideal mixing of alkali and alkaline-earth elements, Neuvill (2005, 2006) proposed to use  
 710 the equation:

$$711 \quad S^{\text{mix}} = W_{NM} x_n y_c^3, \quad (11)$$

712 where  $x_n = \text{Na}_2\text{O}/(\text{Na}_2\text{O}+\text{M}^{2+}\text{O})$  and  $y_c = 1-x_n$ , and  $W_{NM}$  is a constant.

### 2.3.3 Structure of mixed glasses

Equation (11) implies a significant change in the residual entropy that originates from a re-arrangement of the glass structure as  $\text{Ca}^{2+}$  is replaced by  $\text{Na}^+$ . Spectroscopic methods that probe the glass structure allow us to investigate such structural changes.  $^{23}\text{Na}$  and  $^{17}\text{O}$  Nuclear Magnetic Resonance (NMR) spectroscopy data shown a non-random distribution in the case of  $\text{Na}^+$ - $\text{Ca}^{2+}$  mixing, with in particular a prevalence of  $\text{Na}^+$ - $\text{Ca}^{2+}$  pairs in the system (Figure 11B), and several partially resolved non-bridging oxygen peaks such as  $\text{Na}^+$ -NBO, and mixed peaks ( $\text{Na}^+$ ,  $\text{Ca}^{2+}$ )-NBO (Lee and Stebbins, 2003). The observed fractions of  $\text{Na}^+$ -NBO are smaller than those predicted by random distributions of  $\text{Na}^+$  and  $\text{Ca}^{2+}$ , suggesting preference for dissimilar pairs (Lee and Stebbins, 2003) which is also in good agreement (Florian et al., 1996; Lee 2005, Lee and Stebbins 2002 and Lee et al., 2003). In the previous chapter, Raman spectroscopy soda and lime silicate glasses were shown in Figure 9. Different  $Q^n$  contributions are visible in those spectra. From these  $Q^n$  contributions, the ratio of the area between  $Q^3$  and  $Q^2$  units,  $A_{Q3}/A_{Q2}$  can be calculated. Results of such calculation are plotted in Figure 11A. It shows that the fraction of  $Q^3$  units in the glass increases with increasing the  $\text{Na}_2\text{O}/(\text{Na}_2\text{O}+\text{M}^{2+}\text{O})$  ratio.  $\text{M}^{2+}\text{O}$  silicate glasses are thus richer in  $Q^2$  and  $Q^4$  units than alkali silicate glasses (Frantz and Mysen, 1995, Neuville 2005, 2006), because increasing the ionic field strength of metal cation in the glass shifts to the right the equilibrium of the reaction:



This observation will be used in section 2.4 for highlighting how one can build models of the structure, entropy and viscosity of silicate melts. Huang et al. (2016) investigated  $\text{Ca}_3\text{SiO}_5$  composition by using  $^{17}\text{O} \rightarrow ^{29}\text{Si}$  CP-HETCOR NMR experiment and they proposed that free oxygen can also play a small role structure and properties in the mixed glasses, what is possible but this experiment must be considered with caution, firstly it is a particularly difficult composition to manufacture and secondly, only the nominal compositions are given and not those analyzed.

### 2.3.4 Network polymerization

The substitution of 30 mol% of  $\text{CaO}$  by  $\text{Na}_2\text{O}$  in an alkaline-earth silicate glass results in a moderate increase of  $\sim 0.9 \text{ J mol}^{-1} \text{ K}^{-1}$  of  $S^{\text{conf}}(T_g)$  (Figure 11A). This indicates an increase in the structural disorder in the glass, possibly linked to change in the glass network polymerization. Structural changes that may account for the entropy behaviour may be discerned in the Raman spectra of the glasses. In particular, the ratio of the areas of Raman bands assigned to  $Q^3$  and  $Q^2$  units,  $A_{Q3}/A_{Q2}$ , varies with  $\text{M}^{2+}\text{O}/(\text{M}^{2+}\text{O}+\text{M}^{2+}\text{O})$ , indicating a change in the  $Q^n$  speciation distribution (Neuville, 2006). There is a distinct increase of this ratio with adding  $\text{Na}_2\text{O}$  in the alkaline-earth silicate glasses. In the case of  $\text{Na}/\text{Ca}$

747 and Na/Sr mixing, Raman spectroscopy observations shown in Figure 11A are in good agreement with  
748 previous observations by Raman spectroscopy (McMillan, 1984; McMillan et al., 1982; Frantz and  
749 Mysen, 1995) and by  $^{17}\text{O}$  NMR (Maekawa et al., 1991; Buckerman and Müller-Warmuth, 1992; Jones  
750 et al., 2001, Lee and Stebbins, 2003, Lee et al., 2003), all showing a decrease in  $Q^3$  fraction upon  
751 substitution of alkali by alkaline-earth element in silicate glasses. Moreover, the increase in  $Q^2$  units with  
752 adding alkaline-earth elements in soda silicate glasses can be correlated to increasing Boson peak  
753 frequency and intensity (Neuvville, 2006).

754 Note that below  $250\text{ cm}^{-1}$ , there is only a scattering continuum and the Raleigh tail of the exciting line,  
755 except at very low frequency where there is the so-called boson peak (Malinovsky and Sokolov, 1986;  
756 Buchenau et al., 1986). This peak has been ascribed to excitations associated with rotational motions of  
757 almost rigid tetrahedra (Buchenau et al., 1986; Helhen et al., 2000, 2002). Helhen et al. (2002) consider  
758 that this peak, observed for different silicate glasses, increases in intensity and shifts to higher frequency  
759 with higher distortion of the  $\text{SiO}_4$  tetrahedra. Several others interpretations are proposed: - Champagnon  
760 and collaborators proposed that Boson peak can be link with structural homogeneity in the glass  
761 (Champagnon et al., 2009), and the other hand Chumakov and collaborators proposed that Boson peak  
762 can be attributed to some fluctuation of disorder in glass (Chumakov et al., 2014) and finally Schirmacher  
763 and collaborators proposed an intermediate interpretation by considering that the Boson peak can  
764 corresponds to the spatial fluctuations of elastic constants caused by the structural disorder of the  
765 amorphous materials (Schirmacher and Ruocco, 2020, Schirmacher et al., 2015). If we consider that  
766 molecular dynamic simulations provided by Cormack and coworkers suggest that Si-NBO bond length  
767 is about  $0.05\text{ \AA}$  shorter than the Si-BO bond length (Henderson, 1995; Cormack and Du, 2001; Du and  
768 Cormack 2004)<sup>5</sup>, we can propose that  $Q^2$  units are more distorted than  $Q^3$  or  $Q^4$  units. This implies that  
769  $Q^4$  and  $Q^0$  units are regular tetrahedra with  $Q^4$  bigger than  $Q^0$  and they are less distorted than the  $Q^1$ ,  $Q^2$ ,  
770  $Q^3$  units species (Nakamura et al., 2013). It is probable that  $Q^2$  units are the more distorted tetrahedra  
771 with 2 distances T-BO and 2 distances T-NBO which can be in good agreement with the variation of the  
772 frequency of boson peak. So, we proposed that the variation on the Boson peak observed as a function  
773 of chemical change in simple systems with cation substitution can be attributed to tetrahedra distortion  
774 as observed on  $\text{SiO}_2$  glass with pressure. This variation can also result of structural heterogeneity produce

<sup>5</sup> Du and Cormack (2004) proposed from MD simulation that when the alkali content vary between 10 and 50 mole percent the  $d(\text{Si-BO})$  vary between  $1.625$  and  $1.629\text{ \AA}$  and  $d(\text{Si-NBO})$  varies between  $1.559$  and  $1.579\text{ \AA}$ . Henderson (1995) proposed from EXAFS measurements that  $d(\text{Si-O})$  equal  $1.61\pm 0.02\text{ \AA}$  and  $1.58\pm 0.02\text{ \AA}$  for NS1.5 glass which is in good agreement with MD.

775 by the fact that soda silicate glasses are richer in  $Q^3$  species than lime-silicate glasses. These structural  
776 heterogeneities can also be close the idea of percolation channels proposed by Greaves (1985).

777

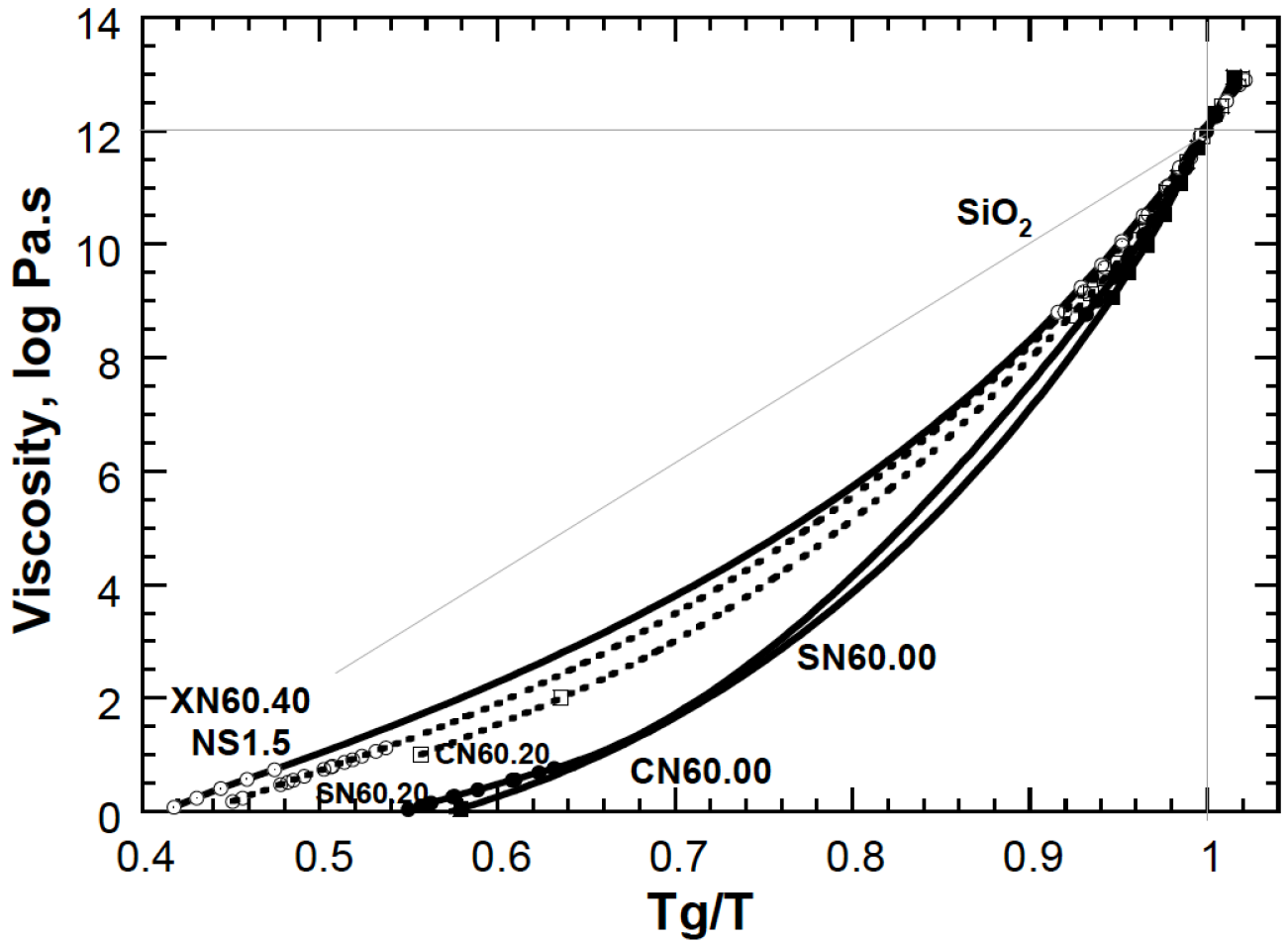
### 778 2.3.5 Fragility

779 Angell (1991) proposed a classification of liquids between strong and fragile: a strong liquid shows a  
780 linear variation like SiO<sub>2</sub> in the diagram  $\log \eta$  versus  $T_g/T$  whereas this linear relation is not preserved in  
781 a fragile liquid (Figure 12). The melt fragility,  $m$ , is related to its thermodynamic properties via the  
782 relationship:

$$783 \quad m = B_e / S^{conf}(T_g) * T_g * (1 + C_p^{conf}(T_g) / S^{conf}(T_g)) \quad , \quad (13)$$

784 In the case of the M<sup>+</sup><sub>2</sub>O-M<sup>2+</sup>O-SiO<sub>2</sub> system, the viscosities of the alkali- alkaline-earth silicate melts  
785 are plotted as a function of  $T_g/T$  in Figure 12. The strongest liquid is the pure soda silicate, XN60.40  
786 (NS1.5), whereas the most fragile liquids are the pure alkaline-earth silicate melts. The Ca- and Sr-silicate  
787 melts have similar fragility, despite the Ca-silicate melt being more viscous than Sr-silicate melt.  
788 Intermediate chemical compositions mixing Na<sup>+</sup> with Ca<sup>2+</sup> or Sr<sup>2+</sup> present an intermediate behavior  
789 between end-members. The behavior of the melt fragility correlates well with melt  $C_p^{conf}$  values, which  
790 decrease of ~ 20 % upon replacing M<sup>2+</sup> with Na (M<sup>2+</sup> = Ca<sup>2+</sup> or Sr<sup>2+</sup>; Neuville, 2005, 2006). This  
791 observation on the decrease of the  $C_p^{conf}$  is in good agreement with the increase of the  $\Delta C_p = C_{pl} / C_{pg}(T_g)$   
792 which varies between 1.2 for the Na-silicate glass up to 1.27 and 1.29 for Ca- and Sr-silicate glasses.  
793 Note that, Angell (1991) proposed that  $\Delta C_p$  vary between 1.1 and 1.3 for a strong and fragile liquid  
794 respectively.





795

796 **Figure 12:** Viscosity of soda- $M^{2+}O$  silicate glasses versus  $T/T_g$ . Error bars are smaller than symbol  
 797 size, from Neuville (2005, 2006).

798

799 **2.3.6 Melt configurational entropy, fragility,  $Q^n$  speciation, mobility and network connectivity**

800 The distribution of cations in the glass network can have important implications for transport properties  
 801 such as conductivity, viscosity and fragility. In the case of the Na/Ca substitution in silicate melts, Roling  
 802 and Ingram (2000) have shown that the mobility of  $Ca^{2+}$  cations is enhanced upon their replacement by  
 803  $Na^+$ . This replacement of  $Ca^{2+}$  by  $Na^+$  produces a positive coupling effect on the movements of divalent  
 804 cations that correlates well with the increase in  $S^{conf}(T_g)$  (Figure 11A). Conversely, the activation energies  
 805 related to movements of  $Na^+$  is slightly changed. The cation mobility strongly depends on the glass  
 806 structure, and the structural changes taking place during the Na/Ca substitution in the Ca-silicate glass  
 807 enhance the mobility of  $Ca^{2+}$ . The modification in network topology will provide new types of empty  
 808 sites that could be used for Ca movements (Cornier and Neuville, 2004). The mobility of the divalent  
 809 cation is then assisted by positive coupling with the more mobile monovalent cation (Magnien et al.,  
 810 2004, 2008).

811

812 To summarize the observations made in the case of the mixing between alkali,  $M^+$ , and alkaline-earth,  
813  $M^{2+}$ , elements in silicate glasses and melts:

- 814 - alkali and alkaline-earth cations do not mix randomly,
- 815 - increased alkali content increases the formation of  $Q^3$  species,
- 816 - diffusivity increase with alkaline-earth element (Roling and Ingram, 2000),
- 817 - fragility increases with alkaline-earth content,
- 818 - the distortion of the tetrahedra suggested by the boson peak variation and the distortion of the  
819 network increases with increasing MO content,
- 820 - the proportion of  $Q^2$  species increases with  $M^{2+}O$  content and in the same way, the intensity and the  
821 frequency position of the boson peak increase. The fact, that the alkaline-earth silicate glasses around  
822 than 60% of silica correspond to a mixing of  $Q^2$  and a small amount of  $Q^4$  species, may be the origin of  
823 the unmixing observed for more than 60% of  $SiO_2$  in the  $M^{2+}O-SiO_2$  binary system (see Figure 9). These  
824 two interconnected  $Q^n$  species can also be an image of the percolation channels (Greaves et al., 1981,  
825 Greaves, 1985, Frischat et al., 2001, Le Losq et al., 2017).

826

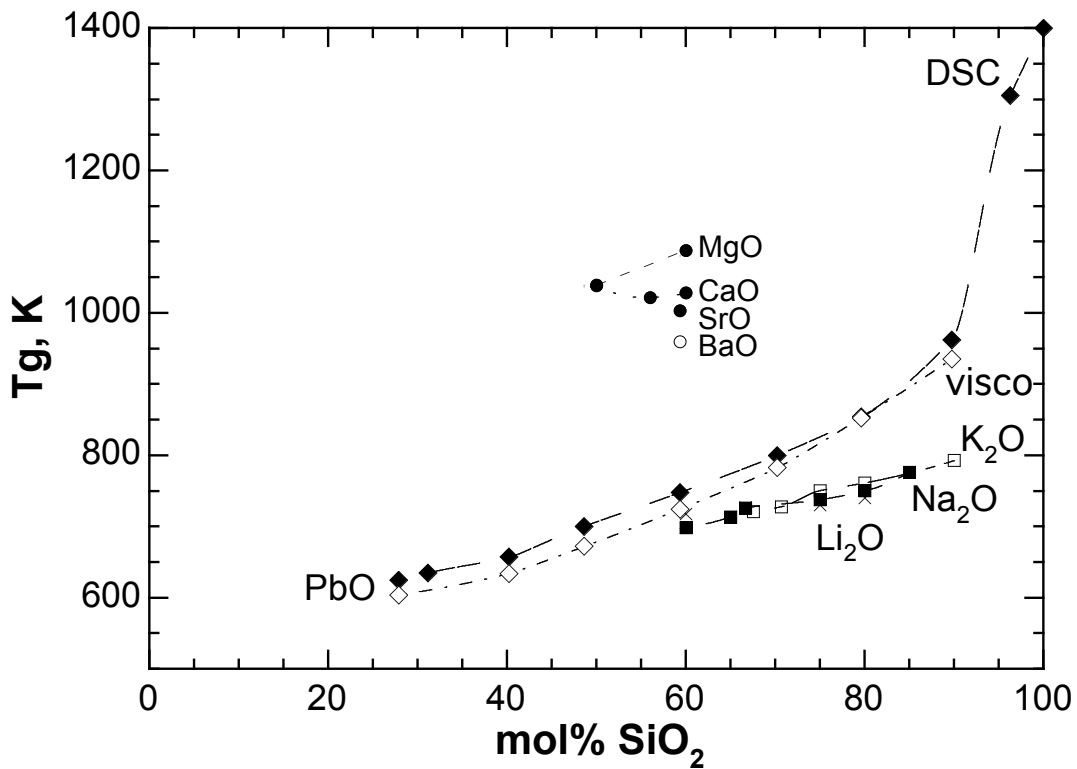
## 827 *2.4 Silicate glasses and others network formers*

828

### 829 *2.4.1 Lead*

830 The replacement of  $SiO_2$  by  $PbO$  produces a small decrease in the glass molar volume until the Si/Pb  
831 ratio reaches a value of 0.5. Further  $PbO$  addition results in a molar volume increase. The  $PbO$  amorphous  
832 molar volume value can be obtained by extrapolation and is  $25.0 \text{ cm}^3$  (Robie et al., 1979; see arrow in  
833 Figure 5) which is similar to the molar volume of Litharge,  $PbO$  with  $Pb^{2+}$  in four-fold coordination.  
834 Variations in the molar volume of lead silicate glasses correlate well with structural observations made  
835 via Raman spectroscopy (chapter 2, this volume, and Ben Kacem et al., 2017). For small amounts of lead  
836 oxide added to silica glass (<20 mole %),  $Pb$  is essentially in six-fold coordination and its introduction  
837 into silica results in the formation of non-bridging oxygens, clearly visible in the  $Q^n$  species distribution  
838 in the Raman spectra (Ben kacem et al., 2017). This is accompanied by a decrease in melt viscosity and  
839 glass transition temperature. At  $PbO$  concentrations higher than 20 mol%, a mixture of essentially two  
840 lead species, in 4- and 6-fold coordinations, exists. Kohara et al. (2010) and more recently Sampaio et al.  
841 (2018) mentioned that  $Pb$  can be distributed between 3-, 4-, 5- and 6-fold coordination but recent X-Ray  
842 diffraction shows that  $Pb$  is essentially distribute in 4- and 6-fold coordination (Drewitt et al., this issue).  
843  $Pb$  in four-fold coordination can be considered as a weak network former (Fayon et al., 1998, 1999; Feller  
844 et al., 2010; Ben Kacem et al., 2017) as  $^{[4]}Pb$  creates a network of interconnected tetragonal pyramid  
845  $PbO_4$  (Morikava et al., 1982). This is visible in Raman spectra, where an intense band at  $140 \text{ cm}^{-1}$  can be

846 assigned to Pb-O-Pb covalent bonds (see chapter 3 and Ben Kacem et al., 2017). This band at 140 cm<sup>-1</sup>  
 847 is clearly at higher frequency than that observed in alamosite, PbSiO<sub>3</sub>, at 110 cm<sup>-1</sup> and attributed to Pb in  
 848 6-fold coordination (Worrell and Henshall, 1978; Ben Kacem, 2017, Pena et al., 2017). The coexistence  
 849 of network former PbO<sub>4</sub> and network modifier PbO<sub>6</sub> entities agree with the pair correlation function  
 850 obtained from the X-ray diffraction data (see chapter 3, Figure 6B (Drewitt et al. 2021)), which show that  
 851 the proportion of PbO<sub>4</sub> increases with decreasing SiO<sub>2</sub>/PbO. The mixing of the tetragonal pyramid PbO<sub>4</sub>  
 852 with SiO<sub>4</sub> tetrahedra is probably mechanical in nature, i.e. the two polyhedra cohabit and are  
 853 interconnected but their mixture does not result in an excess of entropy as indicated by the linear  
 854 decreases of the glass transition temperature between 30 and 80% of SiO<sub>2</sub> (Figure 13). The fast decrease  
 855 in  $T_g$  upon addition of ~10 mol% PbO probably relates to the network modifier role of PbO<sub>6</sub> octahedra,  
 856 containing some NBOs in their first coordination shell.



857  
 858 **Figure 13:** Glass transition temperature as a function of the fraction of SiO<sub>2</sub> in PbO-SiO<sub>2</sub> glasses.  
 859 Data for Ca<sup>2+</sup>, Mg<sup>2+</sup>, Na<sup>+</sup>, K<sup>+</sup>, Li<sup>+</sup> silicate glasses are original data from Neuville, Ca50 and Mg50  
 860 (Neuville and Richet, 1991), Ca60 and NS1.5, NS2, NS4 from Neuville (2006), NS3 from Le Losq et al.  
 861 (2014); Sr60 from Neuville (2005) and Pb-silicate glasses open circle are from viscosity measurements  
 862 and full circle are from DSC measurements. (Ben Kacem et al., 2017). Note that all  $T_g$  are obtained  
 863 using viscosity measurements to be comparable except those obtained by Ben Kacem with DSC.

864

865 The introduction of PbO thus produces the transformation of  $Q^n$  units into  $Q^{n-1}$  units as PbO<sub>6</sub> are  
866 network modifier units. The appearance of these  $Q^{n-1}$  species is documented by changes in the high  
867 frequency envelope (800 - 1200cm<sup>-1</sup>) of the Raman spectra of the glasses (Worrell and Henshall, 1978;  
868 Ben Kacem et al., 2017). The Raman spectra of PbO-SiO<sub>2</sub> glasses corresponds to the combination of two  
869 distinct endmember Raman signals: that of a lead-silicate glass network with  $Q^{n-1}$  species, and that of an  
870 amorphous lead network characterized by a strong peak at 140 cm<sup>-1</sup>. The relative abundances of these  
871 signals, and of their associated networks, vary as a function of the SiO<sub>2</sub>/PbO ratio and this is in good  
872 agreement with observation made using <sup>17</sup>O NMR by Lee and Kim (2015). Lee and Kim (2015) also  
873 observed a small amount of free oxygen as early mention by Sampaio et al. (2018), but this small amount  
874 cannot explain the  $T_g$  and viscosity variations.

875

876 In this sense, lead is an example of an amphoteric<sup>6</sup> element that plays two different roles, network  
877 former or network modifier, depending on melt chemical composition. Another example of an element  
878 presenting such behavior is Fe<sup>3+</sup>, which, depending on its coordination, plays different structural roles  
879 (Moretti, 2005). Indeed, while Fe<sup>3+</sup> in 4- or 5-fold coordination can be considered as network formers,  
880 Fe<sup>3+</sup> in 6-fold coordination behaves as a network modifier in silicate melts. It can be found in the literature  
881 that such elements are “intermediate” and often aluminum is associated with this terminology. However,  
882 the story is more complex than this, and Al<sup>3+</sup> does not really present amphoteric behavior per se as highly  
883 coordinated Al species are not surrounded by NBOs such that <sup>[4]</sup>Al is exclusively a network former  
884 element. Its behavior is however complex, as we shall see in the sections below.

885

#### 886 2.4.2 Al in silicate glasses

887 A well-known feature of silicate mineral structures is that Si cations can be replaced isomorphously  
888 by aluminum cations, provided that either mono or divalent cations can ensure charge compensation of  
889 Al polyhedra to maintain local neutralization of electrical charges in the structure. As such, those mono  
890 or divalent cations are called charge compensators. However, it is also possible to obtain alumina-silica  
891 glasses without the presence of charge compensator cations. From a research point of view, this is very  
892 interesting because Al<sub>2</sub>O<sub>3</sub>-SiO<sub>2</sub> glasses are important materials for the understanding of how network  
893 former elements mix. Al<sub>2</sub>O<sub>3</sub>-SiO<sub>2</sub> glasses have a very high liquidus (Sossman, 1933), and are difficult to  
894 synthesize except by fast quench or sol-gel methods (e.g. see Wang et al., 2020). With those methods, it  
895 is possible to obtain Al<sub>2</sub>O<sub>3</sub>-SiO<sub>2</sub> glasses in three different regions, near 15 mol%, 50 mol% or 60 mol%

<sup>6</sup> An amphoteric element can react both as an acid or a base; see Moretti (2005) for details on this concept for silicate melts.

896 of silica. The molar volume of  $x\text{Al}_2\text{O}_3-(1-x)\text{SiO}_2$  glasses calculated from density measurement (Wang et  
897 al., 2020) varies linearly between 27.3 up to 31  $\text{cm}^3$  for 60 % of  $\text{Al}_2\text{O}_3$  (Figure 6).

898 From the data on  $\text{Al}_2\text{O}_3$  (corundum), the molar volume of Al in six-fold coordination is 25.57  $\text{cm}^3$   
899 (Robie et al., 1979). The molar volume of Al in five-fold coordination is unknown, but the extrapolation  
900 of the  $\text{Al}_2\text{O}_3$ - $\text{SiO}_2$  line in Figure 5 yields a value of  $\sim 32 \text{ cm}^3$  at 0 mol % of  $\text{SiO}_2$ . Poe et al. (1992) proposed  
901 that  $\text{Al}_2\text{SiO}_5$  glass is composed by 50% of  $^{[5]}\text{Al}$ , 40% of  $^{[4]}\text{Al}$  and 10% of  $^{[6]}\text{Al}$ .

902 However, no information on the geometry of the  $^{[5]}\text{Al}$  oxygen polyhedra is available: it could  
903 be a tetragonal pyramid, or a trigonal bi-pyramid. The present data do not allow assessment of this  
904 problem, but it is possible to make an assumption: the geometric shape of  $^{[5]}\text{Al}$  will depend on the nearest  
905 charge compensator cation. For example, the smaller the quadrupolar moment,  $Cq$ , observed in  $^{27}\text{Al}$   
906 NMR is, the more  $^{[5]}\text{Al}$  will look like a square base pyramid. The role of  $^{[4]}\text{Al}$ ,  $^{[5]}\text{Al}$  and  $^{[6]}\text{Al}$  in the glass  
907 and melt structure will be discussed later in section 3.

908

### 909 *2.5 Silicate melts: how can we use existing structural knowledge to model melt properties*

910 With the above information from the traditional glass forming ranges, we understand that we  
911 know for silicate melts and glasses:

912 - the glass has a network of  $Q_n$  units, whose concentrations can be determined via NMR or  
913 Raman spectroscopy (Farnan and Stebbins, 1990; Stebbins et al., 1992; Dupree et al., 1986; Maekawa et  
914 al., 1991; Mysen, 1990; Mysen and Frantz, 1993; 1994; Ispa et al., 2010; Zhang et al., 1996; Sen et al.,  
915 2003; Davis et al., 2010; O'Shaughnessy et al., 2020; Nesbitt et al., 2018, 2021)

916 - glass and melt heat capacities, which can be calculated, and

917 - their rheological properties.

918 It has been a longstanding goal to link those observations via a single model that could predict the  
919 properties and structure of glasses and melts. A pioneering start was the work of Mysen (1995), who  
920 proposed to calculate the melt configuration heat capacity from partial heat capacity values  $C_p^{conf}{}_{Q_n}$   
921 assigned to each  $Q^n$  unit with a fraction  $x_{Q^n}$ :

$$922 \quad C_p^{conf} = \sum x_{Q^n} C_p^{conf}{}_{Q^n}. \quad (14)$$

923 Links between melt thermodynamic parameters, rheology and structure were further established by  
924 subsequent publications (Neuvville and Mysen, 1996; Neuvville 2006; Mysen 1990, 1995, Le Losq et  
925 Neuvville, 2013, 2017, Le Losq et al., 2015, 2017; Russell and Giordano 2017). Recently, Le Losq and  
926 Neuvville (2017) demonstrated how, using the Adam and Gibbs theory and  $Q^n$  values from NMR  
927 spectroscopy, it is possible to determine with a high precision the viscosity of  $\text{Na}_2\text{O}$ - $\text{K}_2\text{O}$ - $\text{SiO}_2$  melts. In  
928 this section, we will show how such a model can be constructed, and what opportunities for extension

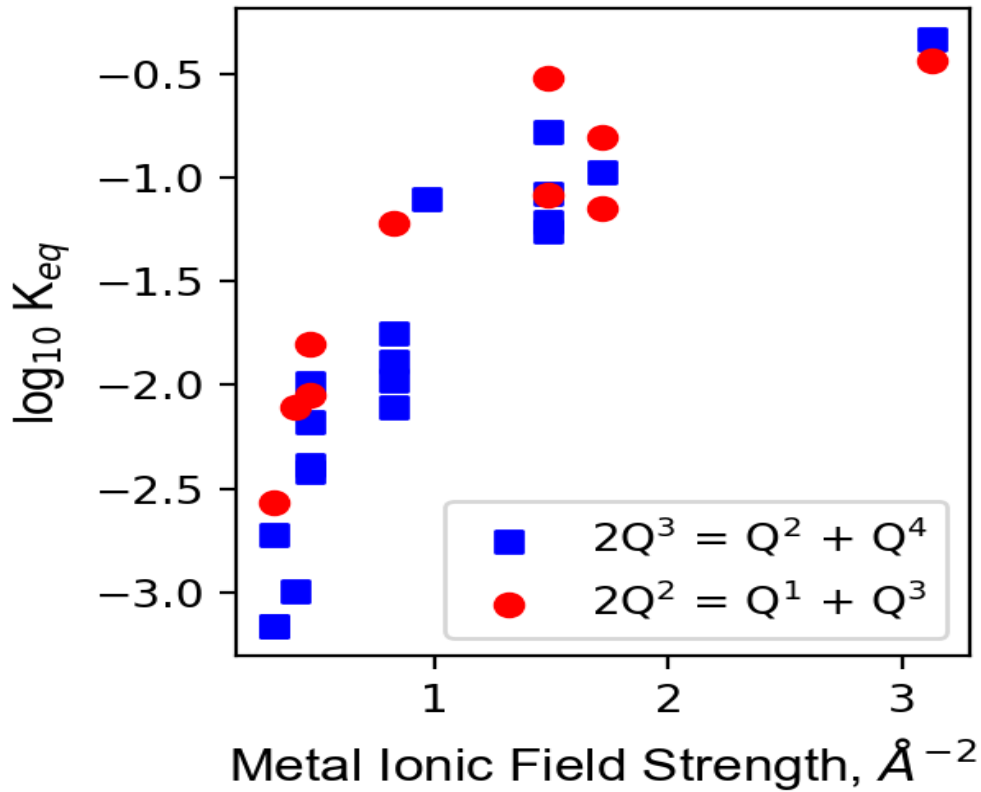
929 are envisioned. The application of such modeling for aluminosilicate melts will further be discussed in  
930 section 3.

931  
932 Using a principle similar to that of equation (14), we may be able to calculate values of  $S^{conf}(T_g)$  and  
933  $B_e$  in eqs. 6 to 9 from partial values assigned to  $Q^n$  units in the glass, i.e. in the melt at the glass transition  
934 temperature. This is possible because  $B_e$  is temperature-independent (Adam and Gibbs, 1965), and  
935  $S^{conf}(T)$  can be estimated from  $S^{conf}(T_g)$  and  $C_p^{conf}$ , which can be easily determined from viscosity data  
936 and modeled in silicate melts, respectively. This implies that we can use glass structural data to build a  
937 model for melts. However, we need to be able to model precisely how the distribution of  $Q^n$  units vary  
938 with glass composition. Fortunately, the distribution of  $Q^n$  units mostly depends on (i) the glass silica  
939 concentration, and (ii) the ionic field strength (IFS) of network modifier metal cations. Numerous  $^{29}\text{Si}$   
940 NMR spectroscopy data were acquired on silicate glasses and allow us to know precisely how  $Q^n$  units  
941 distribute depending on glass composition. They allow, in particular, determining the equilibrium  
942 constants of the  $Q^n$  dissociation reactions

$$943 \quad Q^n = Q^{n-l} + Q^{n+l}, \quad (15)$$

944 which is at play in silicate glasses and melts. This explains the deviations of the  $Q^n$  distribution  
945 measured compared to silicate minerals, where binary combinations of  $Q^n$  units are observed (e.g.  $Q^4$ -  
946  $Q^3$ ,  $Q^3$ - $Q^2$ , etc.). In glasses and melts, randomness implies that the  $Q^n$  distribution departs from the binary  
947 model. The existing  $^{29}\text{Si}$  NMR and Raman data allow one to estimate how the melt composition  
948 influences such deviation. In Figure 14, we collected  $K_{eq}$  equilibrium constants for the dissociation of  $Q^3$   
949 units and of  $Q^2$  units, and reported them as a function of the ionic field strength. In this Figure, most data  
950 are from NMR spectroscopy because data interpretation from  $^{29}\text{Si}$  NMR 1D and 2D methods (Edén,  
951 2012) is less subject to debate, despite some possible complications that highlight that the determination  
952 of  $Q^n$  unit distribution always is an arduous task (Pedone et al. 2010; Charpentier et al. 2013). Indeed,  
953 Raman data requires the use of Raman cross sections, determined by calibration against  $^{29}\text{Si}$  NMR data,  
954 to transform the area of Raman peaks assigned to different  $Q^n$  units into concentrations of those  $Q^n$  units.  
955 This is a first barrier as Raman cross-sections are not straightforward to obtain, a second one being the  
956 fit of the spectra that can be a topic of debate (Nesbitt et al., 2018, 2021; Bancroft et al., 2018). The very  
957 few  $K_{eq}$  values from Raman data used in Figure 14 do not come from possibly controversial traditional  
958 peak fitting methods, but from the use of linear alternative least square methods to retrieve partial Raman  
959 spectra for the different  $Q^n$  units in binary silicate glasses, a method developed by Zakaznova et al. (2007)  
960 and Malfait et al. (2007, 2009). While it is very powerful for binary silicate glasses, it relies on  
961 composition-specific, constant Raman signal shapes for the different  $Q^n$  units. This hypothesis is valid in  
962 binary systems, but this method is limited because (i) partial Raman spectra for one binary system (e.g.

963 Na<sub>2</sub>O-SiO<sub>2</sub>) cannot be used for others and (ii) this starting hypothesis becomes void for ternary and more  
 964 complex systems. This is because partial Raman spectra and Raman cross-sections differ depending on  
 965 the network modifier present into the glass (e.g. Malfait et al., 2009; Woelffel et al. 2015).



966 **Figure 14:** Equilibrium constants of the dissociation of Q<sup>3</sup> and Q<sup>2</sup> units represented as a function of the  
 967 metal ionic field strength. Metal IFS was calculated assuming a coordination number of 6 and ionic  
 968 radius from Whittaker and Muntus (1970). Equilibrium constants were calculated from the data of  
 969 Emerson (1989), Emerson and Bray (1994), Maekawa et al. (1991), Bray et al. (1991), Zhang et al.  
 970 (1996, 1997), Schneider et al., (2003), Voigt et al. (2005), Larson et al. (2006), Malfait et al. (2007),  
 971 Zakaznova-Herzog et al. (2007), Sen et al. (2009), Malfait et al. (2009), Davis et al. (2010) and Herzog  
 972 and Zakaznova-Herzog (2011).

973  
 974  
 975 An idea that arises when seeing Figure 14 is to parametrize the K<sub>eq</sub> values as a function of the mean  
 976 ionic field strength of metals cations in silicate glasses. Indeed, K<sub>eq</sub> values for Q<sup>3</sup> and Q<sup>2</sup> units change  
 977 systematically depending on the ionic field strengths of the metal cation in the glass structure. It thus  
 978 seems possible to calculate K<sub>eq</sub> values from the mean ionic field strengths of metal cations in the glass.  
 979 For ternary and more complex silicate glasses, this relies on the fact that mixing different cations in

980 silicate glasses affects linearly the distribution of  $Q^n$  units. Fortunately, this is a good approximation.  
 981 Indeed, from  $^{29}\text{Si}$  and  $^{23}\text{Na}$  MAS NMR spectroscopy, the  $Q^n$  unit distribution upon Rb-Na mixing in  
 982 alkali trisilicate glasses does not systematically change (Hater et al., 1989). This was also reported during  
 983 Na and Li mixing in  $(\text{Na,Li})_2\text{Si}_2\text{O}_5$  glasses (Ali et al., 1995, Sen et al., 1996). From  $^6\text{Li}$ ,  $^7\text{Li}$  and  $^{29}\text{Si}$  static  
 984 NMR spectroscopy data, Bray et al. (1991) observed a linear change of the  $Q^3$  units fraction upon mixing  
 985 Li and K in disilicate glasses. The  $^{29}\text{Si}$  static NMR data from Emerson and Bray (1994) further suggest  
 986 a slight departure from linearity of the  $Q^3$  unit fraction when mixing  $\text{Na}_2\text{Si}_2\text{O}_5$  and  $\text{Cs}_2\text{Si}_2\text{O}_5$  glasses. Such  
 987 interpretation may be consistent with  $^{17}\text{O}$  Dynamic Angle Spinning NMR data from mixed  $\text{Na}_2\text{Si}_2\text{O}_5$ -  
 988  $\text{K}_2\text{Si}_2\text{O}_5$  glasses (Florian et al., 1996), showing slightly non-linear changes of the fractions of Bridging  
 989 (BO) and Non-Bridging (NBO) oxygen anions with changes in the glasses K/ (K + Na) ratios. Such  
 990 observation agrees with the recent report of Le Losq and Neuville (2017), which showed that the Raman  
 991 areas of  $Q^n$  units in alkali trisilicate glasses vary linearly within error bars.

992

993 From the above review, it thus should be possible to calculate  $K_{eq}$  values for  $Q^3$  and  $Q^2$  unit  
 994 dissociation given the mean IFS of metal cations present in the silicate glass. However, despite a good  
 995 correlation, scattering is visible in Figure 14. Such scattering results from second order effects that may  
 996 be related to some local peculiarities of the effect of each cation on  $K_{eq}$  values as well as our lack of a  
 997 perfect understanding of the coordination number of each cation. To circumvent this problem, we propose  
 998 to calculate the mean  $K_{eq}$  values in silicate glasses based on the combination of  $K_{eq}$  values assigned to  
 999 each cations (from their calculation in the binary  $\text{M}^{x/2x}\text{O-SiO}_2$  systems):

000

$$001 \quad K_{eq} \text{ glass} = \sum K_{eq}^i x_i, \quad (16)$$

002 where  $x_i$  is the fraction of a given cation relative to the sum of all cations. Assuming linear variations  
 003 in the  $Q^n$  unit fractions upon mixing different cations, a valid hypothesis given existing data as indicated  
 004 previously, this will allow obtaining the most precise model for the variations in  $Q^n$  units in Al-free  
 005 silicate glasses (the case of aluminium deserves its own section, such that its effect will be discussed in  
 006 section 3).  $K_{eq}^i$  values determined for each system are provided in Table 1, based on the data reported in  
 007 Figure 14.

008

Metal cation	$K_{eq} \ 2Q^3 = Q^2 + Q^4$	$K_{eq} \ 2Q^2 = Q^1 + Q^3$
Li	0.09(5)	0.2(2)
Na	0.012(4)	0.06(-)



K	0.006(3)	0.012(5)
Rb	0.001(-)	?
Cs	0.001(-)	0.003(-)
Mg	0.464(-)	0.364(-)
Ca	0.106(-)	0.156(-)
Ba	0.078(-)	?

**Table 1:** mean values of the  $K_{eq}$  coefficients for the dissociation of  $Q^3$  or  $Q^2$  units in  $M^+O_2$ - $SiO_2$  or  $M^{2+}O$ - $SiO_2$  glasses, calculated from the data presented in Figure 14. Standard deviations from the mean are provided in parenthesis, when possible.

Now that we can calculate the fractions of  $Q^n$  units for various silicate compositions, it opens doors to calculate the terms of the Adam and Gibbs equation:  $B_e$  and  $S^{conf}(T_g)$ . Le Losq and Neuville (2017) leveraged such ability for  $K_2O$ - $Na_2O$ - $SiO_2$  melts with 60 to 100 mol%  $SiO_2$ , taking into account the ideal mixing of Na and K in silicate melts (Richet, 1984) when developing equations for  $S^{conf}(T_g)$  and  $B_e$ . For  $S^{conf}(T_g)$ , they assumed that, added to the topological entropy  $S^{topo}$ , excess entropies arise from the ideal Si mixing between the different  $Q^n$  units  $S^{mix}_{Si}$  and random mixing of Na and K into the glass network  $S^{mix}_{Na-K}$ , such that:

$$S^{conf}(T_g) = S^{topo} + S^{mix}_{Si} + S^{mix}_{Na-K}, \quad (17)$$

with

$$S^{topo} = \sum_{n=2}^3 x_{Q_{Naenv}^n} S_{Q_{Naenv}^n}^{conf} + \sum_{n=2}^3 x_{Q_{Kenv}^n} S_{Q_{Kenv}^n}^{conf} + x_{Q^4} S_{Q^4}^{conf}, \quad (18)$$

$$S_{Si}^{mix} = \frac{-x_{Si}}{x_O} * 2 * R * \sum_{n=2}^4 x_{Q^n} \ln(x_{Q^n}), \quad (19)$$

and

$$S_{Na-K}^{mix} = \frac{-(x_{Na} + x_K)}{x_O} * 2 * R * (X_K \ln(X_K) + (1 - X_K) * \ln(1 - X_K)), \quad (20)$$

with  $x_{Si}$ ,  $x_O$ ,  $x_{Na}$  and  $x_K$  the atomic fractions of Si, O, Na and K respectively,  $X_K = K/(K+Na)$ ,  $R$  the gas constant, and  $x_{Q^n}$  the  $Q^n$  fractions. We note that, as Le Losq and Neuville (2017) investigated melts with NBO/T lower than 1.5, equations above were limited to  $Q^2$  to  $Q^4$  units. In addition, in the topological contribution (equation 18),  $Q_{Naenv}^n$  and  $Q_{Kenv}^n$  units with their associated  $S_{Q_{Naenv}^n}^{conf}$  and  $S_{Q_{Kenv}^n}^{conf}$  values are distinguished; those are the  $Q^n$  units, with  $n < 4$ , that have NBO bonded preferentially to Na or K, respectively. This is an approximation introduced to take into account the fact that  $Q^n$  units with NBO

033 bonded to Na or K may present different  $S^{conf}$  values, as shown by the difference of  $S^{conf}(T_g)$  between  
 034 sodic and potassic silicate glasses.

035

036 For the calculation of  $B_e$ , the link between  $S^{conf}(T)$  and  $B_e$  needs to be considered. Indeed,

$$037 \quad B_e = \frac{\Delta\mu s_c}{k_B}, \quad (21)$$

038 and

$$039 \quad S^{conf}(T_g) = \frac{N_A}{z (T_g)} s_c, \quad (22)$$

040 with  $\Delta\mu$  the Gibbs free-energy barrier opposed to the cooperative rearrangements of molecular  
 041 subunits of size  $z$  ( $T_g$ ) and intrinsic entropy  $s_c$ ,  $k_B$  the Boltzmann constant and  $N_A$  the Avogadro  
 042 constant (Adam and Gibbs, 1965; Richet, 1984).  $s_c$  represents the entropy of the molecular subunits  
 043 involved in the melt viscous flow and relaxation process. It appears in both eqs. (21) and (22), yielding  
 044 a strong correlation between  $S^{conf}(T_g)$  and  $B_e$  (Neuville and Richet, 1991). From eqs. (20) and (22), we  
 045 can write

$$046 \quad B_e = \frac{\Delta\mu z (T_g) S^{conf}(T_g)}{R}, \quad (23)$$

047 with  $R$  the perfect gas constant ( $=N_A k_B$ ). From eq. (23) and considering that  $\Delta\mu$  and  $s_c$  are  
 048 temperature-independent (Richet, 1984),  $B_e$  should be expressed similarly to  $S^{conf}(T_g)$ , from the melt  
 049 structure recorded at  $T_g$  in glasses. Considering that, Le Losq and Neuville (2017) assumed that  $B_e$  can  
 050 be expressed as the sum of partial molar  $B_e$  terms for the different  $Q_{Menv}^n$  and  $Q^4$  units, with additional  
 051 non-linear contributions arising from the role of  $S^{conf}(T_g)$  in eq. (23). The latter non-linear contributions  
 052 are obtained by directly injecting eqs. (19) and (20) with  $K_1$  and  $K_2$  scaling terms in the expression of  $B_e$ :

$$053 \quad B_e = \sum_{n=2}^3 x_{Q_{Naenv}^n} B_{e_{Q_{Naenv}^n}} + \sum_{n=2}^3 x_{Q_{Kenv}^n} B_{e_{Q_{Kenv}^n}} + x_{Q^4} B_{e_{Q^4}} + K_1 S_{Si}^{mix} + K_2 S_{Na-K}^{mix} \quad (24)$$

054

055 Using this model, Le Losq and Neuville (2017) showed that it is possible to calculate the viscosity of  
 056 the alkali silicate melt with a mean square error of 0.2 log Pa·s. This error is much lower than those of  
 057 parametric models, typical presenting root mean squared errors on their parametrization datasets of ~ 0.6-  
 058 0.7 log Pa·s (e.g. Hui and Zhang, 2017; Giordano et al., 2008).

059

060 Le Losq and Neuville (2017) used cubic splines for interpolation of the  $Q^n$  distribution in their model.  
 061 With the approach presented in this chapter, it is possible to replace this by the  $K_{eq}$ -based model for  $Q^n$   
 062 distribution in silicate melts in order to improve the future deployment and development of such a  
 063 thermodynamic viscosity model. Preliminary tests yield good predictions with standard errors of 0.3 log

064 Pa·s, a value slightly higher than the initial value of 0.2 log Pa·s from Le Losq and Neuville (2017). This  
065 difference arises from the fact that the initial cubic spline modeling of the  $Q^n$  distribution in  $K_2O-Na_2O-$   
066  $SiO_2$  melts is slightly more accurate than the global structural model based on the  $K_{eq}$  values calculations.  
067 Differences are in the range of 1-2%. This actually highlights how sensitive a model can be to melt  
068 structure: an error of only 1-2 % alters measurable the accuracy of the model.

### 070 3. Aluminosilicate glasses and melts

071 Aluminum is a key element in Earth and material sciences because it is present, in various amounts,  
072 in most geologic and industrial glasses, and it drastically affects their properties. Generally, a well-known  
073 feature of the structure of silicate minerals is that silicon ions may be replaced isomorphously by  
074 aluminum ions provided that either mono or divalent cations are available to maintain local neutralization  
075 of electrical charges in the structure (Putnis, 1992). This feature is clearly visible in tectosilicates that  
076 present an interconnected three-dimensional silica-like tetrahedral structure, in which the mono or  
077 divalent cations are accommodated in the framework free volumes. In these minerals, the ratio  
078  $R=M^+_2O/Al_2O_3$  or  $M^{2+}O/Al_2O_3$  is unity. The metal cations play charge compensator roles, and no non-  
079 bridging oxygens are present. This is also generally the case in tectosilicate glasses, albeit some possible  
080 minor amounts of NBOs may be present (Stebbins and Xu, 1997). However, an additional complexity in  
081 aluminosilicate glass is the variable coordination number of Al. Indeed, while Al mostly substitutes for  
082 Si in the  $SiO_4$  tetrahedra in silicate glass, it also is found in five and six-fold coordinations, in proportions  
083 that depend on melt chemical composition, system pressure and temperature, and glass-forming cooling  
084 rate (Ohtani et al., 1985; Risbud et al., 1987; Murdoch et al., 1985; Mc Millan, et al., 1982; Merzbacher  
085 et al., 1990, 1991; Lacy, 1963; Merzbacher and White, 1991; Coté et al., 1992, Stebbins and Xu, 1997,  
086 Sato et al., 1991; Allward and Stebbins, 2005a,b, 2007, Allwardt, et al., 2004; 2007; Stebbins et al., 2000,  
087 2008; Stebbins, 2008; Henderson et al., 2007; Lee 2005, Lee and Stebbins, 2000, 2002, 2009; Neuville  
088 et al., 2004ab, 2006, 2008a,b, 2010; Le Losq et al., 2014). The varying coordination number of Al raises  
089 the question of its role in the melt structure depending on its coordination. Indeed, following the  
090 terminology proposed by Zachariassen (1932), while Al in four-fold coordination is a network former, Al  
091 in six-fold coordination should be a network modifier, and Al in five-fold coordination should probably  
092 also be considered as a network modifier. We will review such questions, and more generally the  
093 connection between aluminosilicate melt structure and properties in this section.

#### 095 3.1 Molar volume, coordination number and structure

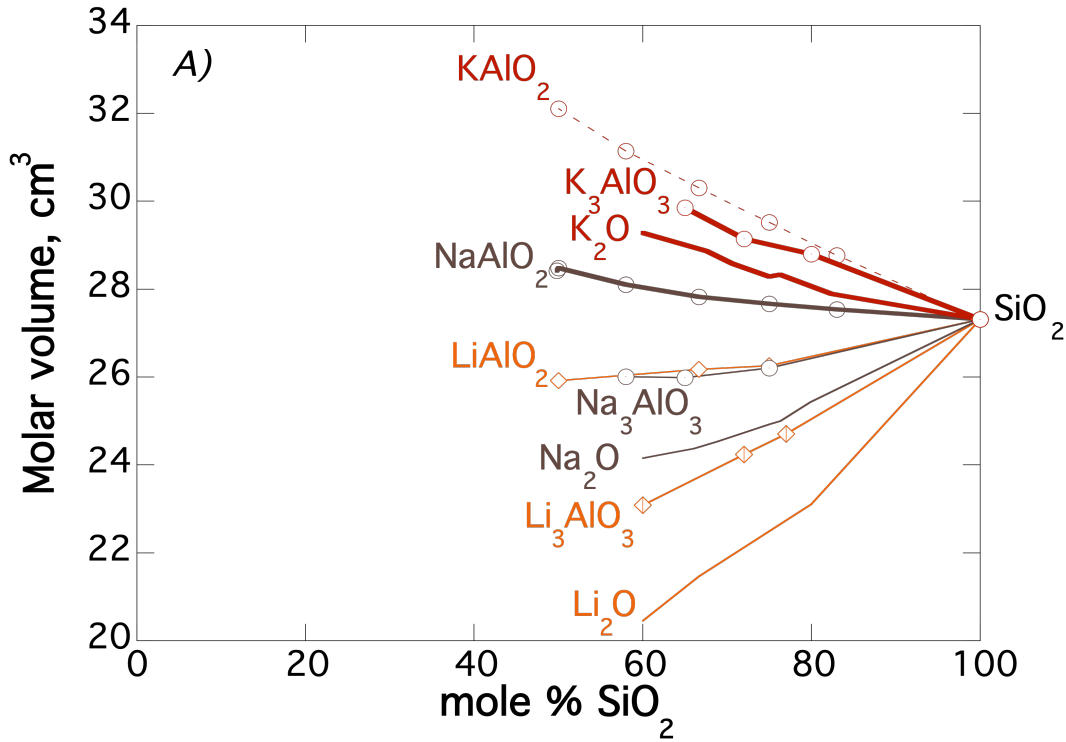
096 Density and molar volume are properties easy to measure in glasses, and bring important pieces of  
097 information regarding their internal structure, and by extension, that of the melt at the glass transition.

098 Variations in the molar volumes of alkali and alkaline-earth silicate and aluminosilicate glasses as a  
099 function of silica concentration show similar trends, except for the heaviest elements, like potassium,  
100 cesium and rubidium (Figure 15). From silica glass with  $V_m=27,31\text{cm}^3$ , it is found that generally the  
101 molar volume decreases with the decrease in  $\text{SiO}_2$ , except for K-, Cs-, Rb- silicate glasses. For the same  
102  $\text{SiO}_2$  content, the magnitude of the decrease of the molar volume depends on the ionic field strength of  
103 the metal cation: it is moderate for  $\text{Na}^+$  and very important for  $\text{Mg}^{2+}$  (for example  $V_m$  of Ca silicate  
104  $=21,21\text{cm}^3$  and  $24,14\text{cm}^3$  for Na-silicate, both at 60 mol % of  $\text{SiO}_2$  – note that we compare Ca and Na  
105 silicate glass and not Mg-silicate at 60 of silica, because this glass is made with a high cooling rate, and  
106 its fictive temperature is probably very different than that for the Na-silicate glass). In the case of  
107 potassium,  $V_m$  always increases regardless of the glass aluminum content. For other cations,  $V_m$  variations  
108 in aluminosilicate glasses are more complex. First, the  $\text{M}^{2+}/\text{Al}$  or  $\text{M}^+/\text{Al}$  ratio directly influences the  
109 variations of  $V_m$  with the glass silica concentration. Secondly, a general concave trend of the  $V_m$  versus  
110  $\text{SiO}_2$  relationship is observed according to previous work (Seifert et al., 1982, Doweidar et al., 1999,  
111 Doweidar 1999). Taking the  $\text{SiO}_2$ - $\text{CaAl}_2\text{O}_4$  binary mixture as an example, and starting from silica,  $V_m$   
112 decreases with silica decrease until 50 mol%  $\text{SiO}_2$  ( $V_m=25,81\text{cm}^3$  for anorthite glass), and then increases  
113 up to a value of  $\sim 27\text{cm}^3$  for the pure  $\text{CaAl}_2\text{O}_4$  end-member for example. Such non-linear  $V_m$  trends  
114 indicate that  $V_m$  modelling in aluminosilicate glasses cannot be obtained from a linear combination of  
115 partial  $V_m$  values assigned to the different oxides. To circumvent this problem, several papers have  
116 modelled the density of glass and melts as a function of their expected  $Q^n$  speciation (Doweidar, 1999,  
117 Doweidar et al., 1999) or other entities like partial volume of oxide components (Lange, 1996, 1997,  
118 Bottinga and Weill, 1970).

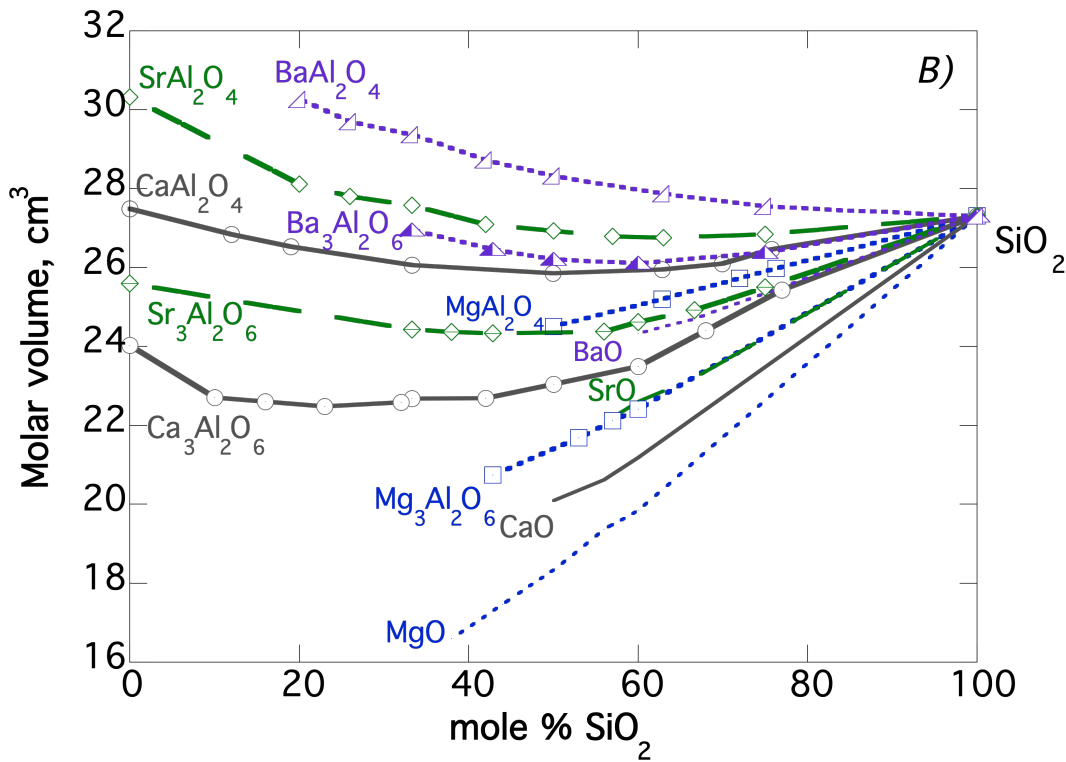
119 One of the most important pieces of information arising from  $V_m$  data analysis is the possibility to  
120 provide knowledge regarding the coordination numbers of metal cations as well as aluminum. We have  
121 mentioned, in section 2.1 (Figure 5), that metal cations' CNs remain almost constant in silicate glasses.  
122 It is also well known that the molar volume of the  $\text{SiO}_4^{4-}$  tetrahedra doesn't change a lot as a function of  
123 the  $Q^n$  species because the  $d(\text{Si-BO})$  or  $d(\text{Si-NBO})$  vary less than  $0.05\text{\AA}$  (Cormack and Du, 2001; Du and  
124 Cormack 2004). This variation corresponds to a variation of around 3% on the distance between Si-BO  
125 and Si-NBO which causes a variation of the volume of the tetrahedra between 12.4 and 9.3% as a function  
126 of the amount of alkali content respectively 10 and 50%, if we used the distances given by Cormack and  
127 collaborators. In the case of aluminum, the molar volume of  $\text{AlO}_4^{5-}$  tetrahedra doesn't change because  
128 Al-O distances stay almost constant as a function of the different  $Q^n$  species for  $\text{Al}^7$ , and the most  
129 important change in the molar volume of Al units come from the change in the coordination of Al and

<sup>7</sup> The distance Al-O increases from 1.76 up to 1.86  $\text{\AA}$  when the coordination number of Al changes from 4 to 6 (Cormier et al., 2000, 2003, Hennet et al., 2016). This implies that Al-O distance vary smaller when Al change of  $Q^n$  species in tetrahedra.

130 not of the  $Q^n$  species of Al. If we consider that the volumes vary very slightly in the ternary diagrams this  
 131 implies that the molar volume variation observed between silicates and aluminosilicates glasses is  
 132 produced essentially by changes in coordination number of alkaline or alkaline-earth. Before discussing  
 133 this, we will quantify the different proportions of aluminum.



134



135

136

137 **Figure 15:** A) molar volume for alkali and B) for alkaline-earth silicate and Al-silicate glasses, data  
138 for NAS, KAS compositions (Le Losq et al. 2017, 2015, Neuvill, 1991, 2006), LAS (Strukelj, 2008), MAS,  
139 CAS system (Neuvill, 1992), SAS data from Novikov et al., (2017), BAS original data and from Novikov  
140 (2017).

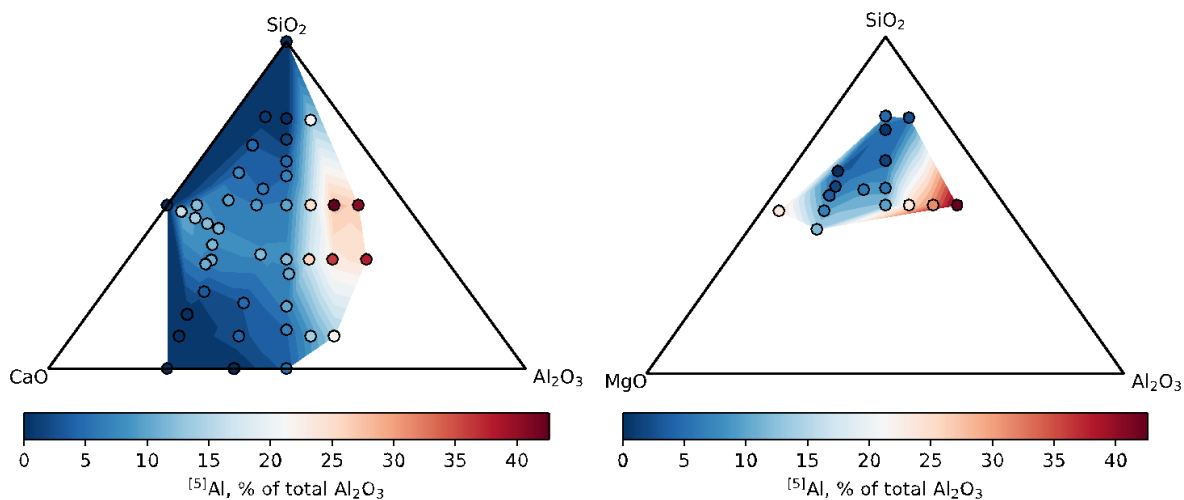
### 143 3.2 Proportion of Al in five-fold coordination

144 Given the role of Al coordination on  $V_m$  and other melt/glass properties, it is clear that Al coordination  
145 should be quantified. Fortunately, through  $^{27}\text{Al}$  NMR spectroscopy, several studies allow drawing a  
146 picture of Al coordination variations with composition, temperature and pressure.

147 The presence of  $^{[5]}\text{Al}$  is systematically observed in the middle of the ternary diagrams of Li  
148 aluminosilicate, and alkaline-earths aluminosilicate, including peralkaline glasses in which Al in five-  
149 fold coordination is not expected considering the stoichiometry (Neuvill et al., 2006, 2007, 2008b,  
150 2010). Moreover, the proportion of  $^{[5]}\text{Al}$  is always maximum for glasses with about 50 mol % of  $\text{SiO}_2$   
151 (Neuvill et al, 2004, 2006, 2008, Novikov et al., 2017). On the contrary, Na or K tectosilicate and  
152 peraluminous glasses have small concentrations of Al in five-fold coordination, which becomes  
153 undetectable in peralkaline compositions (Stebbins and Farnan, 1992; Allwardt et al., 2005a,b; Lee et al.  
154 2009; Le Losq et al., 2014). The variation of NMR chemical shift values for  $^{[5]}\text{Al}$  and  $^{[6]}\text{Al}$  sites with  
155  $\text{SiO}_2$  content are less dependent on silica content than  $^{[4]}\text{Al}$  sites (Figure 13b, from the previous chapter).  
156 The NMR chemical shift values are directly related to the inter-tetrahedral angle or the first-neighbor  
157 cations (Stebbins and Farnan, 1992). This can imply that  $^{[5]}\text{Al}$  and  $^{[6]}\text{Al}$  sites are more connected with Al  
158 in four fold coordination than with Si in different  $Q^n$  species which does not respect the Lowenstein  
159 rule's, but in the majority of studies this rule is avoided (Neuvill et al., 2008a, 2010, Lee and Stebbins,  
160 2009, Hiet et al., 2009). 2D NMR  $^{27}\text{Al}$ - $^{29}\text{Si}$  correlations (Lee and Stebbins, 2009, Hiet et al., 2009) show  
161 that  $^{[5]}\text{Al}$  is more connected with Si than with Al in lanthanum aluminosilicate glasses (Florian et al.,  
162 2007). Highly coordinate Al species, especially  $^{[5]}\text{Al}$ , are likely to have a positive formation enthalpy and  
163 their abundance in the melt is expected to increase with increasing temperature as observed by some  
164 authors (Neuvill et al., 2008b; Stebbins, 2008). However, the  $^{27}\text{Al}$  NMR spectra at high temperature  
165 shifts to lower  $^{27}\text{Al}$  chemical shift values with increasing temperature, this can be interpret as resulting  
166 from the appearance of  $^{[5]}\text{Al}$  and  $^{[6]}\text{Al}$  contributions located at lower chemical shifts than that of  $^{[4]}\text{Al}$   
167 (Kanehashi and Stebbins, 2007, Thompson and Stebbins, 2011, 2012, 2013). Signatures of Al in high  
168 coordination are also clearly visible using X-ray absorption spectroscopy at the Al K-edge (Neuvill et  
169 al., 2008b). In the case of CA50.25 (anorthite melts composition), Neuvill et al (2008b) show an increase  
170 from 8% up to 22% of  $^{[5]}\text{Al}$  between room temperature and 1900 K, in good agreement with high

171 temperature Al NMR (Stebbins, 2008). A significantly higher proportion of  $^{[5]}Al$  is observed in  
 172 magnesium aluminosilicate glasses than in the others aluminosilicate systems on the tectosilicate join  
 173 (Neuvillle et al., 2008b, Novikov et al., 2017, Figure 23B) which can be explained by the promotion of  
 174 highly coordinated Al species with the presence of metal cations with relatively high ionic field strength,  
 175 as shown in boroaluminate by Bunker et al., (1991) and in La-aluminosilicate glass compositions (Florian  
 176 et al. 2007). Such an idea agrees with the increase in the disorder when the cation field strength decreases  
 177 (Mysen et al., 1982; Murdoch et al., 1985; Sharma et al, 1985; Navrotsky et al., 1982, 1985; Lee and  
 178 Stebbins 2000, 2002, Neuvillle et al. 2008a, Wu and Stebbins, 2009; Lee et al., 2016, Le Losq et al.,  
 179 2017).

180  
 181 Several papers on  $^{27}Al$  NMR spectroscopy have shown that, for  $R = M/Al$  varying between infinity  
 182 and 1 (silicate to tectosilicate compositions), Al is essentially in four-fold coordination (Risbud et al.,  
 183 1987, Murdoch et al., 1985; Merzbacher et al., 1990, 1991; Merzbacher and White, 1991; Coté et al.,  
 184 1992, Stebbins and Xu, 1997, Stebbins et al., 2000, 2008; Neuvillle et al., 2004ab, 2006, 2007, 2008a,  
 185 McMillan and Kirkpatrick, 1992; Massiot et al., 2008; Lee and Stebbins, 2009, 2016; Richet et al.,  
 186 2009a; Le Losq et al., 2014; Novikov et al., 2017; Florian et al., 2018, Charpentier et al., 2018). In the  
 187 CAS system, 93 % of Al is in 4-fold coordination, and the proportion of  $^{[5]}Al$  increases slowly up to 7%  
 188 for the anorthite glass composition on the tectosilicate join (Neuvillle, et al., 2006). In the MAS system,  
 189 the proportion of  $^{[5]}Al$  is a little higher, 12% for Mg-anorthite glass (Neuvillle et al., 2008a). For all others  
 190  $M^+$  or  $M^{2+}$  Al-silicate systems, the proportion of  $^{[5]}Al$  is lower and the amounts decrease with increasing  
 191  $z/r$  ( $z$  : cation charge and  $r$  atomic radius, see Neuvillle et al., 2008a or Stebbins et al., 2008, Novikov et  
 192 al., 2017). Figure 16 A and B show the total amount of  $^{[5]}Al$  in mol % in the CAS and MAS system.



193  
 194 **Figure 16:** Percentage of  $^{[5]}Al$  of total Al<sub>2</sub>O<sub>3</sub> in the CAS (left) and MAS (right) systems. Data from  
 195 Neuvillle et al. (2004, 2006, 2007, 2008b, 2010, Massiot et al., 2008; Licheron et al., 2011).

196

### 197 3.3 Molar volume, $AlO_4^{4-}$ and implications for the coordination number of metal cations

198 In the previous sections, we saw that the molar volume of Si in the different  $Q^n$  species can vary by  
199 less than 10% when  $n$  varies from 4 to 0 and that the molar volume of Al stays almost constant for Al in  
200 four-fold tetrahedra. Despite this, the molar volume  $V_m$  of a lime aluminosilicate glass with 50% of  $SiO_2$   
201 (wollastonite to anorthite glasses) can vary from 20 to 25.9  $cm^3$  between the wollastonite and anorthite  
202 compositions, this represents an increase of 25 %. This increase is 12 % between silicate glasses and the  
203 glasses on the  $R = 3$  join, and of 12 % again between the join  $R = 3$  and the join  $R = 1$  with  $R = MO/Al_2O_3$   
204 with  $M = Mg, Ca$ . This huge increases of  $V_m$  is a maximum at 50 mol % silica.

205 In the case of calcium aluminate glasses, the molar volume difference between C3A ( $Ca_3Al_2O_6$ ) and  
206 CA ( $CaAl_2O_4$ ) glasses is only 6.8 % (Figure 15B). In Figure 15B, the increase of molar volume between  
207 join  $R=3$  and 1 can also result from a change in the coordination number of calcium because the aluminum  
208 stays in four-fold coordination between C3A and CA glasses. In this case, Ca varies between regular  
209 octahedra where Ca is in 6-fold coordination to a distorted site in 7-8-fold coordination (Cormier et al.,  
210 2001, 2003, Neuvillle et al., 2008b, 2010, Cicconi et al., 2016; Drewitt et al., 2012, 2017, Jakse et al.,  
211 2012; Takahashi et al., 2015; Hennet et al., 2016).

212

213 Generally, the coordination number of alkali or alkaline-earth elements is difficult to determine, but  
214 changes in the  $V_m$  of a glass can inform us about CN changes. For instance, the above variation in the  
215 CN of Ca is in good agreement with the changes observed via XANES at the Ca  $K$ -edge in Ca  
216 aluminosilicate glasses (Neuvillle et al., 2004b, 2008, Cormier and Neuvillle, 2004; Cicconi et al., 2016).  
217 In particular, Cicconi et al. (2016) observed a shift to greater energy and a decrease in intensity of the  
218 pre-edge in the XANES spectra at the Ca  $K$ -edge between wollastonite to anorthite glasses. This shift  
219 can also be correlated with the new peak  $\omega_2$  observed in the depolarized Raman spectra, VH, (see Figure  
220 13, chapter 3 this volume, Drewitt et al., 2021). The peak  $\omega_2$  decreases when  $R$  goes from infinity to 1  
221 (to silicate to tectosilicate glasses)

222

223 In the case of the NAS system ( $Na_2O-Al_2O_3-SiO_2$ ), the peak  $\omega_2$  is also clearly visible for silicate  
224 glasses in the VH Raman spectra and it disappears for  $R = Na_2O/Al_2O_3 = 1$  (Hehlen and Neuvillle, 2015).  
225 This peak  $\omega_2$  exists in all silicate glasses with  $M^+ = Na, K$  and  $M^{2+} = Mg, Ca, Sr, Ba$  (Hehlen and Neuvillle,  
226 2015, 2020) and its intensity decreases when Al replaces  $M^+$  or  $M^{2+}$ . In the NAS glass system, a shift is  
227 also observed in the chemical shift,  $\delta$ , of  $^{23}Na$  NMR between NS3 and albite glass (Le Losq et al., 2015)  
228 following a trend that can be correlated with variations in XANES at the Na  $K$ -edge between the NS3  
229 and albite glasses (Neuvillle et al., 2004).



230

231 In the case of the SAS (SrO-Al<sub>2</sub>O<sub>3</sub>-SiO<sub>2</sub>) system, Novikov et al. (2017) also observed some change in  
232 the first XANES oscillation which can also be attributed to a change in CN of strontium.

233

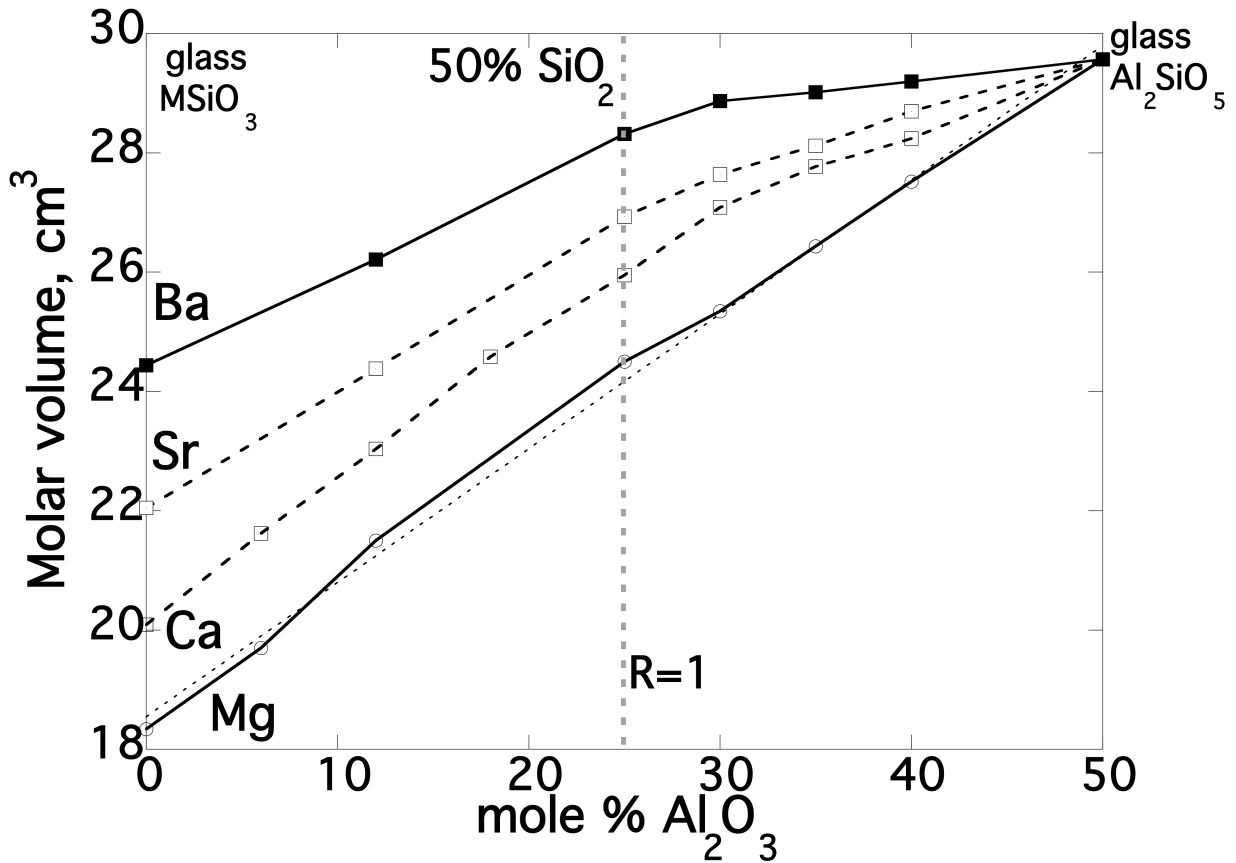
234 To summarize, <sup>23</sup>Na NMR, XANES at the Na, Sr, Ca K-edge, and depolarized Raman spectra, (VH),  
235 all show changes that can be correlated with an observed increase in the molar volume between silicate  
236 and tectosilicate glasses.  $V_m$  varies between 4% and 16% with changing the M<sup>+</sup>/Al or M<sup>2+</sup>/Al ratio at a  
237 given silica content and depends clearly on the metal cation size. The  $V_m$  changes can be assigned to  
238 changes in the coordination of metal cations as their role in the aluminosilicate network varies with the  
239 M/Al ratio. Similarly, features observed in NMR, XANES or Raman spectroscopies can be directly  
240 correlated with such change in the role of alkali or alkaline-earth elements between network modifier and  
241 charge compensator. The concept of network modifier and charge compensator was introduced by  
242 Zachariazen but never really demonstrated. Now, with the technical evolution of spectroscopy methods,  
243 but with measuring the molar volume determined from density measurements, it is possible to have an  
244 idea of the role alkaline elements.

245

246 In Figure 17, the molar volume of various glasses is shown as a function of mole percent of Al<sub>2</sub>O<sub>3</sub> at  
247 constant silica. The glass compositions vary between MSiO<sub>3</sub> up to Al<sub>2</sub>SiO<sub>5</sub>, M=Mg, Ca, Sr, Ba. Four  
248 trends are clearly visible for the four alkaline-earth aluminosilicate glass families. In the case of MgSiO<sub>3</sub>-  
249 Al<sub>2</sub>SiO<sub>3</sub>, the molar volume varies almost linearly with Al<sub>2</sub>O<sub>3</sub> (the linear variation corresponds to the  
250 dashed line). This can imply:

- 251 - i) that the coordination number of Mg is almost constant in this system and is not really affected by  
252 the Mg/Al substitution, an idea in good agreement with XANES at the Mg K-edge (Trcera et al., 2009);  
253 -ii) that the molar volume depends on the proportion of Al in five-fold coordination.

254



255

256 *Figure 17: molar volume at constant  $\text{SiO}_2 = 50 \text{ mol}\%$  for four alkaline-earth aluminosilicate glass*  
 257 *compositions. (The dashed line between  $\text{MgSiO}_3$  and  $\text{Al}_2\text{SiO}_5$  glasses correspond to this equation*  
 258  *$18.547 + 0.22497 * \text{Al}_2\text{O}_3$ ). Values are calculated from density measurements from Neuville (1992) for Ca*  
 259 *and Mg system peralkaline compositions, Neuville et al. (2006, 2008) for Ca and Mg Per-aluminate*  
 260 *compositions, Novikov et al. (2017) for Sr compositions, Novikov (2017) for Ba compositions and  $\text{Al}_2\text{SiO}_5$*   
 261 *are from Wang et al. (2020).*

262

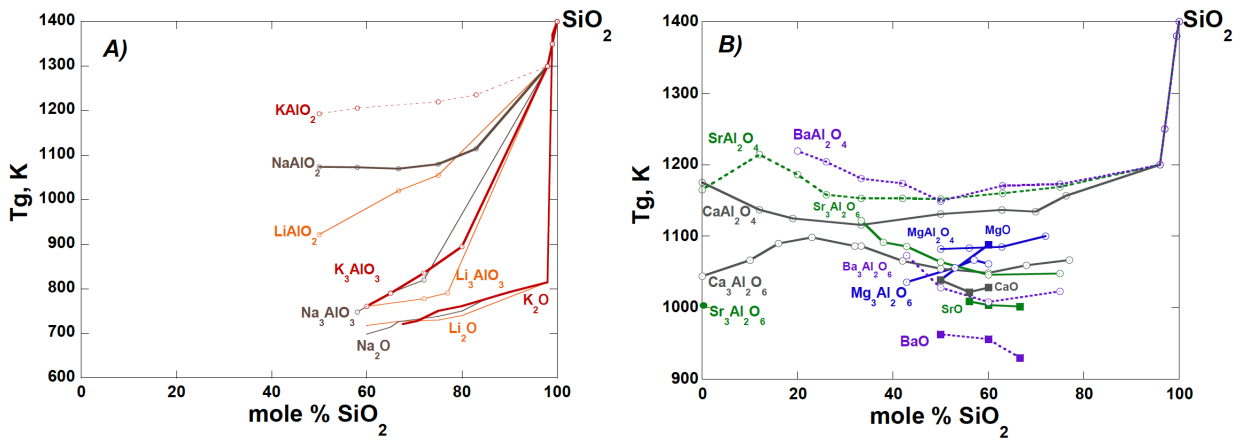
263 For the Ca, Sr and Ba aluminosilicate glasses the changes observed in the slopes near 25 mol % of  
 264  $\text{Al}_2\text{O}_3$  correspond to the tectosilicate line ( $R = M^{2+}O / \text{Al}_2\text{O}_3 = 1$ ), characterized by an increase in the  
 265 proportion of  $^{[5]}\text{Al}$  in the glass (Neuville et al., 2006, 2008, Novikov et al., 2017, Novikov 2017). This  
 266 Figure clearly shows two domains, one where  $V_m$  is affected by aluminum, the peraluminous domains,  
 267 and one where  $V_m$  depends on an increase in the coordination of the alkaline-earth element, the peralkaline  
 268 domain (Cicconi et al., 2016; Novikov et al., 2017).

269

### 270 3.3 Glass transition temperature

271 In general, a decrease in  $T_g$  occurs with decreasing  $\text{SiO}_2$  content at all  $R$  ratios ( $R = M^{2+}O_2 / \text{Al}_2\text{O}_3$  or  
 272  $M^{2+}O / \text{Al}_2\text{O}_3$ ) (Figure 18). It is particularly important at silica contents between 100 and  $\sim 75 \text{ mol}\%$ . In

273 detail, this  $T_g$  decrease is more significant in Al-free silicate melts than in tectosilicate glasses; the lower  
 274  $R$ , the lower the effect of changing  $\text{SiO}_2$  on  $T_g$ . Typically, at  $R=1$  in tectosilicate compositions, the  
 275 decrease in  $T_g$  is of  $\sim 300$  K for  $\text{MAl}_2\text{Si}_2\text{O}_8$  glasses, and 200 K and 300 K for respectively  $\text{KAlSiO}_4$  and  
 276  $\text{NaAlSiO}_4$  glasses. The large contrast between  $T_g$  variations in Al-free silicate and tectosilicate glass  
 277 compositions results from the changing role of metal cations upon aluminum addition into the melt  
 278 network. Indeed, while in silicate glasses, alkali and alkaline-earth elements are network modifiers that  
 279 break the 3D tetrahedral network, in aluminosilicate glasses they ensure the charge compensation of  
 280  $\text{AlO}_4^-$  tetrahedral units and thus participate in increasing melt polymerization. This translates to higher  
 281  $T_g$  along the  $\text{M}^+\text{AlO}_2\text{-SiO}_2$  or  $\text{M}^{2+}\text{Al}_2\text{O}_4\text{-SiO}_2$  binaries than along the  $\text{M}^+\text{O}_2\text{-SiO}_2$  or  $\text{M}^{2+}\text{O-SiO}_2$  binaries.



282  
283

284 *Figure 18: Glass transition temperature  $T_g$ , in K, of silicate and aluminosilicate glasses with alkali*  
 285 *elements (A) and alkaline-earth elements (B). The glass transition temperatures were determined from*  
 286 *viscosity measurements, i.e. they correspond to the temperature at which  $\log \eta = 12$  Pas. Data from*  
 287 *Neuville (1991) for Li, K silicates; Neuville (2006) and Le Losq et al. (2014) for sodic systems, (Neuville,*  
 288 *1992) for Ca and Mg, Novikov et al. (2017) for Sr and Novikov (2017) for Ba.*

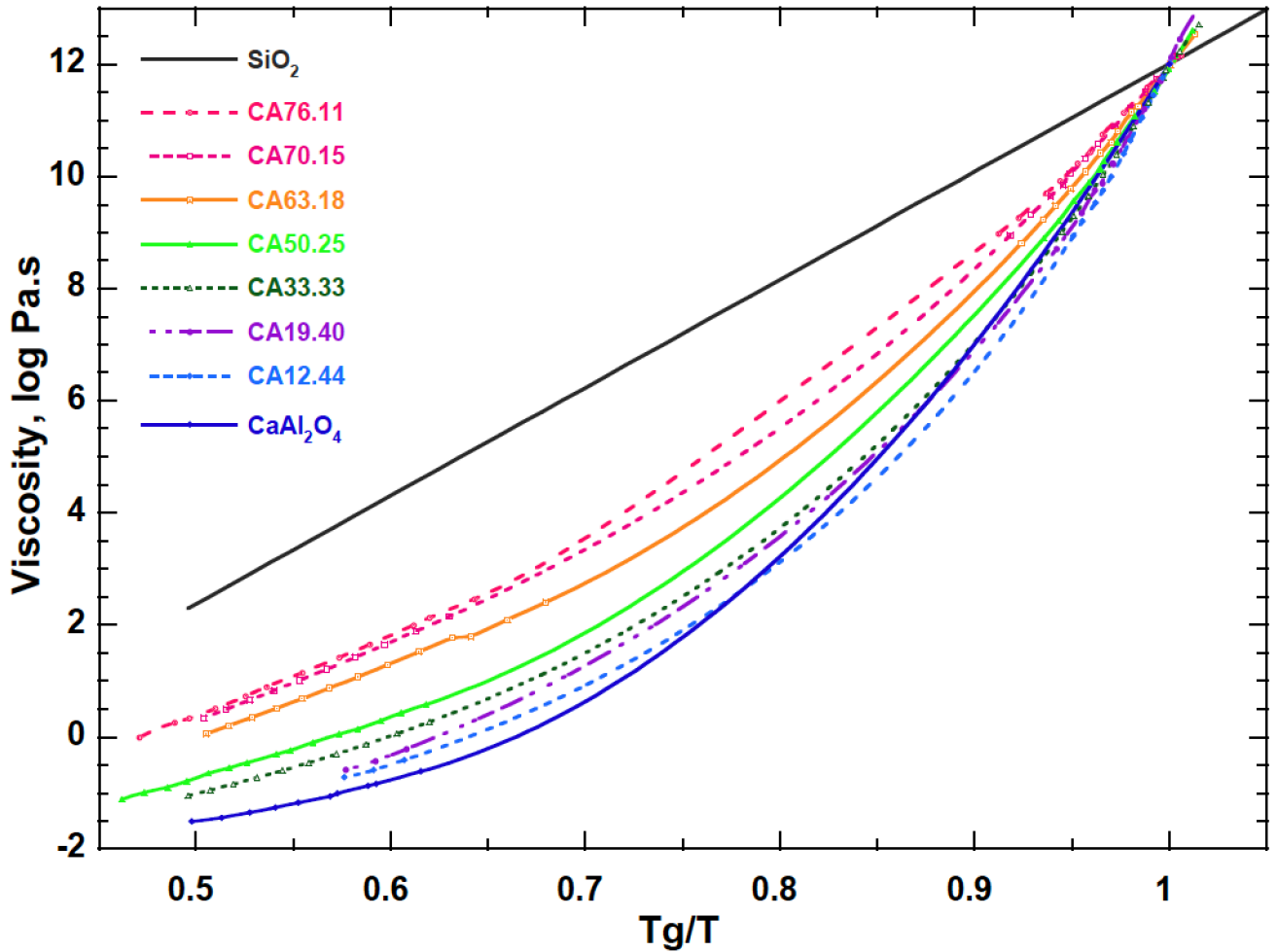
289

### 290 3.4 Link between structure and properties of aluminosilicate melts: example of the $\text{CaO-Al}_2\text{O}_3\text{-SiO}_2$ 291 system

292 To discuss and illustrate the links between glass structure and glass/melt properties, the  $\text{CaO-Al}_2\text{O}_3\text{-SiO}_2$   
 293  $\text{SiO}_2$  (CAS) glass system will be taken as an example in the following. The CAS system has the advantage  
 294 having the largest glass forming domain (Neuville et al., 2006). The observations and interpretations  
 295 made in this system can be extended to other ternary system. In general, in the CAS system, an important  
 296 decrease in  $T_g$  is observed with decreasing  $\text{SiO}_2$  content, which results from network depolymerization,  
 297 except at  $R = 1$ . In the latter case, melt polymerization is almost constant and the decrease in  $T_g$  results  
 298 from the formation of weaker Si-O-Al bonds as Al substitutes for Si in  $Q^4$  units (Navrotsky et al., 1985;

299 [Neuvville et al., 2004](#), [Cormier et al., 2001, 2005](#), [Hennet et al., 2016](#)).  $T_g$  varies by about four hundred  
300 degrees between pure  $\text{SiO}_2$  ( $T_g \sim 1480$  K; [Richet and Bottinga 1984](#)) and the center of the ternary system  
301 ( $T_g = 1115$  K for  $\text{CA}33.33$ ,  $\text{M}^{2+}\text{AX.Y}$  where  $\text{M}^{2+}$ =alkaline-earth element and  $\text{A}=\text{Al}_2\text{O}_3$ ,  $\text{X} = \text{SiO}_2\%$  i.e.  
302 33.3 mol%,  $\text{Y} = \%\text{Al}_2\text{O}_3$  and  $\text{M}^{2+}\text{O}=(100-(\text{X}+\text{Y}))$  in this case,  $\text{CaO}=33.3\%$ ). At  $R=1$ , glasses with less  
303 than 30 mol%  $\text{SiO}_2$  display a continuous increase in  $T_g$  upon decreasing  $\text{SiO}_2$  content, and  $T_g$  reaches a  
304 new local maximum for the  $\text{CaAl}_2\text{O}_4$  composition at 1175 K; the minimum in  $T_g$  at  $R=1$  is centered  
305 between 40 and 50 mol%  $\text{SiO}_2$ . The observed behavior in  $T_g$  at  $R = 1$  results from the competition between  
306 Si and Al as network formers. As indicated by the difficulty of forming glasses at high Al concentrations  
307 (e.g. along the  $\text{SiO}_2$ - $\text{Al}_2\text{O}_3$  binary) as well as a lowering of  $T_g$  with addition of Al. Al can be considered  
308 as a relatively poor network former compared to Si. This is further corroborated by variations in the melt  
309 fragility (i.e. the derivative of the melt viscosity as a function of T at  $T_g$ ): the strongest existing melt is  
310  $\text{SiO}_2$ , and Al-rich melts have higher fragility, with the most fragile being  $\text{CaAl}_2\text{O}_4$  in the CAS system  
311 (Figure 19). This is also in good agreement with the variation of the  $C_p^{conf}$  of  $\text{SiO}_2$  and  $\text{CaAl}_2\text{O}_4$ , which  
312 varies between 8.2 to 13.8 J/mol K. This  $\Delta C_p$  between liquid and glass at  $T_g$  can be expressed in term of  
313  $C_{pl}/C_{pg}$  ratio as proposed by [Angel \(1991\)](#). This ratio varies between 1.1 for  $\text{SiO}_2$ , the strongest melt to  
314 1.37 for  $\text{CaAl}_2\text{O}_4$ , the more fragile melt in Figure 19.

315

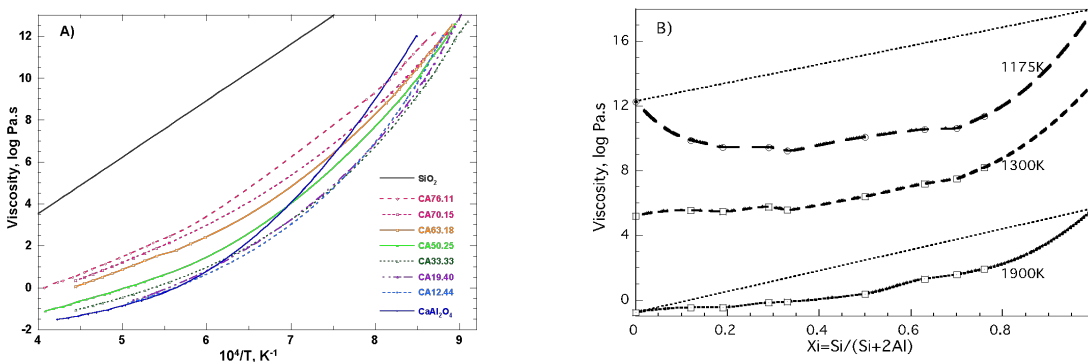


316  
317 *Figure 19: “Angel plot” showing  $\log \eta$  versus  $T_g/T$  for melts with  $R=CaO/Al_2O_3=1$  in the CAS system.*

318  
319 As mentioned previously, the CAS system presents one of the largest glass-forming domains. Indeed,  
320 it is possible to quench glasses even without silica, e.g. like the C12A7 composition (CXAY with C=CaO,  
321 A=Al<sub>2</sub>O<sub>3</sub>, X and Y are their relative proportions), using classic quench rates. With increasing quench  
322 rates, e.g. via laser levitation heating, it is possible to make glasses between C3A and CA1.5 (from 75  
323 down to 40 mol% CaO). In this condition, the addition of a small amount of SiO<sub>2</sub> in CaO-Al<sub>2</sub>O<sub>3</sub> glasses  
324 extends the glass forming ability and lowers the melt liquidus temperature. Other macroscopic properties  
325 are also markedly changed with silica introduction in CaO-Al<sub>2</sub>O<sub>3</sub> melts/glasses, suggesting extensive  
326 structural modifications. For instance, an anomalous behavior of  $T_g$  is clearly observed at low silica  
327 content, with a maximum in  $T_g$  visible at ~20 mol% SiO<sub>2</sub> along the Ca<sub>3</sub>Al<sub>2</sub>O<sub>6</sub>-SiO<sub>2</sub> binary (Figure 18B;  
328 Higby et al., 1990; Neuville 1992; Neuville et al., 2004; Cormier et al., 2005; Neuville et al., 2010). Note  
329 that this anomalous behavior of  $T_g$  results from the change in the polymerization of Al which varies  
330 between  $Q^2$  to  $Q^4$  species along the join  $R=3$  between C3A and CA20.40 glasses (Neuville et al., 2004,  
331 Cormier et al., 2001, 2003, 2005).

332  
 333  
 334  
 335  
 336  
 337  
 338  
 339  
 340  
 341  
 342  
 343  
 344  
 345

To explore further the properties of CAS glass compositions, viscosity along the join R=1 (CaAl<sub>2</sub>O<sub>4</sub> – SiO<sub>2</sub> binary) is plotted in Figure 20. At high temperatures, viscosity decreases constantly with addition of CaAl<sub>2</sub>O<sub>4</sub> (Figure 20B). At supercooled temperatures, near  $T_g$ , melt viscosity decreases by ~ 7 orders of magnitude with adding 30 mol% CaAl<sub>2</sub>O<sub>4</sub> to silica, then a further addition of 30 mol% CaAl<sub>2</sub>O<sub>4</sub> yields a decrease in viscosity of 1 order of magnitude. Between 40 and 0 mol% SiO<sub>2</sub>, melt viscosity increases ~ 5 orders of magnitude. The deviation from a linear variation (Figure 20B) is 4 orders of magnitude at 1175 K, and less than 2 orders of magnitude at 1900 K. It thus decreases with increasing temperature. These changes thus deviate strongly and negatively from a linear variation, particularly at undercooled conditions. Such behavior may originate from mixing between Si and Al in  $Q^4$  units that occurs in such tectosilicate melts (Seifert et al., 1982), this mixing resulting in excess entropy and leading to non-linear, convex variation of the melt viscosity as a function of the  $Si/(Si+Al)$  ratio (e.g., Neuvillle and Mysen, 1996).



346  
 347  
 348  
 349  
 350

Figure 20: A) Viscosity of melts between silica and CaAl<sub>2</sub>O<sub>4</sub> compositions, CAX.Y mean: X=SiO<sub>2</sub> %, Y=Al<sub>2</sub>O<sub>3</sub>, CaO=100-(X+Y). B) viscosity at constant temperature, 1150, 1200, 1800 K as a function of  $Xi=Si/(Si+2Al)$ . SiO<sub>2</sub> data are from Hetherington et al. (1964) Leko, (1979) and Urbain et al. (1982), CaAl<sub>2</sub>O<sub>4</sub> from Urbain (1983), Neuvillle (1992).

351  
 352  
 353  
 354  
 355

In all others glass systems, alkali or alkaline-earth aluminosilicate, viscosity shows similar behavior along the join  $R=1$ , an important decrease between 100 and 70% of SiO<sub>2</sub>, and for lower silica content, a smaller decrease of the viscosity (Alkaline see Le Losq et al., 2017, Mg, Neuvillle 1992, Sr, Novikov et al 2017, Ba, Novikov 2017).

356  
 357  
 358

As already mentioned, the configurational heat capacity,  $Cp^{conf}$ , is required in order to determine the configurational entropy,  $S^{conf}(T)$ , from equations (6) and (7). In the CaO-Al<sub>2</sub>O<sub>3</sub>-SiO<sub>2</sub> system, the

359 configurational heat capacity can be determined from the difference between the heat capacity of the melt  
 360 at T and that of the glass at  $T_g$  (equation 8). Several models exist, like those of Richet (1987) and Richet  
 361 and Bottinga (1985), and allow one to calculate the configurational heat capacity with precision. The  
 362 more recent works of Courtial (1993) and Richet and Neuville (1992) allow refining the heat capacity  
 363 modelling in the CaO-Al<sub>2</sub>O<sub>3</sub>-SiO<sub>2</sub> system, with using the following partial molar heat capacity equations  
 364 (J mol<sup>-1</sup> K<sup>-1</sup>) for the glass and liquid (the estimated uncertainties is about 1% for the partial molar heat  
 365 capacities following Courtial and Richet, 1993):

$$366 \quad C_{pg \text{ SiO}_2} = 127.2 - 0.010777T - 431270/T^2 - 1463.9/T^{0.5}, \quad (25)$$

$$367 \quad C_{pg \text{ Al}_2\text{O}_3} = 175.46 - 0.005839T - 1347000/T^2 - 1370/T^{0.5}, \quad (26)$$

$$368 \quad C_{pg \text{ CaO}} = 39.159 + 0.01865T - 152300/T^2, \quad (27)$$

$$369 \quad C_{pl \text{ SiO}_2} = 81.37, \quad (28)$$

$$370 \quad C_{pl \text{ Al}_2\text{O}_3} = 85.78 - 130.216T, \quad (29)$$

$$371 \quad C_{pl \text{ CaO}} = 86.05. \quad (30)$$

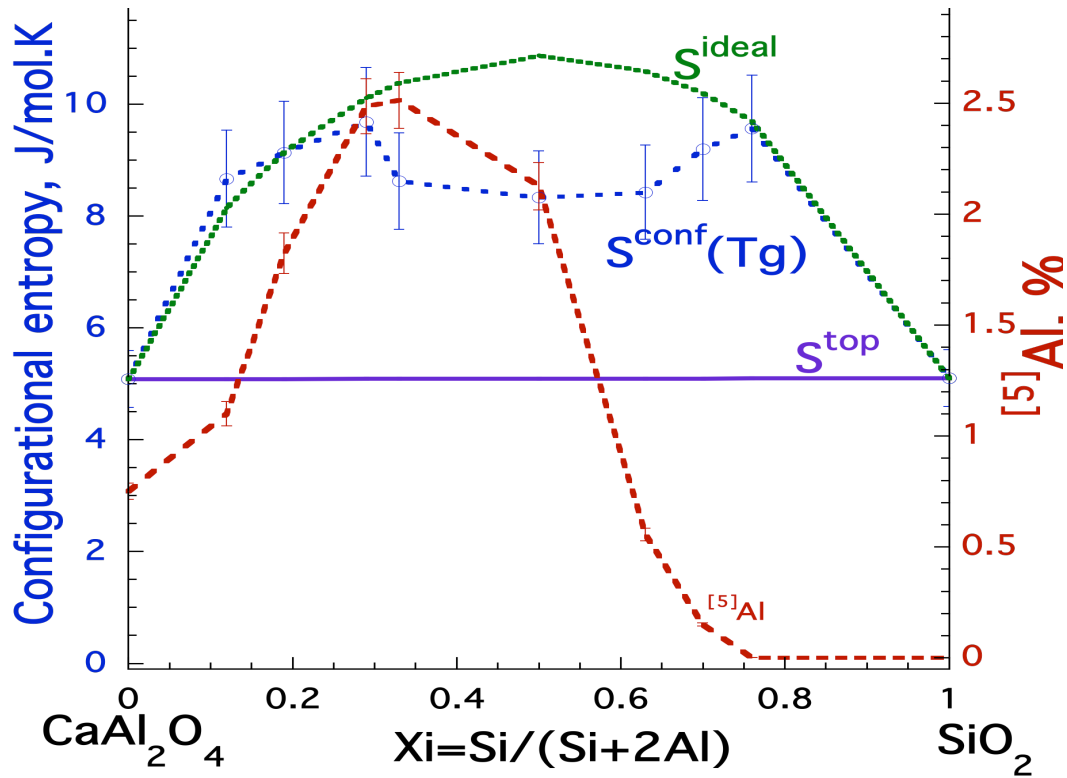
372

373 With these partial molar heat capacity terms,  $C_p^{conf}(T_g)$  can be calculated easily and used for the  
 374 calculation of  $S^{conf}(T_g)$ , which are plotted in Figure 21. It is clearly visible that  $S^{conf}(T_g)$  of silica glass is  
 375 almost the same than that of CaAl<sub>2</sub>O<sub>4</sub>, CA glass. Assuming that  $S^{conf}(T_g)$  can be decomposed into  
 376 topological and excess terms, we can model the observed variations as

$$377 \quad S^{topo} = X_{\text{SiO}_2} S^{conf}(T_g)_{\text{SiO}_2} + (1 - X_{\text{SiO}_2}) S^{conf}(T_g)_{\text{CaAl}_2\text{O}_4}, \quad (31)$$

378  $S^{topo}$  is thus assumed to vary linearly between the two end-members SiO<sub>2</sub> and CaAl<sub>2</sub>O<sub>4</sub> glasses. This  
 379 term  $S^{topo}$ , is independent of temperature and corresponds to a simple mechanical mixing between two  
 380 entities. The term  $S^{ideal}$ , defined in equation 10, can be taken as equal to the entropy obtained from an  
 381 ideal random mixing of two species, in this case Si and Al. At high or low concentration of silica,  $S^{conf}(T_g)$   
 382 variations seem to follow the ones predicted assuming such an ideal mixing between Si and Al. This  
 383 suggests that CaAl<sub>2</sub>O<sub>4</sub> randomly replace Si<sub>2</sub>O<sub>4</sub> in the melt/glass structure. However, between 33 and 75  
 384 percent of silica,  $S^{conf}(T_g)$  variations depart from the predictions of this ideal mixing model. In this silica  
 385 concentration range, a decrease of ~25 % in  $S^{conf}(T_g)$  is observed, and there is a maximum difference of  
 386 ~2.5 J mol<sup>-1</sup> K<sup>-1</sup> between  $S^{conf}(T_g)$  values and the ideal model at around 50 mol% SiO<sub>2</sub> (Figure 21).

387



388

389 *Figure 21: Configurational entropy at the glass transition temperature,  $S^{conf}(T_g)$  (Neuville, 1992), and*  
 390 *real proportion of  $^{[5]}Al$  in mole percent in glasses along the  $SiO_2$ - $CaAl_2O_4$  binary (Neuville et al., 2004,*  
 391 *2004). Each  $S^{conf}(T_g)$  value was calculated from the viscosity data obtained for each composition.*

392

393 The observed  $S^{conf}(T_g)$  variations (Figure 21) suggest that :

394

-i) at low or high silica concentrations, Si and  $^{[4]}Al$  mix almost randomly in the melt/glass structure,

395

-ii) a deviation from ideal mixing exists at intermediate silica contents. The latter deviation can be

396

rationalized upon considering that Al in five-fold coordination represents around 2,5 % of total Al in the

397

CA50.25 glass.

398

Excess  $^{[5]}Al$  tends to decrease  $S^{conf}(T_g)$  and in parallel increase the glass transition temperature, as  
 399 shown by Le Losq et al. (2014) in the  $Na_2O$ - $Al_2O_3$ - $SiO_2$  system. A similar effect is potentially observed  
 400 here, with the presence of  $^{[5]}Al$  possibly producing a decrease in  $S^{conf}(T_g)$  and also an increase in  $T_g$   
 401 because  $^{[5]}Al$  and  $^{[4]}Si$  do not interact and do not mix randomly. One should be careful with extrapolating  
 402 such behavior because it is only valid close to the glass transition. Indeed, at high temperatures (close or  
 403 above the liquidus), Neuville et al (2008b) proposed that  $^{[5]}Al$  plays a role similar to  $^{[5]}Si$ , a transient  
 404 species ensuring the exchange of O atoms during viscous flow according to Stebbins (1991). Similarly,  
 405 in polymerized aluminosilicate networks, we can infer that five-fold coordinated network formers (Si or  
 406 Al) ensure cationic mobility at high temperature. In depolymerized networks,  $Q^1$ ,  $Q^2$  and  $Q^3$  units ensure

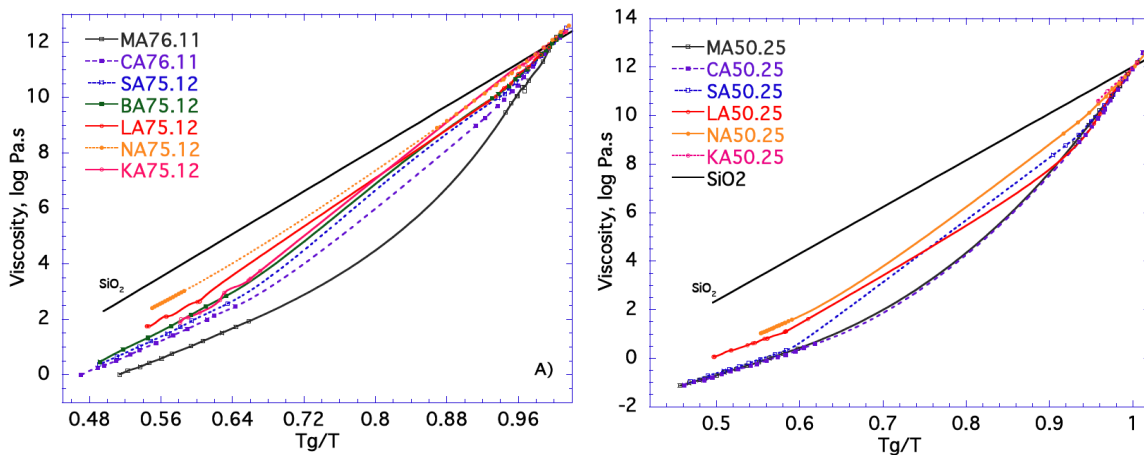


407 network mobility (Stebbins, 1991; Farnan and Stebbins, 1990, 1994; Neuville et al., 2008b, Le Losq et  
 408 al., 2014). Such assumptions agree well with the data near the C3A domain (see section 4). From Figure  
 409 21, it is further possible to make the assumption that  $^{51}\text{Al}$  plays a different role in silica-rich or alumina-  
 410 rich glasses and melts. Indeed, in silica-rich networks ( $>60$  mol%  $\text{SiO}_2$ ),  $^{51}\text{Al}$  increases network  
 411 connectivity and this results in a decrease in  $S^{conf}(T_g)$ . In an aluminate-rich network, a few percent of  $^{51}\text{Al}$   
 412 plays a role similar to  $^{41}\text{Al}$ , which exchanges randomly with Si.

413  
 414 Other systems show behaviors along the tectosilicate join similar to that previously presented for  
 415  $\text{CaAl}_2\text{O}_4\text{-Si}_2\text{O}_4$ . In particular, Raman spectra along all tectosilicate joints in the LAS, NAS, KAS, MAS,  
 416 SAS, BAS systems show similar variations. They all present a linear decrease in the frequency of the  
 417 bands assigned to T-O symmetric and asymmetric stretching of  $Q^4$  units with decreasing  $\text{SiO}_2$   
 418 concentration. This correlates very well with increasing  $^{27}\text{Al}$  NMR chemical shifts with decreasing silica  
 419 content in tectosilicate glasses (see Figure 12 previous chapter, Drewitt et al., 2021). Those Raman and  
 420 NMR variations arise from the variation of the T-O distance between Si-O and Al-O, as the Si-O distance  
 421 is shorter than the Al-O distance.

422  
 423 In the Figure 22, the viscosities of tectosilicate melts with 75 and 50 mol % silica are plotted as a  
 424 function of  $T_g/T$ . The strongest glass in the Angell plot corresponds to the  $\text{SiO}_2$  composition, and the  
 425 more fragile the composition, the greater the curvature. The fragility of melts decreases from Mg, Ca, Sr  
 426 to Ba for the alkaline-earth elements. Alkali tectosilicate compositions show similar fragilities at 50 mol  
 427 % silica (Figure 22B). At 75 mol % (Figure 22A), Li and K tectosilicate compositions also present a  
 428 similar fragility while the Na-tectosilicate composition is the strongest one.

429

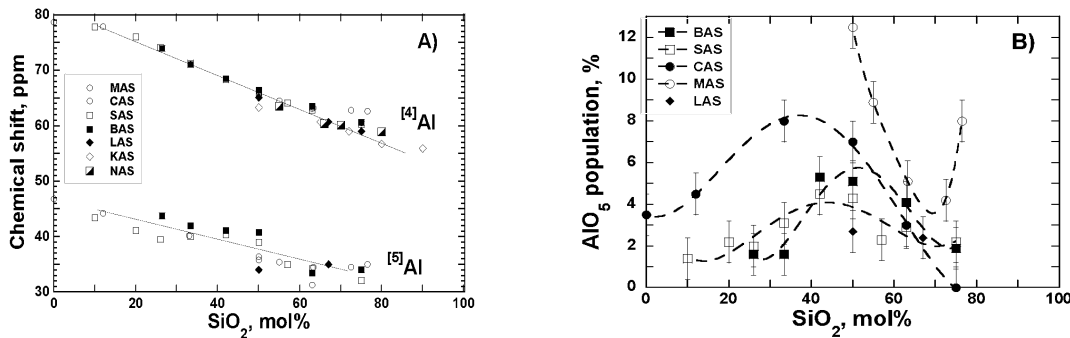


430  
 431 *Figure 22: Viscosity of MAX.Y melts versus  $T_g/T$ , with  $M = \text{Li}_2, \text{Na}_2, \text{K}_2, \text{Mg}, \text{Ca}, \text{Sr}, \text{Ba}$ .  $X = \text{SiO}_2$ ,*  
 432  *$Y = \text{Al}_2\text{O}_3$ , and  $\text{MO} = 100 - (\text{SiO}_2 + \text{Al}_2\text{O}_3)$  in mole%, A) for 75 mole % of  $\text{SiO}_2$ , and B for 50 mole % of*

433  $\text{SiO}_2$ . (data are from *Le Losq, 2012 for LAS, Le Losq et al., 2017, for NAS and KAS, Neuville 1991 for*  
 434 *CAS and MAS, Novikov et al.2017, for SAS, and Novikov, 2018 for BAS).*

435  
 436 *3.5 From the CAS system to other chemical systems*

437 For tectosilicate glasses and melts, the structure seems to present a random distribution and random  
 438 substitution between  $\text{SiO}_4^{4-}$  and  $\text{AlO}_4^{5-}$  units, in violation of the Loewenstein's aluminum avoidance  
 439 principle (*Loewenstein, 1954*). The Si/Al substitution is clearly confirmed by the linear variation of the  
 440 chemical shift of the  $^{27}\text{Al}$  NMR and of the frequency of the Raman band in the  $800 - 1200\text{cm}^{-1}$  domain.  
 441 We can propose that alkali or alkaline-earth elements are in the free-volumes of the  $\text{Al}_x\text{-Si}_{(1-x)}\text{O}_2$  network,  
 442 ensuring the charge compensation of  $\text{AlO}_4^{5-}$  units. The Figure 23 shows the proportion of  $^{[5]}\text{Al}$  in  
 443 tectosilicate glasses versus  $\text{SiO}_2$  content. The proportion of  $^{[5]}\text{Al}$  is a maximum in the middle of the  
 444 ternary system, in the peraluminous domain for all ternary systems MAS (with  $\text{S}=\text{SiO}_2$ ,  $\text{A}=\text{Al}_2\text{O}_3$ ,  
 445  $\text{M}=\text{Li}_2\text{O}$ ,  $\text{Na}_2\text{O}$ ,  $\text{K}_2\text{O}$ ,  $\text{MgO}$ ,  $\text{CaO}$ ,  $\text{SrO}$ ,  $\text{BaO}$ ), and increases with the decrease of  $z/r^2$  (*Lee and Stebbins,*  
 446 *1999, 2000, Allward et al, 2003, 2007, Stebbins, 2008, 2016; Stebbins and Farnan, 1992; Stebbins et al.,*  
 447 *1999; Neuville et al., 2004, 2006, 2008, 2010, Le Losq et al., 2017, Lee et al., 2016; Novikov et al., 2017,*  
 448 *Stebbins et al., 2008, Lee et al., 2009, Hiet et al., 2009, Alu et al., 2018*). In the NAS and KAS system,  
 449  $^{[5]}\text{Al}$  is not detected in tectosilicate compositions, and it is only present in peraluminous domain  
 450 (*Allwardt, et al., 2003; Le Losq et al., 2014*).



451  
 452 *Figure 23: A) NMR chemical shift of  $^{[4]}\text{Al}$  and  $^{[5]}\text{Al}$  and B) proportion of  $^{[5]}\text{Al}$  in LAS, MAS, CAS,*  
 453 *SAS, BAS system along the join  $R=1$ , the tectosilicate join (note that there is not  $^{[5]}\text{Al}$  in Na and K*  
 454 *tectosilicate glasses). Data from *Le Losq (2012), Neuville et al., (2008, 2006), Novikov et al., (2017),*  
 455 *Novikov, (2017). Error bar are smaller than symbol size.**

456  
 457 In tectosilicate glasses, the NMR chemical shifts of  $^{[5]}\text{Al}$  and  $^{[4]}\text{Al}$  decrease linearly with the silica  
 458 content (*Figure 23A*), due to an increase in the mean T-O-T inter-tetrahedral angle as Al substitutes for  
 459 Si in tetrahedral units (*Stebbins and Farnan, 1992; Neuville et al., 2006, 2008*). At a given silica content,

460 small variations in the  $^{27}\text{Al}$  NMR chemical shift are observed, and correlate with the electronegativity  
461 and size of the first-neighbor metal cations in the glass structure. These variations arise from small  
462 changes in the Si/Al distribution and in the mean inter-tetrahedral T-O-T angle as the metal cation field  
463 strength and property changes.

464  
465 In peralkaline glasses, the degree of polymerization plays a small role on the  $^{41}\text{Al}$  environment. Mysen  
466 et al. (2003) showed that, in sodium aluminosilicates, Al remains mostly in  $Q^4$  units. Using Raman and  
467 viscosity data, Le Losq et al. (2014) corroborated such a view for this system. Other studies suggest that  
468 this remains true probably in most aluminosilicate compositions at silica contents higher than 40 mol%  
469 (Neuvill et al., 2004b, 2008, Novikov et al., 2017); a strong preference of  $^{41}\text{Al}$  for the most polymerized  
470 structural units is expected according to experimental (Mysen et al., 1981; Cormier et al., 2000; 2005,  
471 Neuvill et al., 2004b, 2008, Novikov et al., 2017) and numerical studies (Cormier et al., 2003, Cormier  
472 2019).

### 474 *3.6 Alkaline-earth mixing in aluminosilicate glasses and melts*

475 The substitution of one alkaline-earth element by another has little affect on glass Raman spectra  
476 (Merzbacher and White, 1991, Neuvill et al. 2008b). The Si/Al substitution actually has a greater  
477 influence on the aluminosilicate network than the alkaline-earth element substitution (see also chapter 3,  
478 this volume). In the case of Ca-Mg aluminosilicates, this agrees with an ideal mixing of Ca and Mg in  
479 aluminosilicates as inferred from macroscopic viscosity measurements (Neuvill and Richet, 1991). This  
480 random distribution was confirmed by  $^{17}\text{O}$  NMR data, which show that NBOs, are equally associated  
481 with Mg or Ca cations (Farnan and Stebbins, 1990, 1994; Allwardt and Stebbins, 2004). However, the  
482 network is more perturbed by the presence of Mg than by Ca because of the higher ionic field strength  
483 of Mg (Navrotsky et al., 1982; Roy and Navrotsky, 1985) and the Ca/Mg coordination number should  
484 play an important role. The coordination number of Mg is well characterized (Kroeker and Stebbins,  
485 2000, Trcera et al. 2009, Fiske and Stebbins, 1994): it is 4 in silicate glasses, and increases up to 5-6 in  
486 aluminosilicate glasses, in agreement with glass molar volumes variations (Figure 15). Turning to Ca, in  
487 silicate glasses it is mainly located in distorted sites with 6-7 oxygen neighbors (Cormier et al., 2003,  
488 Neuvill et al., 2004b, 2008, Cicconi et al., 2016). Its CN increases with substitution by Al as shown by  
489 the variation of the molar volume between  $\text{CaSiO}_3$  and  $\text{Al}_2\text{SiO}_5$  glasses (Figure 17). At high  $\text{Al}_2\text{O}_3$   
490 content ( $R \geq 1$ ), in Ca/Mg aluminosilicate glasses, Ca is in 7-8 fold coordination (Shimoda et al., 2007a)  
491 whereas Mg is in 6-fold coordination (Shimoda et al., 2007b, Trcera et al. 2009), as corroborated by data  
492 like molar volume, X-ray diffraction spectra, XANES spectra at the Ca and Mg *K*-edge, and  $^{43}\text{Ca}$  and  
493  $^{25}\text{Mg}$  NMR experiments (Kroeker and Stebbins, 2000, Trcera et al. 2009, Fiske and Stebbins, 1994).

494 The above discussion raises a paradox: Ca and Mg always have different coordination numbers but  
495 seem to mix randomly in silicate and aluminosilicate melts and glasses. First, this may highlight the  
496 difficulty determining alkali or alkaline-earth environments that are loosely held in large sites with fairly  
497 irregular coordination (Cormier and Neuvill, 2004, Neuvill et al., 2008). Nevertheless, there is a  
498 general consensus for lower coordination for Mg than Ca. The low Mg coordination number and the  
499 possibility to have MgO<sub>4</sub> tetrahedra in Mg-silicate glass suggest that Mg will not be available for charge  
500 compensation of Al in tetrahedral position. Alternatively, its small size favors its localization in network  
501 tetrahedral cavities, yielding important distortions of the aluminosilicate network to accommodate such  
502 Mg coordination, which could result in the formation of highly-coordinated Al. This interpretation might  
503 justify the modifier role played by Mg despite their low coordination (Shimoda et al., 2007b, Guignard  
504 and Cormier, 2008, Trcera et al. 2009), in agreement with recent NMR data suggesting that substitution  
505 of Na by Mg in aluminosilicates in glass promotes melt depolymerisation (Sreenivasan et al. 2020).  
506 Similar observations can be made regarding the role of Zn in silicate or aluminosilicate glasses (Novikov,  
507 2017). The fact that the viscosities of the Mg or Zn glass compositions are lower than that of Ca glass  
508 compositions for the same amount of SiO<sub>2</sub>, confirms the role of network modifier of Mg and Zn while  
509 they are preferably in 4-fold coordination. (Neuvill, 1992; Neuvill and Richet, 1991; Toplis and  
510 Dingwell, 2004, Neuvill et al., 2008).

511  
512 In mixed CMAS glasses, Raman, NMR and neutron diffraction data (Allwardt and Stebbins, 2004,  
513 Allwardt et al., 2003, Lee et al., 2003, Lee and Stebbins, 2003; Neuvill et al., 2006, 2008, Guignard and  
514 Cormier, 2008; Cormier and Coello, 2013, Cormier 2019) are in good agreement with random mixing  
515 between Ca and Mg in the melt structure, as initially proposed by Neuvill and Richet (1991). This  
516 implies that intermediate CMAS melts can be considered as being derived from the random mixing of  
517 their CAS and MAS end-members, e.g. Ca<sub>3</sub>Al<sub>2</sub>Si<sub>3</sub>O<sub>12</sub> - Mg<sub>3</sub>Al<sub>2</sub>Si<sub>3</sub>O<sub>12</sub> for garnet-like glasses and  
518 CaAlSi<sub>2</sub>O<sub>8</sub> - MgAlSi<sub>2</sub>O<sub>8</sub> for anorthite-like compositions. An interesting observation is that Ca/Mg mixing  
519 shows a random distribution and the network polymerization is not really affected by the Ca/Mg  
520 substitution, but the proportion of <sup>51</sup>Al increases with the Ca/Mg substitution (Neuvill et al., 2008b).

521  
522

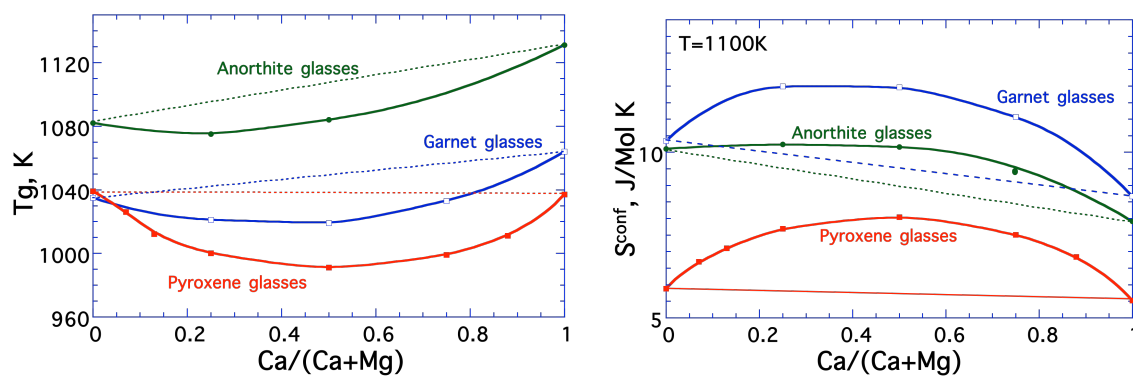


Figure 24: A) glass transition temperature and B) configurational entropy at 1100 K upon Ca/Mg mixing in pyroxene ( $\text{CaSiO}_3\text{-MgSiO}_3$ ), garnet ( $\text{Ca}_3\text{Al}_2\text{Si}_3\text{O}_{12}\text{-Mg}_3\text{Al}_2\text{Si}_3\text{O}_{12}$ ) and anorthite ( $\text{CaAl}_2\text{Si}_2\text{O}_8\text{-MgAl}_2\text{Si}_2\text{O}_8$ ) glass compositions, with respectively 0, 12.3 and 25.0 mol%  $\text{Al}_2\text{O}_3$ . Data for pyroxene and garnet glasses are from Neuville and Richet (1991) and original data for anorthite glasses.

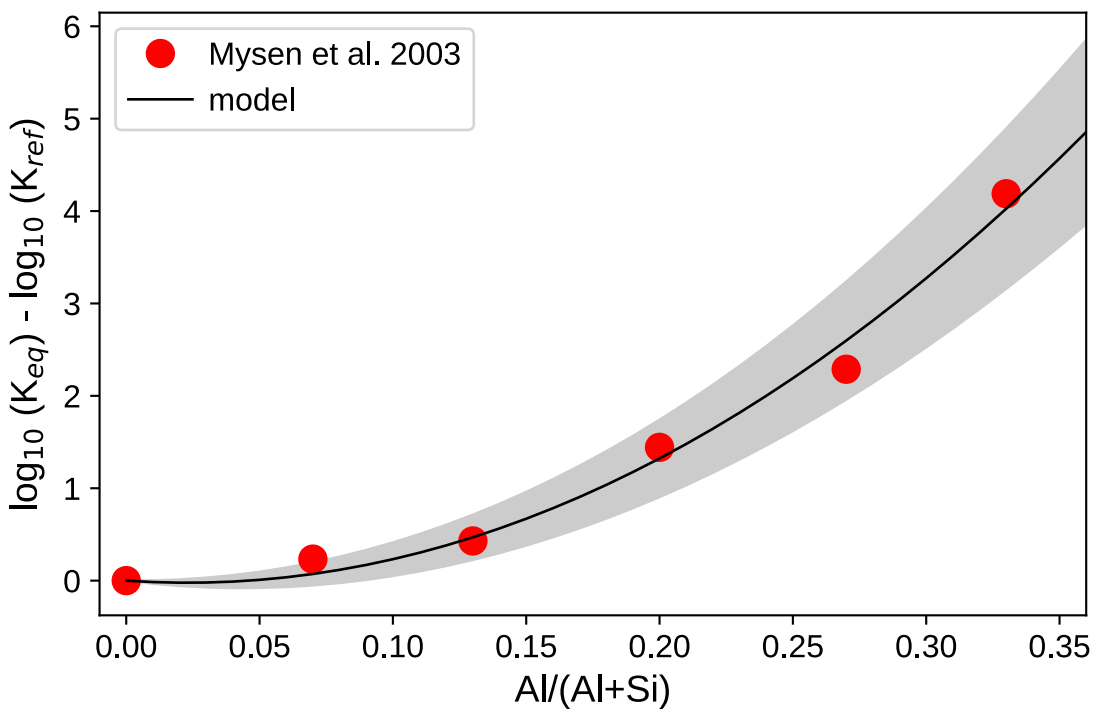
Unfortunately, knowledge regarding the mixing between Sr/Ca, Ba/Mg or more generally between an alkali with an alkaline-earth element in aluminosilicate compositions remain scarce, and it is not possible to propose a general conclusion. It is possible to say that Si and Al are almost randomly distributed in tectosilicate glass compositions, and metal cations are located in cavities of the 3D polyhedral network and ensure the charge compensation of the  $\text{AlO}_4^{5-}$  tetrahedra. This assumption is in good agreement with the linear variation of the  $T\text{-O}$  distances from 1.66 up to 1.76 Å between  $\text{SiO}_2$  and  $\text{CaAl}_2\text{O}_4$  glasses (Figure 13b, chapter 3, this issue). The  $T\text{-O}$  distances are also well correlated with the linear variation of the NMR chemical shift of  $^{27}\text{Al}$  and the linear variation of the frequency of the  $Q^f$  species along the tectosilicate joint (compiled in Figure 13a,b chapter 3, this issue). They may mix randomly like Ca and Mg, but a non-random distribution with increasing network segregation has also been reported in alkali tectosilicate melts (Le Losq et al., 2017). This highlights the complexity of the structure of aluminosilicate melts and glasses, a problem when considering the modelling of their properties. Other problems are the presence of excess NBOs,  $^{[5]}\text{Al}$  and tri-coordinated oxygens (Stebbins and Xu, 1997, Le Losq et al. 2014). For instance, the presence of  $^{[5]}\text{Al}$  can be important, reaching concentrations up to 12% of the  $\text{Al}_2\text{O}_3$  in the middle of the MAS ternary system, and the presence of  $^{[5]}\text{Al}$  results in increasing the glass transition temperature and decreasing configurational entropy. Metal cations could be located in cavities of the 3D polyhedral network, in a manner consistent with the Compensated Continuous Random Network model (Greaves and Ngai, 1995; Greaves and Sen, 2007; Le Losq et al., 2017); they ensure the charge compensation of the  $\text{AlO}_4^{5-}$  tetrahedra. In the potassium aluminosilicate ternary, a non-random distribution of Si and Al between framework units may be accompanied by an increasing segregation of metal cations in clusters or channels. This has been proposed to explain the variations in

550 the structure and properties of potassium tectosilicate melts, for instance (Le Losq and Neuville, 2013;  
 551 Le Losq et al., 2017). This is a problem when considering the modelling of their properties, and a large  
 552 number of approximation may be necessary as we shall see in the later section.

553

### 554 3.7 Models for alkali aluminosilicate melts

555 The above sections allow us to have a glimpse into the complexity of aluminosilicate melts. Even  
 556 leaving aside the potential effects of parameters like  $^{[5]}Al$ , there is no data for the distribution of  $Q^n$   
 557 species in aluminosilicate melts because  $^{29}Si$  NMR spectroscopy loses resolution with aluminosilicate  
 558 compositions due to Si-Al interactions resulting in significant signal broadening and increased  
 559 complexity of the peaks. Mysen et al. (2003) quantified the fractions of the different  $Q^n$  species in Na  
 560 aluminosilicate glasses by modelling the  $^{29}Si$  NMR data. Their findings allow us to constrain the  $K_{eq}$   
 561 value for the dissociation  $2 Q^3 = Q^2 + Q^4$  in sodium aluminosilicate glasses (Figure 25). We observe that  
 562 Al introduction into the glass network promotes the dissociation of  $Q^3$  units.



563

564 *Figure 25: Relative value of the equilibrium constant  $K_{eq}$  of the reaction  $2 Q^3 = Q^2 + Q^4$  obtained*  
 565 *from  $Q^n$  data in Na aluminosilicate melts calculated by Mysen et al. (2003), reported as a function of the*  
 566  *$Al/(Al+Si)$  ratio of glasses.  $K_{ref}$  is the value of  $K_{eq}$  in the glass without Al. The black line represents a*  
 567 *polynomial modelling of the data, and the grey areas are the two-sigma confidence interval of the model*  
 568 *predictions. Using this model, it is possible to estimate the  $Q^n$  distribution in alkali aluminosilicate*  
 569 *glasses, but one must note that such relation remains unknown for other elements like K, Ca or Mg.*

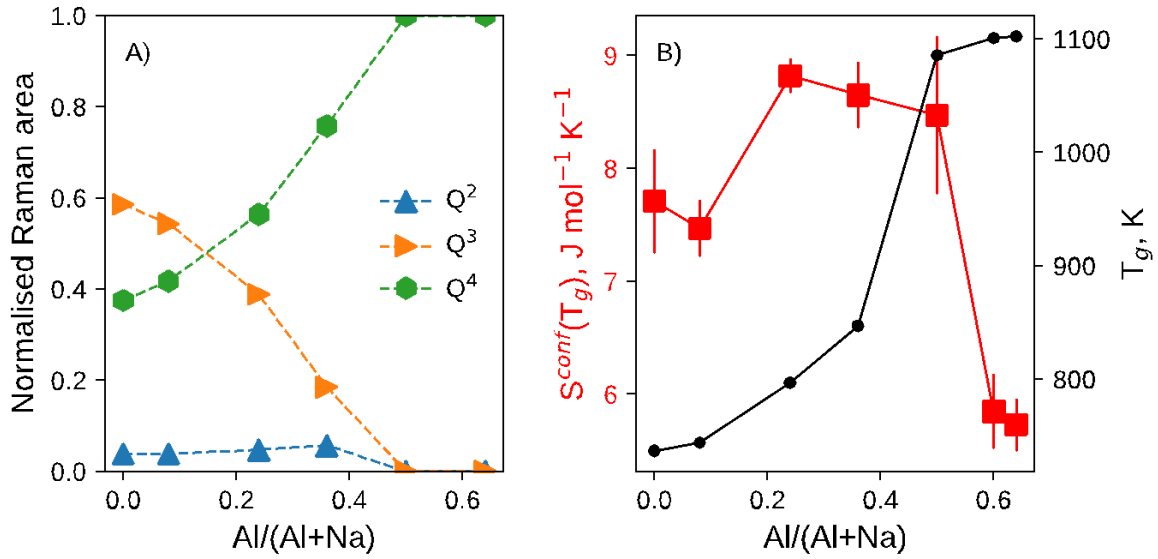
570

571 This result is the only experimental one to the knowledge of authors that could be used to model the  
572  $Q^n$  distribution in aluminosilicates based on the principle of using partial  $K_{eq}$  values as highlighted in  
573 section 2.5. Other models (Doweidar, 1999 for example), like the associate solution one, are purely  
574 theoretical and remain unconstrained by experimental data, as they are not available. This does not  
575 prevent one from building models of glass and melt properties. For instance, Doweidar (1999) simply  
576 used a binary model for calculating the density of  $\text{Na}_2\text{O}-\text{Al}_2\text{O}_3-\text{SiO}_2$  glasses from partial molar values of  
577 different Na- $Q^n$  units. The structural model employed there is clearly not appropriate, but interestingly,  
578 this does not prevent a good prediction of glass densities. A better attempt to link melt composition,  
579 structure and viscosity is that of Starodub et al. (2019), who calculated the  $Q^n$  distribution in  $\text{Na}_2\text{O}-\text{K}_2\text{O}-$   
580  $\text{Al}_2\text{O}_3-\text{SiO}_2$  melts from an associate solution model, and then linked the fractions of  $Q^n$  units and the  
581 concentrations of cations to the parameters of the Avramov-Milchev equation for calculation of melt  
582 viscosity. This is an interesting model, but it suffers from two problems. First, they did not select the  
583 viscosity data used for fitting their model, as they used the large SciGlass database, and the results of  
584 their model will thus suffer from the propagation of large errors affecting some experimental data.  
585 Secondly, the Avramov-Milchev (Avramov and Milchev, 1988) equation works well but it is less  
586 attractive than the Adam-Gibbs theory because it does not allow one to link the chemical, structural,  
587 thermodynamic and dynamic dimension of the problem.

588

589 An extension of the model presented in section 2.5 could allow one to circumvent such caveats. We  
590 will explore if such a model is possible to implement below for the  $\text{Na}_2\text{O}-\text{K}_2\text{O}-\text{Al}_2\text{O}_3-\text{SiO}_2$  system. A  
591 first step would be to combine the silicate structural model (section 2.5) to the relationship presented in  
592 Figure 25. This will allow one to approximate the  $Q^n$  speciation in aluminosilicate glasses. Then, we need  
593 to know the effects of Na-K mixing in aluminosilicate melts and of Al concentration on the glass  
594 configurational entropy. Combining viscosity and Raman data with thermodynamic calculations, Le  
595 Losq et al. (2014) have shown that Al introduction in  $\text{NaSi}_2\text{O}_7$  yields a rapid network polymerisation  
596 (Figure 26A) that is accompanied by a jump in glass configurational entropy and an increase in glass  $T_g$   
597 (Figure 26B). At  $\text{Al}/(\text{Al}+\text{Na})$  higher than 0.5, we see a continuous decrease in  $S^{conf}(T_g)$  that is  
598 accompanied by increasing  $T_g$ .

599



600

601 *Figure 26: A) Fractions of the  $Q^n$  units Raman signal, and B) entropy and glass transition temperature*  
 602 *of Na aluminosilicate glasses with 75 mol%  $SiO_2$  but varying  $Al/(Al+Na)$  ratios. Data from Le Losq et*  
 603 *al. (2014).*

604

605 Variations in  $S^{conf}(T_g)$  are thus complex functions of the melt  $Al/(Al+M)$  ratio. As an approximation,  
 606 one could assume that Al and Si mix randomly in  $Q^4$  units in the silicate network, as proposed for Na  
 607 tectosilicate melts by Neuville and Mysen (1996). Note that it is important to remember that unlike the  
 608 Ca or Mg aluminosilicate system, the ternary system  $Na_2O-Al_2O_3-SiO_2$  does not contain Al in 5-fold  
 609 coordination except in the peraluminous domain (Lee et al., 2003, Le Losq et al., 2014). This hypothesis  
 610 implies that the Lowenstein Al-O-Al avoidance rule will not be respected, and is thus in contradiction  
 611 with the interpretation of NMR data of Na aluminosilicate glasses (Lee and Stebbins, 1999, Lee et al.,  
 612 2003). However, this hypothesis allows reproduction of the variations in configurational entropy  
 613 observed when Al substitutes Si in Na aluminosilicate melts (Neuville and Mysen, 1996; Le Losq, 2012).  
 614 One may thus consider it as adequate for the aim of building a model of configurational entropy  
 615 variations. An additional point is to consider that  $Q^4_{Al}$  charged-balanced by Na ( $Q^4_{Al,Naenv}$ ) or K ( $Q^4_{Al,Kenv}$ )  
 616 probably present different partial configurational entropies (respectively  $S^{conf}_{Q^4_{Al,Naenv}}$  and  $S^{conf}_{Q^4_{Al,Kenv}}$ ).  $S^{topo}$   
 617 (eq. 16) could then be written as:

618

$$\begin{aligned}
 619 \quad S^{topo} = & \sum_{n=2}^3 x_{Q^n_{Si,Naenv}} S^{conf}_{Q^n_{Si,Naenv}} + \sum_{n=2}^3 x_{Q^n_{Si,Kenv}} S^{conf}_{Q^n_{Si,Kenv}} + x_{Q^4_{Si}} S^{conf}_{Q^4_{Si}} + \\
 620 \quad & x_{Q^4_{Al,Naenv}} S^{conf}_{Q^4_{Al,Naenv}} + x_{Q^4_{Al,Kenv}} S^{conf}_{Q^4_{Al,Kenv}}. \quad (32)
 \end{aligned}$$

621



622 From this equation, we need to discriminate the fraction of charge-compensator and network modifiers  
623 (Na, K), in order to calculate the variation in the fractions of the  $Q^n$  units. This could be done easily  
624 assuming that the fractions of charge-compensator and network modifiers Na and K are just equal to the  
625 weighted average fractions of Na and K. This assumes no preference of Na and K to specific  
626 environments, an hypothesis that surely could be challenged.

627  
628 We see that many hypotheses have been already proposed in order to start building a model to express  
629  $S^{conf}(T_g)$ . This is without even considering the calculation of any entropy resulting from cationic mixing,  
630  $S^{mix}$ . The picture becomes even more complex at this point. Indeed, while variations of  $S^{conf}(T_g)$  upon  
631 mixing Na and K in silicate melts can be explained by a random mixing of those cations (Richet, 1984;  
632 see section 2.4, eq. 18): mixing Na and K in the presence of Al results in a different behaviour. Entropy  
633 variations upon mixing Na and K in tectosilicate melts (R=1) are far from ideal (Le Losq and Neuville,  
634 2013). Viscosity, Raman, NMR and molecular dynamic simulation data all indicate that Na and K  
635 actually are present in different environments in tectosilicate melts (Le Losq et al., 2017), with K tending  
636 to be present in large percolation channels in the polyhedral Al-Si network. This was recently challenged  
637 by a new analysis of viscosity data along the  $\text{SiO}_2\text{-(Na,K)AlO}_2$  binary by Robert et al. (2019). Those  
638 authors fitted viscosity data of mixed Na-K tectosilicate melts, leaving the  $A_e$  parameter (eq. 6) free. This  
639 yields results where it is possible to fit viscosity upon Na-K mixing in tectosilicate melts assuming a  
640 random Na-K distribution, like in silicate melts. In such cases, most of the variations in viscosity seemed  
641 to be explained by variations in  $A_e$ . While this is an interesting take on this problem, this is probably not  
642 a good representation of the reality. Indeed, many authors demonstrated that the pre-exponential term in  
643 viscosity equations converge to a singular value (Persikov, 1991; Giordano and Dingwell, 2003,  
644 Giordano et al., 2008, Giordano and Russell 2018). The  $A_e$  parameter is unlikely to vary largely in  
645 aluminosilicate melts (e.g. Russell and Giordano, 2005, 2017 and references therein). It thus seems  
646 improbable that  $A_e$  varies largely upon substitution of Na by K at fixed  $\text{SiO}_2$  and  $\text{Al}_2\text{O}_3$  contents. Raman  
647 spectroscopy data and molecular dynamic simulations (Le Losq and Neuville, 2013; Le Losq et al., 2017,  
648 Le Losq et al., 2019) further indicate that Na tectosilicate and K tectosilicate melts do not have the same  
649 structure, such that Na and K do not mix randomly in such systems. The mixing of Na- and K-  
650 tectosilicates thus appears to be of a mechanical mixing, and should accordingly yield a pseudo-linear  
651 variation of  $S^{conf}(T_g)$ . This agrees with conclusions from Le Losq and Neuville (2013) as well as Le Losq  
652 et al. (2017), which report pseudo-linear variations in  $S^{conf}(T_g)$  upon Na-K mixing.

653  
654 Considering that mixing Na and K compensators does not affect entropy, we need to consider  
655 three sources for the calculation of  $S^{mix}$ : (i) the ideal mixing of Si between different  $Q^n$  units, (ii) the

656 ideal mixing of Si and Al in  $Q^4$  units and (iii) the ideal mixing of Na and K network modifiers. We thus  
 657 have:

$$658 \quad S_{Si-Al}^{mix} = -2 \frac{x_{Si \in Q^4} + x_{Al}}{x_o} R \left[ \frac{Al}{Al+Si} \log \frac{Al}{Al+Si} + \left(1 - \frac{Al}{Al+Si}\right) \log \left(1 - \frac{Al}{Al+Si}\right) \right], \quad (33)$$

660 with  $x_{Si \in Q^4}$  the mole fraction of Si in  $Q^4$  units,

$$661 \quad S_{Si}^{mix} = \frac{-x_{Si}}{x_o} * 2 * R * \sum_{n=2}^4 x_{Q_{Si}^n} \log \left(x_{Q_{Si}^n}\right), \quad (34)$$

662 and assuming a distribution of Na and K as charge-compensator and network modifier that varies  
 663 linearly with Al/(Al+M), we finally have

$$664 \quad S_{Na-K modifiers}^{mix} = MODS \times \left[ -2R \frac{x_{Na} + x_K}{x_o} (X_K \log(X_K) + (1 - X_K) \log(1 - X_K)) \right], \quad (35)$$

665 with MODS the fraction of modifiers contributing to  $S^{mix}$ ; MODS is equal to  $(1 - Al/(Na+K))$  for  $Al <$   
 666  $(Na+K)$ , and is equal to 0 for  $Al \geq (Na+K)$ .

667 The sum of equations 32 to 35 allows the calculation of  $S^{conf}(T_g)$ .  $B_e$  can be calculated following a  
 668 similar logic to that used for silicate melts (section 2.5):

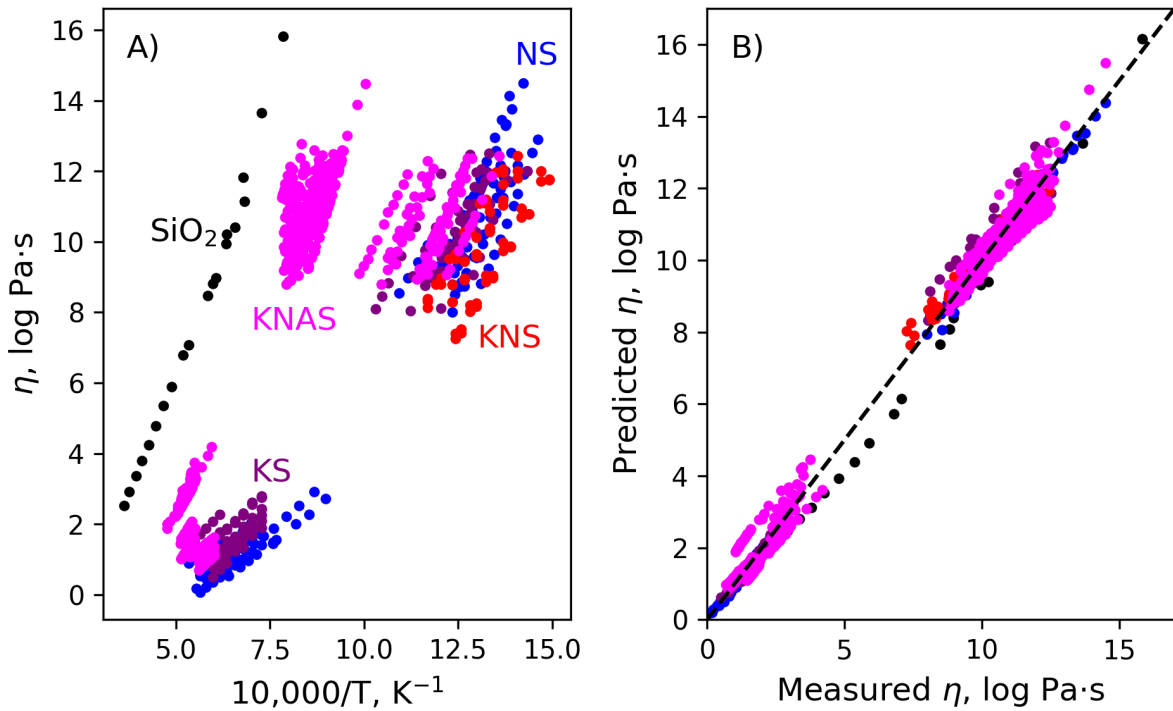
$$669 \quad B_e = \sum_{n=2}^3 x_{Q_{Si,Naenv}^n} B_{e Q_{Si,Naenv}^n} + \sum_{n=2}^3 x_{Q_{Si,Kenv}^n} B_{e Q_{Si,Kenv}^n} + x_{Q_{Si}^4} B_{e Q_{Si}^4} +$$

$$670 \quad x_{Q_{Al,Naenv}^4} B_{e Q_{Al,Naenv}^4} + x_{Q_{Al,Kenv}^4} B_{e Q_{Al,Kenv}^4} + K_1 S_{Si}^{mix} + K_2 S_{Na-K modifiers}^{mix} + K_3 S_{Si-Al}^{mix}, \quad (36)$$

671 with  $K_1$ ,  $K_2$  and  $K_3$  being proportionality constants accounting for the influence of the intrinsic entropy  
 672 in  $B_e$  (section 2.4; Le Losq and Neuville, 2017).  $A_e$  is left as a common parameter.

673 Using the equations described above, and selecting viscosity data from the literature for parameter  
 674 tuning via least-square (see Figure 27), we are able to build a model for the viscosity of melts in the  
 675  $Na_2O-K_2O-SiO_2-Al_2O_3$  system, with compositions from 50 mol% (in aluminosilicates; 60 in silicates) to  
 676 100 mol%  $SiO_2$ , and NBO/T ranging from 0 to 1.33. Root-mean-square-errors between viscosity  
 677 predictions and measurements are equal or lower than 0.5 log Pa·s. This demonstrates that building a  
 678 structural model of the properties of aluminosilicate melts is possible. However, the above model is

688 incomplete because it relies on many hypotheses, and does not take into account (yet) many specifics  
 689 like the role of  $^{[5]}Al$  on  $S^{conf}(T_g)$ . Despite this, this is an encouraging step toward the construction of  
 690 structural models that usually achieve a high degree of precision in the predictions they make. New  
 691 developments in modelling the melt structure and in linking it with melt properties will surely allow  
 692 improvements of such structural models in the future.  
 693



694  
 695 *Figure 27. A) Viscosity data used for the model calibration. Data (n=817) are those compiled by Le*  
 696 *Losq and Neuville (2017) for silicates (NS, KS, KNS and SiO<sub>2</sub>), and for aluminosilicates (KNAS) they*  
 697 *were compiled from Riebling (1966), Taylor and Rindome (1970), Urbain et al. (1982), Le Losq (2012),*  
 698 *Le Losq and Neuville (2013), Le Losq et al. (2014), and Le Losq et al. (2017). The model parameters*  
 699 *were optimised by No-U-Turn Markov Chain Monte Carlo sampling via the PyMC3 Python library. The*  
 700 *root-mean-squared error between predictions and measurements is around 0.36 log unit.*

701  
 702 *4. Aluminate glasses and melts*

703 Aluminate glasses and melts are of interest from a fundamental structural point of view: they contain  
 704 only Al as a network former and, hence, allow better understanding of the role of Al in glasses and melts.  
 705 The study of aluminate materials is also very important to understand the formation and evolution of  
 706 parental bodies in the universe (Leger et al., 2009; Batalha et al., 2011). Aluminate materials further  
 707 represent a technological material of interest because of their good IR transmission and ultralow optical  
 708 losses (Higby et al., 1990) that make them attractive candidates for low loss optical fibers such as infrared

709 waveguides (Lines et al., 1989, King and Shelby, 1996). In addition, calcium aluminate glasses have been  
710 found to be photosensitive to ultraviolet radiations, leading to potential applications in photometric  
711 devices for information storage purposes (Hosono et al., 1985). They also have excellent mechanical  
712 properties, such that calcium aluminate glass fibres have been proposed for the reinforcement of cement  
713 composites (Wallenberger et al., 2004, El Hayek, 2017).

714 Looking at aluminate glasses allows one to better understand the fundamental role of aluminum in  
715 glasses and liquids, a task somehow difficult in aluminosilicate compositions because of the  
716 superposition of many complexities (see section 3). Numerous studies have probed the structure of  
717 calcium aluminate crystals, glasses and melts (e.g. McMillan and Piriou, 1983, Hannon and Parker, 2000,  
718 Benmore et al., 2003; Neuville et al., 2008, 2010, Licheron et al., 2011, Drewitt et al., 2012, 2017). From  
719 those, it appears that four compositional “domains” can be distinguished:  $\text{Al}_2\text{O}_3$ ,  $\text{Al}_2\text{O}_3$ -CA, CA-C3A  
720 and C3A-CaO with  $\text{CA}=\text{CaAl}_2\text{O}_4$ ,  $\text{C3A}=\text{Ca}_3\text{Al}_2\text{O}_6$ .

#### 722 4.1 $\text{Al}_2\text{O}_3$

723 Crystalline  $\text{Al}_2\text{O}_3$  has corundum structure with Al in 6-fold coordination (Rankin, 1915). Several  
724 studies, using  $^{27}\text{Al}$  NMR at high temperature show that  $\text{Al}_2\text{O}_3$  liquid is a mixture of 60%  $^{[6]}\text{Al}$  - 40%  $^{[4]}\text{Al}$ .  
725 This was confirmed more recently by XANES at the Al *K*-edge and FDMNES simulation (Neuville et  
726 al., 2009). Recently, Shi et al. (2019) proposed, from new X-ray diffraction at high temperature  
727 measurements, that Al is essentially in five-fold coordination in the  $\text{Al}_2\text{O}_3$  liquid; this interpretation is  
728 based on the Al-O distance. The  $^{27}\text{Al}$  NMR chemical shift is 53 ppm (Couture et al., 1990; Florian et al.,  
729 1995, Ansell et al., 1997), a value that can be interpreted as  $^{[5]}\text{Al}$ , or as a mixture of  $^{[4]}\text{Al}$  and  $^{[6]}\text{Al}$ . When  
730 assuming a mixture of  $^{[4]}\text{Al}$  and  $^{[6]}\text{Al}$ , the high temperature  $^{27}\text{Al}$  NMR data allow determining an Al NMR  
731 relaxation time in excellent agreement with the relaxation time obtained from viscosity measurements  
732 (Urbain, et al. 1982). Besides, when comparing XANES data at the Al *K*-edge measured at high  
733 temperature in the liquid state to spectra simulated using the FDMNES code (Joly, 2001), the assumption  
734 of a mixture of  $^{[4]}\text{Al}$  and  $^{[6]}\text{Al}$  provides the best reproduction of the experimental data (Neuville et al.,  
735 2009). From all the high temperature NMR and XANES spectroscopies and/or neutron diffraction  
736 measurements, it is at the moment preferable to consider that, in liquid alumina, Al is present as a mixture  
737 of  $^{[4]}\text{Al}$  and  $^{[6]}\text{Al}$ .

738 We have essentially mentioned  $\text{Al}_2\text{O}_3$  in its crystalline or liquid forms, however, some studies have  
739 shown that it is possible to obtain  $\text{Al}_2\text{O}_3$  in its amorphous form, it is usually obtained by fast quenching  
740 and in thin film form (Lee et al., 2010; Kim et al., 2014). In that case, Al is essentially a mix of 4- and 5-  
741 fold coordination with a small amount of 6-fold coordination (Lee et al., 2010; Kim et al., 2014). The

742 difference between the Al coordination between glass and liquid state can be easily explained by the high  
743 cooling rate.

#### 744 4.2 $Al_2O_3$ - $CaAl_2O_4$ compositions.

746 With the introduction of calcium (or others alkaline-earth elements) in alumina liquid, a first  
747 crystalline phase can be found: grossite,  $CaAl_4O_7$ , called CA2, with  $AlO_4$  tetrahedra only in  $Q^4$  units  
748 although one of the O atoms forms an “oxygen tricluster” which links three  $AlO_4$  tetrahedra (Stebbins et  
749 al, 2001, Iuga et al., 2005, Neuville et al., 2010). With increasing Ca content up to the  $CaAl_2O_4$  crystal  
750 composition, the amount of tricluster oxygen decreases and Al stays in four fold coordination. The  
751  $CaAl_4O_7$  composition always crystallizes while  $CaAl_2O_4$  (CA) can be quenched to a glass by fast quench  
752 methods. In the CA glass,  $^{41}Al$  is dominant and  $^{51}Al$  representing 3,5 % of total Al (Neuville et al., 2006).  
753 In the CA liquid,  $^{41}Al$  remains dominant but the proportion of  $^{51}Al$  increases up to around 40 mol % near  
754 2000 K, as observed from XANES at the Al K-edge and neutron diffraction (Neuville et al., 2008a,  
755 Drewitt et al., 2012). Oxygen triclusters also probably are present but remain unquantified during these  
756 changes. The coordination of calcium, which is 7-fold in the glasses, increases in the melts as indicated  
757 by the evolution of the pre-edge of Ca K-edge XANES spectra between room temperature and  
758 superliquidus temperatures (Neuville et al., 2008a).

#### 760 4.3 CA-C3A compositions.

761 For compositions between  $50 > Al_2O_3 > 25$  mol%, Al is only in tetrahedral coordination in both the  
762 glasses and the crystals, with a number of bridging oxygens varying between 4 to 2 respectively for CA  
763 and C3A (McMillan and Piriou, 1983, Neuville et al., 2004, 2006, 2010, Licheron et al. 2011, Drewitt et  
764 al., 2017). In C3A crystal or glass ( $Ca_3Al_2O_6$ ), Al can be found in  $Q^2$  units, and, with increasing  
765 temperature, Al K-edge XANES show very small changes (Neuville et al., 2008a). The later observation  
766 implies that Al stays in  $Q^2$  species with increasing temperature without creation of  $^{51}Al$ . The cationic  
767 mobility is only insured by  $Q^2$  species, and not by highly coordinated units as proposed by Stebbins and  
768 Farnan (1992) for polymerized melts. Calcium cations in crystalline C3A and glass is in 6-fold  
769 coordination, and, near 2000 K, a small pre-edge in Ca K-edge XANES spectra is observed; this implies  
770 that the Ca coordination increases with increasing temperature (Neuville et al., 2008a).

#### 772 4.4 C3A-CaO compositions

773 For compositions with  $Al_2O_3 < 25$  mol%, no glass or stable crystalline phases are observed. The  
774 knowledge of Al and Ca coordination in such conditions remains very scarce, if not non-existent.

4.5 Link with observations in other binary systems

In SrO-Al<sub>2</sub>O<sub>3</sub> and BaO-Al<sub>2</sub>O<sub>3</sub> systems, the liquidus temperatures are higher than in the CaO-Al<sub>2</sub>O<sub>3</sub> system. This observation seems logical since there is agreement with an increase of liquidus temperature with increasing the size of the alkaline-earth elements in alkaline-earth aluminosilicate systems (Médugin et al., 2004, Licheron et al., 2011, Shan et al., 2018). Turning to MgO-Al<sub>2</sub>O<sub>3</sub>, Mg<sup>2+</sup> forms a very stable spinel with alumina; it is not possible to quench the MgAl<sub>2</sub>O<sub>4</sub> composition or other magnesium aluminate composition even with using fast-quench methods. In MgAl<sub>2</sub>O<sub>4</sub> crystals, Mg and Al are in 4 and 6-fold coordinations, respectively, at room temperature and that can change with temperature (Andreozzi et al., 2000, Neuville et al., 2009).

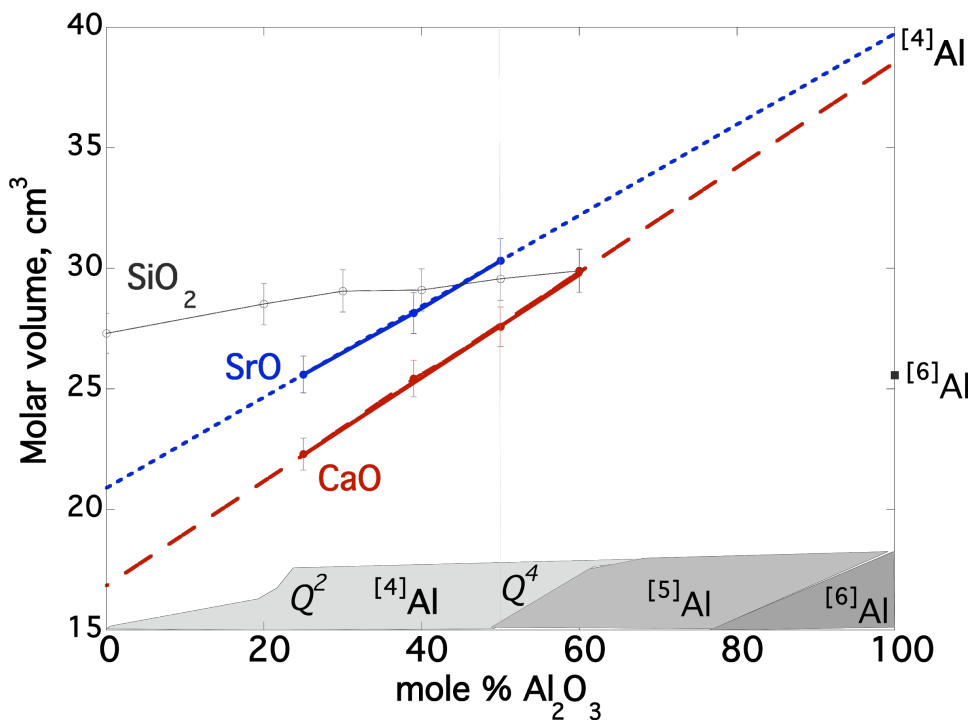
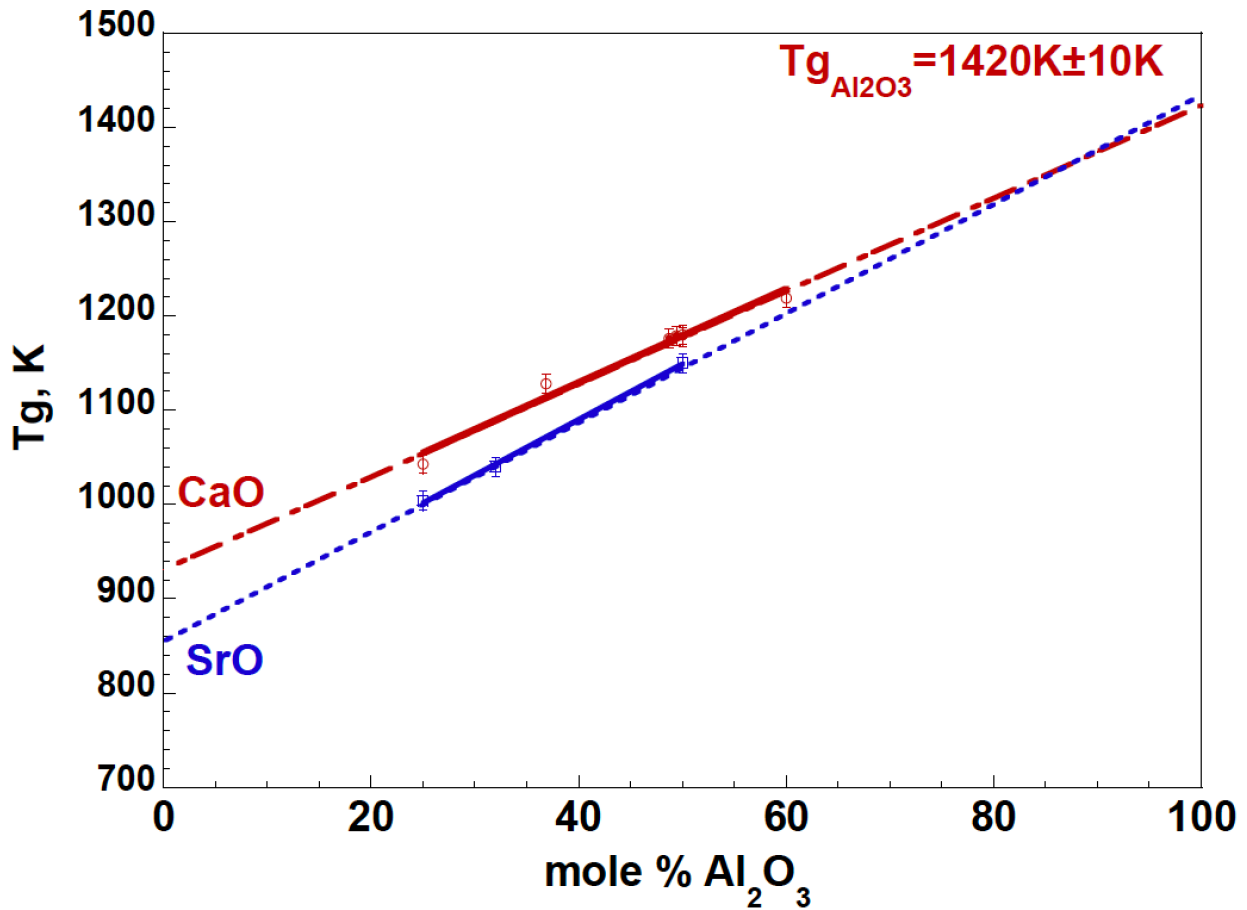


Figure 28: Coordination of Al between MO-Al<sub>2</sub>O<sub>3</sub> and variation of molar volume of aluminate glasses. Molar volumes are calculated from the density measurements for Al<sub>2</sub>O<sub>3</sub>-SiO<sub>2</sub> (Wang et al., 2020), Al<sub>2</sub>O<sub>3</sub>-CaO (Neuville et al., 2006, 2010, Licheron et al., 2011), and Al<sub>2</sub>O<sub>3</sub>-SrO (Licheron et al., 2011). Solid lines correspond to fits of the data with a line, and dashed lines show the extrapolation of those fits to end members.

Figure 28 summarizes the evolution of the Al coordination in aluminate glasses and also shows how the molar volume of glass changes with Al<sub>2</sub>O<sub>3</sub> content. The glasses CxA or SxA, with x varying between 3 and 1, are made by levitation and fast quench, and all these glasses show Al in 4-fold coordination (Neuville et al., 2006, 2008b, 2010, Licheron et al., 2010). For Ca or Sr aluminates, a linear variation of

797 the molar volume with the alumina content is observed between 25 and 50 mole percent of alumina, and  
 798 Ca is in 6-fold coordination and Al in 4-fold coordination (Neuville et al., 2008b). If we consider linear  
 799 extrapolations of these trends, it is possible to propose, considering only Al in four-fold coordination and  
 800 Ca and Sr in 6-fold coordinations, that the respective partial molar volumes of Al<sub>2</sub>O<sub>3</sub>, CaO and SrO are  
 801 respectively of 39.1, 17.0 and 21.0 cm<sup>3</sup> mol<sup>-1</sup>. Such estimations are in very good agreement with the  
 802 values proposed by Robie (1978) for the molar volume of CaO and SrO.  
 803



804  
 805 *Figure 29: Glass transition temperature obtained from DSC measurements with and heating rate of*  
 806 *10°/min for aluminate glasses. Full line corresponds to linear variation fitting datas and dashed line*  
 807 *corresponds to extrapolation up to end members.*

809 To complete the observations made on the molar volume, the glass transition temperatures for C<sub>x</sub>A  
 810 and S<sub>x</sub>A glasses were measured and plotted in Figure 28. The glass transition temperature of the different  
 811 C<sub>x</sub>A and S<sub>x</sub>A glasses were obtained by DSC measurements with a heating rate of 10 °/min. Two linear  
 812 trends are observed along the binaries CaO-Al<sub>2</sub>O<sub>3</sub> and SrO-Al<sub>2</sub>O<sub>3</sub>. They converge to similar values when  
 813 extrapolated to the alumina end-member. From this, we can propose an “apparent” partial glass transition  
 814 temperature for Al<sub>2</sub>O<sub>3</sub> at 1420 ± 10 K. Following this logic, we also propose partial T<sub>g</sub>s for CaO and SrO

815 in 6-fold coordination at  $932 \pm 10$  and  $857 \pm 10$  K. The estimated  $T_{g_i}$  for  $Al_2O_3$  with Al in four-fold  
816 coordination is in very good agreement with calculation of phase diagrams using CALPAHD program  
817 (Pitsch, et al. 2021 submitted).

818 Recently Shan et al (2018) made some calcium-strontium peraluminous glasses at 58% mole of  $Al_2O_3$   
819 using levitation device and fast cooling rate. They investigated macroscopic properties of these glasses  
820 and they showed that an ideal mixing term between Ca and Sr clearly exist to explain Vickers micro-  
821 hardness and glass transition temperatures variation between Ca/Sr aluminate glasses.

822

### 823 5. Conclusion and perspectives

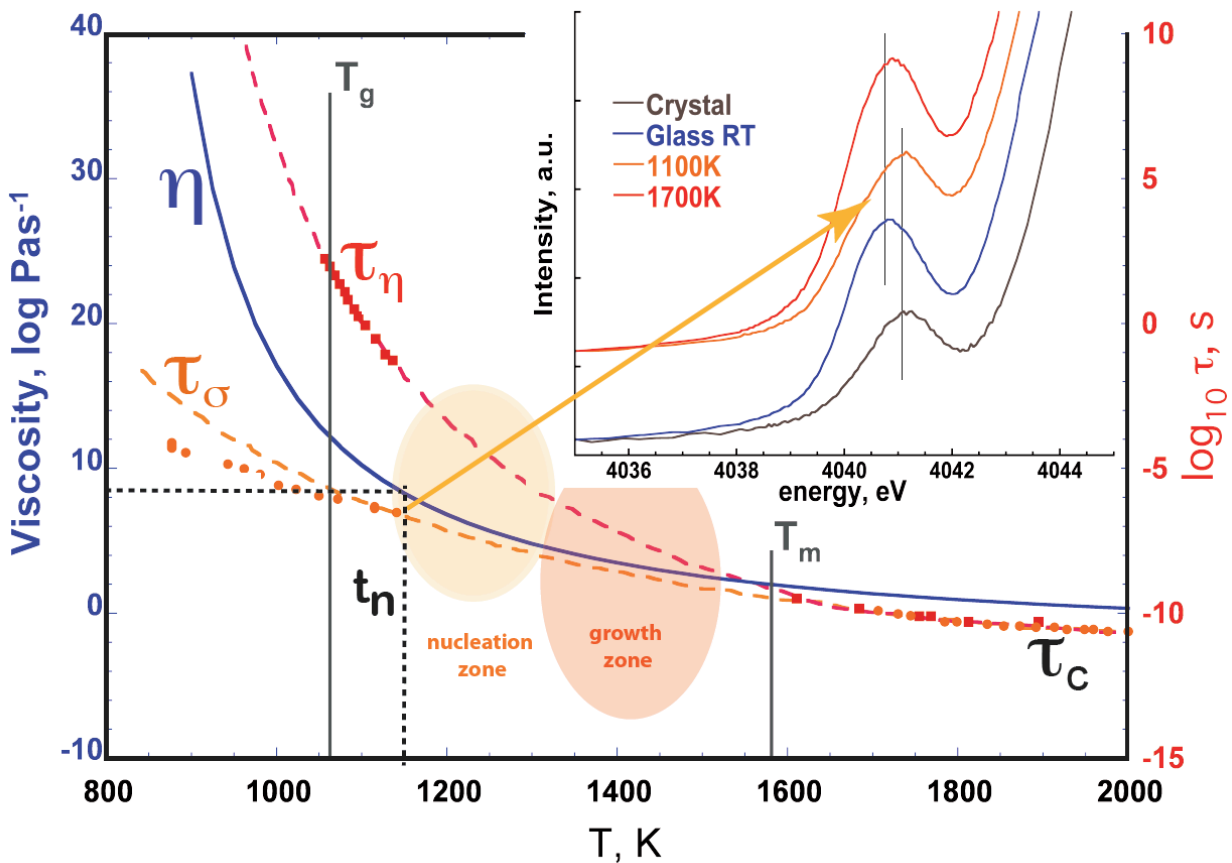
824 Since the 1980s, it has been possible to study the structure of a liquid at high temperature by  
825 several spectroscopic methods: Raman, NMR, X-ray absorption and X-ray and neutron diffraction  
826 techniques. This allows us to understand the local order and the medium range order directly in the liquid  
827 state and thus be able to link the high temperature structure to the measurements of properties directly  
828 accessible at high temperature, like heat capacity, viscosity, conductivity, diffusivity. We have seen that  
829 this kind of approach is very promising because it allows us to have a global view of a glass and a liquid  
830 and thus to better understand the structural changes that take place in a liquid. This improved  
831 understanding of silicate glasses and liquids has great applications in both volcanology and geochemistry  
832 where we are better able to understand changes in eruptive dynamism, mass transfers and also chemical  
833 balances during crystallization processes for example. But this work allows also a better understanding  
834 of industrial processes during melting, glass-forming or even during the processes of glass-ceramic.

835 To summarize the changes that can occur in a cooling liquid, Figure 30, obtained for a  
836 composition of  $Ca_3Al_2Si_3O_{12}$  liquid, shows both the changes that occur in the liquid state and during its  
837 cooling. We can see that at high temperature, beyond the liquidus,  $T_m$ , 1580K, the relaxation times  
838 obtained from the  $^{27}Al$  NMR,  $\tau_{NMR}$ , measurement of conductivity,  $\tau_\sigma$ , or viscosities,  $\tau_\eta$  converge and are  
839 similar. It simply means that in the liquid state all cations whatever their roles in the melts, move in  
840 relation to each other. From structural point of view, it is a liquid state, characterized by the particularly  
841 intense pre-edge of the XANES spectra at the Ca  $K$ -edge at high temperature. On the other hand, when  
842 the temperature decreases, there is a decoupling between the various relaxations, this means that the  
843 atoms begin to move differently, the network modifiers like Ca, continue to move as shown by the  
844 relaxation  $\tau_\sigma$ , while the relaxation calculated from the viscosity measurements,  $\tau_\eta$ , shows a strong  
845 increase, meaning that the tetrahedral network composed of tetrahedral  $SiO_4$  and  $AlO_4$  moves more  
846 slowly, which translates into an increase in the viscosity curve. This decoupling between the various  
847 families of atoms appears at about 1100K for this chemical composition, several orders of magnitude



848 separate the relaxation times obtained from the conductivity measurements,  $\tau_\sigma$ , from those obtained from  
 849 viscosity measurements,  $\tau_\eta$ . These differences show, on the one hand, that the aluminosilicate network  
 850 freezes with a significant increase of  $\tau_\eta$ , and viscosity and that calcium atoms put themselves in a position  
 851 close to that which they will have in the crystalline phase, as shown by the changes observed in the pre-  
 852 edge of the XANES spectra at the Ca K-edge. In the end, we find that close to  $T_g$ , the Ca is probably in a  
 853 crystallographic site almost identical to the one it will have in a crystal.

854



855

856 *Figure 30: viscosity of  $Ca_3Al_2Si_3O_{12}$  liquid from Neuville and Richet (1991), relaxation  $\tau_\eta$  is calculated*  
 857 *from viscosity measurements,  $\tau_\sigma$  and  $\tau_{NMR}$ , are from Gruener et al., (2001) and pre-edge XANES spectra*  
 858 *at the Ca K-edge are from Neuville et al., (2008b)*

859

860 Figure 30 completes the Figure 4 of this chapter, which helped to understand the links between potential  
 861 movements in a liquid, various entropic states and viscosity, but this latter figure indicates that at high  
 862 temperature all atoms can move quickly relative to each other and that at lower temperatures, atoms are  
 863 in different potentials energy states and that changes will take more time.

864

865 In 2021, it is therefore possible and necessary to understand the structure and properties of a  
 glass or/and a liquid throughout its history during a natural or industrial process. The current

866 computational techniques discussed in the following chapters can show and predict these different states,  
867 and it is easy to imagine that the new techniques based on Machine Learning will allow modeling of the  
868 structure, and physical properties and be able to predict them globally (Le Losq et al., 2021), this will  
869 have great consequences for both earth sciences and materials sciences.

870

## 871 6. References

872 Adam, G. and J.H. Gibbs, (1965) On the temperature dependence of cooperative relaxation properties in  
873 glass-forming liquids, *J. Chem. Phys.* 43 139–146.

874 Ali F., A.V. Chadwick, G.N. Greaves, M.C. Jermy, K.L. Ngai, M.E. Smith, Examination of the mixed-  
875 alkali effect in (Li,Na) disilicate glasses by nuclear magnetic resonance and conductivity  
876 measurements, *Solid State Nucl. Magn. Reson.* 5 (1995) 133–143.

877 Allu A., Gaddam A., Sudheer Ganiseti, Sathravada Balaji, Renée Siegel, Glenn C. Mather, Margit  
878 Fabian, Maria J. Pascual, Nicoletta Ditaranto, Wolfgang Milius, Jürgen Senker, Dmitrii A. Agarkov,  
879 Vladislav. V. Kharton, and Ferreira J. (2018) Structure and Crystallization of Alkaline-Earth  
880 Aluminosilicate Glasses: Prevention of the Alumina-Avoidance Principle. *The Journal of Physical*  
881 *Chemistry B.* 122, 4737-4747

882 Allwardt, J.R., Lee, S.K., and Stebbins, J.F. (2003) Bonding preferences of non-bridging O atoms:  
883 evidence from  $^{17}\text{O}$  MAS and  $^3\text{QMAS}$  NMR on calcium aluminate and low-silica Ca-aluminosilicate  
884 glasses. *American Mineralogist*, 88, 949-954.

885 Allwardt J.R. and Stebbins J.F. (2004) Ca-Mg and K-Mg mixing around non-bridging O atoms in silicate  
886 glasses: An investigation using  $^{17}\text{O}$  MAS and  $^3\text{QMAS}$  NMR. *American Mineralogist*, 89, 777–784.

887 Allwardt, J.R., Stebbins, J.F., Schmidt, B.C., Frost, D.J., Withers, A.C., and Hirschmann, M.M. (2005a)  
888 Al coordination and density of high-pressure aluminosilicate glasses. *American Mineralogist*, 90,  
889 1218-1222.

890 Allwardt, J.R., Poe, B.T., and Stebbins, J.F. (2005b) The effect of fictive temperature on Al-coordination  
891 in high-pressure (10 GPa) Na aluminosilicate glasses. *American Mineralogist*, 90, 1453-1457.

892 Allwardt, J.R., Stebbins, J.F., Terasaki, H., Du, L.D, Frost D.J., Withers, A.C., Hirschmann, M.M.,  
893 Suzuki A., and Ohtani E. (2007) Effect of structural transitions on properties of high-pressure silicate  
894 melts:  $^{27}\text{Al}$  NMR, glass densities, and melt viscosities. *American Mineralogist*, 92, 1093-1104.

895 Andreozzi, G.B., Princivalle, F., Skogby, H. and Della Giusta, A. (2000) Cation ordering and structural  
896 variations with temperature in  $\text{MgAl}_2\text{O}_4$  spinel: an X-ray single-crystal study. *Americ. Mineral.*, 85,  
897 1164-1171.

898 Angell C.A. ,1991. Relaxation in liquids, polymers and plastic crystals strong/fragile patterns and  
899 problems. *J. Non-Cryst. Solids* 131-133, 13-31.

900 Ansell, S., Krishnan, S., Weber, J. K. R., Felten, J. F., Nordine, P. C., Beno, M. A., Price, D. L. and  
901 Saboungi, M.-L. (1997) Structure of liquid aluminum oxide. *Phys. Rev. Let.*, 78, 464-466.

902 Avramov I. and Milchev A. (1988) Effect of disorder on diffusion and viscosity in condensed systems.  
903 *J. Non-Cryst Solids* 104, 253–260.

904 Batalha, N.M., Borucki, W.J., Bryson, S.T., Buchhave, L.A., Caldwell, D.A., Jørgen Christensen-  
905 Dalsgaard, Ciardi, D., Dunham, E.W., Fressin, F., III, T.N.G., Gilliland, R.L., Haas, M.R., Howell,  
906 S.B., Jenkins, J.M., Kjeldsen, H., Koch, D.G., David W. Latham, Lissauer, J.J., Marcy, G.W., Rowe,  
907 J.F., Sasselov, D.D., Seager, S., Jason H. Steffen, Torres, G., Basri, G.S., Brown, T.M., Charbonneau,  
908 D., Christiansen, J., Bruce Clarke, Cochran, W.D., Dupree, A., Fabrycky, D.C., Fischer, D., Ford,  
909 E.B., Jonathan Fortney, Girouard, F.R., Holman, M.J., Johnson, J., Isaacson, H., Klaus, T.C., Pavel  
910 Machalek, Moorehead, A.V., Morehead, R.C., Ragozzine, D., Tenenbaum, P., Joseph Twicken, Quinn,  
911 S., VanCleve, J., Walkowicz, L.M., Welsh W.F., Devore, E., Gould, A., 2011. Kepler’s First Rocky  
912 Planet: Kepler-10b. *Astrophys. J.* 729, 27. <https://doi.org/10.1088/0004-637X/729/1/27>

913 Bacon C.R. (1977) High-temperature heat content and heat capacity of silicate glasses: experimental  
914 determination and a model for calculation. *Amer. J. Sci.*, 277, 109

915 Bancroft M., Nesbitt H.W., Henderson G.S., O’Shaughnessy C., Withers A.C. and Neuville D.R. (2018)  
916 Lorentzian dominated lineshapes and linewidths for Raman symmetric stretch peaks (800–1200  
917  $\text{cm}^{-1}$ ) in Qn (n=1–3) species of alkali silicate glasses/melts. *Journal of Non-Crystalline Solids.* 484,  
918 72-83.

919 Ben Kacem I, Gautron L., Coillot D., Neuville D.R. (2017) Structure and properties of lead silicate  
920 glasses and melts. *Chemical Geology*, 461, 104-114.

921 Benmore C.J., Weber J K R, Sampath S, Siewenie J, Urquidi J and Tangeman J A (2003) A neutron and  
922 x-ray diffraction study of calcium aluminate glasses. *J. Phys.: Condens. Matter* 15 (2003) S2413–  
923 S2423.

924 Bockris J.O.M., Mackenzie J.D. and Kitchener E., 1955. Viscous flow in silica and binary liquid silicates.  
925 *Farad. Soc. Lond. Trans.* 51, 1734-1749.

926 Bødker M.S., Youngman R.E., Mauro J. and Smedskjaer M.M. (2020) Mixed Alkali Effect in Silicate  
927 Glass Structure: Viewpoint of  $^{29}\text{Si}$  Nuclear Magnetic Resonance and Statistical Mechanics. *J. Phys.*  
928 *Chem. B*, 124, 10292–10299. DOI: 10.1021/acs.jpcc.0c07980

929 Bottinga Y. and Weill D.F. (1970) Densities of liquid silicate systems calculated from partial molar  
930 volumes of oxide components *Amer. J. Sci.*, 269, 169

931 Bottinga Y. and D.F. Weill, The viscosity of magmatic silicate liquids: a model for calculation, *Am. J.*  
932 *Sci.* 272 (1972) 438–475

933 Bender S., Franke R., Hartmann E., Lansmann V., Jansen M., Hormes J. (2002) X-ray absorption and

934 photoemission electron spectroscopic investigation of crystalline and amorphous barium silicates.  
935 Journal of Non-Crystalline Solids 298, 99–108

936 Bray, P.J., J.F. Emerson, D. Lee, S.A. Feller, D.L. Bain, D.A. Feil, NMR and NQR studies of glass  
937 structure, J. Non-Cryst. Solids 129 (1991) 240–248.

938 Brauer D.S. Bioactive glasses - structure and properties. Angew Chem Int Edit. 2015;54(14):4160–81.

939 Brückner R. (1970) Properties and structure of vitreous silica. II. J. Non-Cryst. Solids 5, 177-216.

940 Buckerman W-A, Müller-Warmuth W., 1992. A further <sup>29</sup>Si NMR study on binary alkali silicate glasses.  
941 Glastechn. Ber. 65, 18-21.

942 Bunker, B.C., Kirkpatrick, R.J., Brow, R.K., Turner, G.L., and Nelson, C. (1991) Local structure of  
943 alkaline-earth boroaluminate crystals and glasses. II, <sup>11</sup>B and <sup>27</sup>Al MAS NMR spectroscopy of  
944 alkaline-earth boroaluminate glasses. Journal of the American Ceramic Society, 74,1430-1438.

945 Carmichael I.S.E., Nicholls J., Spera F.J., Wood B.J. and Nelson S.A. (1977) High-temperature of silicate  
946 liquids: application to the equilibration and ascent of basic magma. Phil. Trans. R. Soc. Lond., A. 286,  
947 373.

948 Champagnon B., Wondraczek L., Deschamps T. (2009) Boson peak, structural inhomogeneity, light  
949 scattering and transparency of silicate glasses Journal of Non-Crystalline Solids, 355, 712–714

950 Charpentier T., Okhotnikov K., Novikov A., Hennet L., Fischer H., Neuville D.R., Florian P. (2018)  
951 Structure of strontium aluminosilicate glasses from molecular dynamics simulations, neutron  
952 diffraction and nuclear magnetic resonance studies. The Journal of Physical Chemistry. 122(41):  
953 9567-9583. DOI: 10.1021/acs.jpcc.8b05721

954 Chumakov A. I., Monaco G., Fontana A. Bosak, R. P. Hermann, D. Bessas, B. Wehinger, W. A.  
955 Crichton, M. Krisch, R. Rüffer, G. Baldi, G. Carini Jr., G. Carini, G. D'Angelo, E. Gilioli, G. Tripodo,  
956 M. Zanatta, B. Winkler, V. Milman, K. Refson, M. T. Dove, N. Dubrovinskaia, L. Dubrovinsky, R.  
957 Keding, and Y. Z. Yue (2014) Role of Disorder in the Thermodynamics and Atomic Dynamics of  
958 Glasses. Physical Review Letters, 112, 025502

959 Cicconi M.R., de Ligny D., Gallo T. M., Neuville D.R. (2016) Ca Neighbors from XANES spectroscopy:  
960 a tool to investigate structure, redox and nucleation processes in silicate glasses, melts and crystals.  
961 American Mineralogist, 101, 1232-1236.

962 Clupper D.C., Hench L.L., 2003. Crystallization kinetics of tape cast bioactive glass 45S5. J. Non-Cryst.  
963 Solids 318, 43-48.

964 Cormack A.N. and Du J., 2001. Molecular dynamics simulations of soda-lime silicate glasses. J. Non-  
965 Cryst. Solids. 293-295, 283-289.

966 Cormier L. and Neuville D.R. (2004) Ca and Na environments in Na<sub>2</sub>O-CaO-Al<sub>2</sub>O<sub>3</sub>-SiO<sub>2</sub> glasses:  
967 influence of cation mixing and cation-network interactions. Chem. Geol., 213, 103-113

968 Cormier L., Neuville D.R. and G. Calas (2000) Structure and properties of low-silica calcium  
969 aluminosilicate glasses. *J. Non-Crystal. Solids*.274, 110-114.

970 Cormier L, Ghaleb D., Neuville D.R., Delaye JM, Calas G. (2003) Network polymerization of calcium  
971 aluminosilicate glasses: a Molecular Dynamics and Reverse Monte Carlo study. *J. Non-Crystal.*  
972 *Solids.*, 332, 255-270.

973 Cormier L., Neuville D.R. and G. Calas (2005) Structure of low-silica calcium aluminosilicate glasses.  
974 *J. Amer. Ceram. Soc.*, 88, 2292-2299.

975 Cormier L. and Cuello G. (2013) Structural investigation of glasses along the MgSiO<sub>3</sub>-CaSiO<sub>3</sub> join:  
976 diffraction studies. *Geochimica et Cosmochimica Acta* 122 (2013) 498-510.

977 Cormier L. 2019 Neutron and X-Ray Diffraction of Glass. *Hand Book of glass*. 1045-1090

978 Coté, B., Massiot, D., Taulelle, F., Coutures, J.-P. (1992) 27Al NMR spectroscopy of aluminosilicate  
979 melts and glasses. *Chemical Geology*, 96, 367-370.

980 Courtial P. (1993) Propriétés thermodynamiques des silicates fondus et des minéraux au voisinage de la  
981 fusion. Thèse Université Paris 7

982 Courtial P. and Richet P. (1993) Heat capacity of magnesium aluminosilicate melts. *Geochimie and*  
983 *Cosmochimica Acta* Vol. 57, pp. 1267-1275

984 Coutures, J.-P., Massiot, D., Bessada, C., Echegut, P., Rifflet, J.-C., and Taulelle, F. (1990) Etude par  
985 RMN 27Al d'aluminates liquides dans le domaine 1600-2100°C. *C.R. Acad. Sci. Paris*, 310, 1041-  
986 1045.

987 Davis R.O., and Jones G.O. (1953) Thermodynamic and kinetic properties of glasses. *Adv. Phys.*, 2, 370

988 Davis M., Kaseman D., Parvani S., Sanders K., Grandinetti P., Massiot D., Florian P. (2010) Q(n) Species  
989 Distribution in K<sub>2</sub>O·2SiO<sub>2</sub> Glass by 29Si Magic Angle Flipping NMR. *J. Phys. Chem. A* 2010, 114,  
990 5503–5508

991 Day D. E. (1976) Mixed alkali glasses - Their properties and uses. *J. Non-Cryst. Solids* 21, 343–372.

992 Descamps M. (2017) États amorphe et vitreux des composés moléculaires et pharmaceutiques –  
993 Propriétés générales. *Techniques de l'Ingénieur.*, PHA2030 v1

994 Dingwell D.B. and S.L. Webb, (1990) Relaxation of silicate glass. *Eur. J. Mineral.*, 2 427.

995 Doremus R.H. (1973) *Glass science* ; John Wiley and Sons N.Y. 349p

996 Doweidar H. (1999) Density-structure correlations in silicate glasses, *J. Non-Cryst. Solids* 249, 194–200

997 Doweidar, H., S. Feller, M. Affatigato, B. Tischendorf, C. Ma, E. Hammarsten: (1999) Density and molar  
998 volume of extremely modified alkali silicate glasses, *Phys. Chem. Glasses* 40, 339–344

999 Drewitt J.W.E, L. Hennet, Zeidler A., Jahn S., P.S. Salmon, Neuville D.R. and Fischer H.E. (2012)  
000 Structural transformations on vitrification in the fragile glass forming system CaAl<sub>2</sub>O<sub>4</sub>. *Physical*  
001 *Review Letters*. 109 (23), 235501-235506.

002 Drewitt J.W.E, Barnes A.C., Jahn S., Kohn S.C., Walter M.J., Novikov A., Neuville D.R., Fischer H.E.

003 and Hennet L. (2017) Structure of liquid tri-calcium aluminate. *Physical Review B*. 95, 064203-  
004 064214.

005 Drewitt J., Hennet L., Neuville D.R., (2021) The structure of glasses from short distance order to long  
006 distance. In Neuville D.R., Henderson G.S, Dingwell D. B. (2021) "Magmas, melts, liquids and  
007 glasses: Experimental insights " Review in *Mineralogy and Geochemistry*. in press – DOI :

008 Du J. and Cormack A.M. (2004) The medium range structure of sodium silicate glasses: a molecular  
009 dynamics simulation. *Journal of Non-Crystalline Solids* 349, 66–79

010 Dulong, P.L., and Petit, A.T. (1819) Recherches sur quelques points importants de la théorie de la chaleur.  
011 *Annales de chimie et de physique*, 10, 395–413.

012 Dupree R., D. Holland, D.S.Williams (1986) The structure of binary alkali silicate glasses, *J. Non-Cryst.*  
013 *Solids* 81, 185–200, [http://dx.doi.org/10.1016/0022-3093\(86\)90269-3](http://dx.doi.org/10.1016/0022-3093(86)90269-3).

014 Dupree, N. Ford, D. Holland, Examination of the  $^{29}\text{Si}$  environment in the  $\text{PbO-SiO}_2$  system  
015 by magic angle spinning nuclear magnetic resonance. Pt. 1. Glasses. *Phys. Chem. Glasses* 28 (1987)  
016 78-87.

017 Edén, M. (2012) NMR studies of oxide-based glasses. Annual Reports Section “C” (Physical Chemistry),  
018 108, 177.

019 Emerson J.F., Stallworth P.E. and Bray P.J. (1989) HIGH-FIELD  $^{29}\text{Si}$  NMR STUDIES OF ALKALI  
020 SILICATE GLASSES. *Journal of Non-Crystalline Solids* 113 (1989) 253-259

021 Emerson J.F., P.J. Bray, Nuclear magnetic resonance and transmission electron microscopy studies of  
022 mixed-alkali silicate glasses, *J. Non-Cryst. Solids* 169 (1994) 87–95.

023 English S., 1923. The effect of composition on the viscosity of glass, Part II. *J. Soc. Glass. Tech.*, 8, 205-  
024 251.

025 Eppler R.A. (1966), Viscosity of Molten  $\text{B}_2\text{O}_3$ . *Journal of the American Ceramic Society*, 49, 679-680.  
026 <https://doi.org/10.1111/j.1151-2916.1966.tb13202.x>

027 Fanderlik I. (1990) *Silica Glass and Its Application*. Elsevier, Amsterdam.

028 Farnan I., and Stebbins J.F. (1990) High-temperature  $^{29}\text{Si}$  NMR investigation of solid and molten  
029 silicates. *J. Amer. Chem. Soc.*, 112, 32

030 Farnan, I., and Stebbins, J.F. (1994) The nature of the glass-transition in a silica-rich oxide melt, *Nature*,  
031 265, 1206-1209.

032 Fayon, F., Bessada, C., Massiot, D., Farnan, I., Coutures, J.P., 1998.  $^{29}\text{Si}$  and  $^{207}\text{Pb}$  NMR study of local  
033 order in lead silicate glasses. *J. Non-Cryst. Solids* 232, 403–408.

034 Fayon, F., Landron, C., Sakurai, K., Bessada, C., Massiot, D., 1999.  $\text{Pb}^{2+}$  environment in lead silicate  
035 glasses probed by Pb-LIII edge XAFS and  $^{207}\text{Pb}$  NMR. *J. Non-Cryst. Solids* 243, 39–44.

036 Feller, S., Lodden, G., Riley, A., Edwards, T., Croskrey, J., Schue, A., Liss, D., Stentz, D., Blair, S.,  
037 Kelley, M., Smith, G., Singleton, S., Affatigato, M., Holland, D., Smith, M.E., Kamitsos, E.L.,  
038 Varsamis, C.P.E., Loannou, E., 2010. A multispectroscopic structural study of lead silicate glasses  
039 over an extended range of compositions. *J. Non-Cryst. Solids* 356, 304–313.

040 Fiske P.S and Stebbins J.F. (1994) The structural role of Mg in silicate liquids: A high-temperature  $^{25}\text{Mg}$ ,  
041  $^{23}\text{Na}$ , and  $^{29}\text{Si}$  NMR study. *American Mineralogist*, Volume 79, pages 848-861, 1994

042 Florian P., Massiot D., Poe B., Farnan I. and Couture J.P. (1995) A time resolved  $^{27}\text{Al}$  NMR study of  
043 the cooling process of liquid alumina from  $2450^\circ\text{C}$  to crystallisation. *Sol. Stat. Magnet. Reson.*, 5,  
044 233-238.

045 Florian P., K.E. Vermillion, P.J. Grandinetti, I. Farnan, J.F. Stebbins, Cation distribution in mixed alkali  
046 disilicate glasses, *J. Am. Chem. Soc.* 118 (1996) 3493–3497.

047 Florian, P., Sadiki, N., Massiot, D., and Coutures J.P (2007)  $^{27}\text{Al}$  NMR study of the Structure of  
048 Lanthanum- and Yttrium-Based Aluminosilicate glasses and melts. *Journal of Physical Chemistry B*,  
049 111, 9747-9757.

050 Florian P., Novikov A., Drewitt J.W.E, Hennet L., Sarou-Kanian V., Massiot D., Fischer H.E. and  
051 Neuville D.R. (2018) Structure and Dynamics of High-Temperature Strontium Aluminosilicate Melts.  
052 *Physical Chemistry Chemical Physics*. 20, 27865-27877

053 Fulcher G.S. (1925) Analysis of recent measurements of the viscosity of glasses. *J. Am. Ceram. Soc.*, 8, 339

054 Fontana and Plummer (1966) A study of viscosity-temperature relation-ship in the  $\text{GeO}_2$  and  $\text{SiO}_2$   
055 system. *Phys Chem Glass*, 7, 139.

056 Frantz J.D. and Mysen B.O., 1995. Raman spectra and structure of  $\text{BaO-SiO}_2$ ,  $\text{SrO-SiO}_2$  and  $\text{CaO-SiO}_2$   
057 melts to  $1600^\circ\text{C}$ . *Chem. Geol.* 121, 155-176.

058 Frischat G.H., Poggemann J.F, Heide G. (2001) Nanostructure and atomic structure of glass seen by  
059 atomic force microscopy. *Journal of Non-Crystalline Solids* 345&346, 197–202

060 Frischat G.H. and Sebastian K, (1985) Leach resistance of nitrogen-containing  $\text{Na}_2\text{O-CaO-SiO}_2$  glasses.  
061 *J. Am. Ceram. Soc.*, 68, C305-C307.

062 Galeener F.L., Leadbetter A.J, Stringfellow M.W. (1983) Comparison of the neutron, Raman and infrared  
063 vibrational spectra of vitreous  $\text{SiO}_2$ ,  $\text{GeO}_2$ ,  $\text{BeF}_2$ . *Physical Review B*, 27, 1052-1079.

064 Gahay V.M.C., Tomozawa M. (1989) “The origine of phase separation in silicate melts and glasses.” *J.*  
065 *Non-Cryst. Solids*, 109, 27-34.

066 Gaskell P, , MC Eckersley, AC Barnes, P Chieux (1991) Medium-range order in the cation distribution  
067 of a calcium silicate glass. *Nature*, 350, pages675–677

068 Georges A.M. and Stebbins J.F. (1998) Structure and dynamics of magnesium in silicate melts: A high-  
069 temperature  $^{25}\text{Mg}$  NMR study *American Mineralogist*, Volume 83, pages 1022–1029, 1998

070 Gibbs J.H. and Dimarzio E.A. (1958) Nature of the glass transition and the glassy state. *J. Chem. Phys.*,  
071 28, 373

072 Giordano D. and Russell J. K. (2018) Towards a structural model for the viscosity of geological melts.  
073 *Earth Planet. Sci. Lett.* 501, 202–212.

074 Giordano D., Russell J. K. and Dingwell D. B. (2008) Viscosity of magmatic liquids: A model. *Earth*  
075 *Planet. Sci. Lett.* 271, 123–134.

076 Giordano, D., Dingwell, D.B., (2003). Non-Arrhenian multicomponent melt viscosity: a model. *Earth*  
077 *Planet. Sci. Lett.* 208, 337–349 Erratum *Earth Planet. Sci. Lett.* 221, 449.

078 Goldstein M. (1969) Viscous liquids and the glass transition: a potential energy barrier picture. *J. Chem.*  
079 *Phys.*, 51, 3728

080 Goldstein M. (1976) Viscous liquids and the glass transition. V. Sources of the excess specific heat of  
081 the liquid. *J. Chem. Phys.*, 64, 4767

082 Goldstein M. (2011) On the reality of the residual entropy of glasses and disordered crystals: The entropy  
083 of mixing. *Journal of Non-Crystalline Solids* **357**, 463–465.

084 Greaves, G.N., Fontaine, A., Lagarde, P., Raoux, D., and Gurman, S.J. (1981) Local structure of silicate  
085 glasses. *Nature*, 293, 611-616.

086 Greaves, G. N. Exafs and the structure of glass. *J. Non-Cryst. Solids* 71, 203–217 (1985).

087 Greig J.W (1927) Immiscibility in silicate melts. *American Journal of Science*. s5-13 (73) 1-44; DOI:  
088 <https://doi.org/10.2475/ajs.s5-13.73.1>

089 Grest G.S. and Cohen M.H. (1980) Liquids, glasses, and the glass transition: a free-volume approach ; in  
090 "Advances in Chemical Physics", 48, Prigogine I. and Rice S.A. eds John Wiley and Sons N.Y., 545

091 Gruener G. P. Odier, D. De Sousa Meneses, P. Florian, and P. Richet (2001) Bulk and local dynamics in  
092 glass-forming liquids: A viscosity, electrical conductivity, and study of aluminosilicate melts. *Phys.*  
093 *Rev. B* 64, 024206

094 Guignard, M. and Cormier, L. (2008) Environments of Mg and Al in MgO-Al<sub>2</sub>O<sub>3</sub>-SiO<sub>2</sub> glasses: a study  
095 coupling neutron and X-ray diffraction and Reverse Monte Carlo simulations. *Chemical Geology*.  
096 256, 111–118

097 Hannon, A.C. and Parker, J.M. (2000) The structure of aluminate glasses by neutron diffraction. *Journal*  
098 *of Non-Crystalline Solids*, 274, 102–109.

099 Hater W., W. Müller-Warmuth, M. Meier, G.H. Frischat, High-resolution solid-state NMR studies of  
100 mixed-alkali silicate glasses, *J. Non-Cryst. Solids* 113 (1989) 210–212.

101 El Hayek R., Ferey F., Florian P., Pisch A. and Neuville D.R. (2017) Structure and properties of lime  
102 alumino-borate glasses and melts. *Chemical Geology*, 461, 75-81.

103 Hehlen B., Courtens E., Yamanka A. and Inoue K., 2002. Nature of the Boson peak of silica glasses from  
104 hyper-Raman scattering. *J. Non-Cryst. Solids* 307, 185-190.

105 Hehlen B. and Neuville D.R. (2015) Raman response of network modifier cations in alumino-silicate  
106 glasses. *The Journal of Physical Chemistry B*. 119, 4093–4098.

107 Hehlen B. and Neuville D.R. (2020) Non-network-former cations in oxide glasses spotted by Raman  
108 scattering. *Physical Chemistry Chemical Physics*., 22, 12724 – 12731. DOI: 10.1039/D0CP00630K.

109 Hench L.L., 1991. *Bioceramics : from concept ot clinic*. *J. Am. Ceram. Soc.* 74, 1487-1510.

110 Henderson G.S., Neuville D.R., Cormier L. (2007) An O K-edge XANES study of Calcium Aluminates.  
111 *Can. J. Chem.*, 85, 801-806.

112 Henderson G.S. (1995) A Si K-edge EXAFS/XANES study of sodium silicate glasses. *Journal of Non-*



113 Crystalline Solids, 183, 43-50.

114 Hennet L. Drewitt J.W.E., Neuville D.R., Cristiglio V., Kozaily J., Brassamin S., Zanghi D., Fischer H.E.

115 (2016) Neutron diffraction of calcium aluminosilicate glasses and melts. *Journal of Non-Crystalline*

116 *Solids*. 451, 89-93.

117 Herzog F. et Zakaznova-Herzog V.P. (2011) Quantitative Raman spectroscopy: Challenges, shortfalls,

118 and solutions—Application to calcium silicate glasses. *American Mineralogist*, 96914–927

119 Hetherington G. Jack, H, Kennedy J.C. (1964) The viscosity of vitreous silica. *Physics and Chemistry of*

120 *Glass*. 5, 130-137.

121 Hiet, J., Deschamps, M., Pellerin, N., Fayon, F., Massiot, D., (2009) Probing chemical disorder in glasses

122 using silicon-29 NMR spectral editing. *Phys. Chem. Chem. Phys.* 11, 6935. doi:10.1039/b906399d

123 Higby, P. L., Ginther, R.J., Aggarwal, I.D., Friebele, E.J., (1990) Glass formation and thermal properties

124 of low-silica calcium aluminosilicate glasses. *J. Non-Cryst. Solids* 126, 209-215.

125 Hill R. and Brauer D.S. (2011) Predicting the bioactivity of glasses using the network connectivity or

126 split network models. *Journal of Non-Crystalline Solids* 357, 3884–3887

127 Hosono H. Yamazaki K, and abe Y. (1985) Dopant-Free Ultraviolet-Sensitive Calcium Aluminate

128 Glasses. *J. Am. Ceram. Soc.*, 68, C-304-C-305

129 Hudon P, Baker D.R. (2002a) The nature of phase separation in binary oxide melts and glasses. I. Silicate

130 systems. *Journal of Non-Crystalline Solids* 303, 299–345

131 Hudon P, Baker D.R. (2002b) The nature of phase separation in binary oxide melts and glasses. II.

132 Selective solution mechanism. *Journal of Non-Crystalline Solids* 303 (2002) 346–353

133 Hung I, Gan Z., Gor'kov P.L., Kaseman D.C., Sen S., LaComb M., Stebbins J.F. (2016) Detection of

134 “free” oxide ions in low-silica Ca/Mg silicate glasses: Results from  $17\text{O} \rightarrow 29\text{Si}$  HETCOR NMR.

135 *Journal of Non-Crystalline Solids*, 445–446, 1-6

136 Hui H. and Zhang Y. (2017) Toward a general viscosity equation for natural anhydrous and hydrous

137 silicate melts. *Geochimica et Cosmochimica Acta* 71 (2007) 403–416

138 Imaoka M. and Yamazaki T. (1963) Studies of the Glass-formation Range of Silicate

139 Systems. *Investigations on the Glass-formation Range*, 2. *J. Ceram. Assoc. Japan* , 79, 215-232.

140 Inaba S., Fujino S., Sakai K. (2010) Non-contact measurement of the viscosity of a soda–lime–silica melt

141 using electric field tweezers. *Phys. Chem. Glasses: Eur. J. Glass Sci. Technol. B*, 51, 304–308

142 Ispa S., Charpentier T., Mauri F. and Neuville D.R. (2010) Structural properties of Lithium and Sodium

143 tetrasilicate glasses: molecular dynamics simulations vs NMR experimental and first principles data.

144 *Solid State Sciences*, 12, 183-192.

145 Iuga D., Morais C., Gan Z., Neuville D.R., Cormier L., Massiot D. (2005)  $27\text{Al}/17\text{O}$  NMR correlation

146 in crystalline and vitreous materials. *J. Amer. Chem. Soc.*, 127, 11540-11542.

147 Jakse N., Bouhadja M., Kozaily J., Hennet L., Drewitt J.W.E., Neuville D.R., Fischer H. E., Cristiglio

148 V., Pasturel A. (2012) Interplay between non-bridging oxygen, triclusters, and fivefold Al  
149 coordination in low silica content calcium aluminosilicate melts. Applied Physics Letters, 101,  
150 201903-201908.

151 Joly, Y. (2001) X-ray absorption near edge structure calculations beyond the muffin-tin approximation.  
152 Phys. Rev. B, 63, 125120.

153 Jones A.R., Winter R., Greaves G.N, and Smith I.H., 2001. MAS NMR study of soda-lime silicate glasses  
154 with variables degree of polymerisation. J. Non-Cryst. Solids 293-295, 87-92.

155 Kanehashi, K. and Stebbins J.F. (2007) In situ high temperature  $^{27}\text{Al}$  NMR study of structure and  
156 dynamics in a calcium aluminosilicate glass and melt. Journal of Non-Crystalline Solids 353, 4001–  
157 4010.

158 Kashio S., Iguchi y., Goto t., Nishina y., Fuwa t. (1980) Raman Spectroscopic Study on the Structure of  
159 Silicate Slag. Transactions of the Iron and Steel Institute of Japan, 20, 251-253  
160 <https://doi.org/10.2355/isijinternational1966.20.251>

161 Kauzmann, W., 1948. The nature of the glassy state and the behavior of liquids at low temperatures.  
162 Chem. Rev. 43, 219-243.

163 Kim H-M, Miyaji F. And Kokubo T., 1995. Bioactivity of  $\text{Na}_2\text{O}$ - $\text{CaO}$ - $\text{SiO}_2$  glasses. J. Amer. Ceram.  
164 Soc. 78, 2405-2411.

165 King W. and Shelby J. (1996) Strontium calcium aluminate glasses. Physics and chemistry of glasses, 37,  
166 1-14.

167 Kim N. Bassiri R, Fejer M.M, Stebbins J.F. (2014) The structure of ion beamsputtered amorphous  
168 alumina films and effects of Zn doping: High-resolution  $^{27}\text{Al}$  NMR. Journal of Non-Crystalline Solids  
169 405, 1–6.

170 Kohara S., Ohno, M., Takata T., Usuki L, Morita H., Suzuya S., Akola S., Pusztai L. (2010) Lead silicate  
171 glasses: Binary network-former glasses with large amounts of free volume. PHYSICAL REVIEW B  
172 82, 134209

173 Koike A. and Tomozawa M., 2007, IR investigation of density changes of silica glass and soda-lime  
174 silicate glass caused by microhardness indentation. Journal of Non-Crystalline Solids, 353, 2318-2327

175 Koike A, Tomozawa M., Ito S., (2007), Sub-critical crack growth rate of soda-lime-silicate glass and less  
176 brittle glass as a function of fictive temperature. Journal of Non-Crystalline Solids, 353, 2675-2680

177 Kroecker, S. and Stebbins, J.F. (2000) Magnesium coordination environments in glasses and minerals:  
178 New insight from high-field magnesium-25 MAS NMR. American Mineralogist, 85, 1459–1464.

179 Kusabiraki K. and Shiraishi K.T.(1981) The infrared spectrum of vitreous fayalite. Journal of Non-  
180 Crystalline Solids. 44, 365-368.

181 Kusabiraki K. (1986) Infrared spectra of vitreous silica and sodium silicates containing titanium. Journal

182 of Non-Crystalline Solids, 79, 208-212

183 Lacy, E.D., 1963. Aluminium in glasses and melts. *Phys. Chem. Glasses* 4, 234-238.

184 Lange R. A. (1996) Temperature independent thermal expansivities of sodium aluminosilicate melts.

185 *Geochim. Cosmochim. Acta* 60, 4989-4996.

186 Lange R. A. (1997) A revised model for the density and thermal expansivity of K<sub>2</sub>O-Na<sub>2</sub>O-CaO-MgO-

187 Al<sub>2</sub>O<sub>3</sub>-SiO<sub>2</sub> liquids from 700 to 1900 K: extension to crustal magmatic temperatures. *Contrib.*

188 *Mineral. Petrol.* 130, 1-11.

189 Lange R. A. and Carmichael I. S. E. (1987) Densities of Na<sub>2</sub>O-K<sub>2</sub>O-CaO-MgO-Fe<sub>2</sub>O<sub>3</sub>-Al<sub>2</sub>O<sub>3</sub>-TiO<sub>2</sub>-

190 SiO<sub>2</sub> liquids: New-measurements and derived partial molar properties. *Geochim. Cosmochim. Acta*

191 51,2931-2946.

192 Lange RA, Navrotsky A (1992) Heat capacities of Fe<sub>2</sub>O<sub>3</sub>-bearing silicate liquids. *Contrib Mineral Petrol*

193 110:311-320

194 Lee S.K., Park S.Y, Yi Y.S., and Moon J. (2010) Structure and Disorder in Amorphous Alumina Thin

195 Films: Insights from High-Resolution. *J. Phys. Chem. C* 2010, 114, 13890–13894

196 Leko BK (1979) Viscosity of vitreous silica. *Fiz Khim Stekla* 5 : 258-278

197 Larson C. Doerr, Affatigato M, Feller S, Holland D and Smith M E (2006), A <sup>29</sup>Si MAS NMR study of

198 silicate glasses with a high-lithium content. *J. Phys.: Condens. Matter* 18, 11323–11331

199 doi:10.1088/0953-8984/18/49/023

200 Leko V. K., Gusakova N. K., Meshcheryakova E. V., and Prokhorova T. I. (1977) The effect of impurity

201 alkali oxides, hydroxyl groups, Al<sub>2</sub>O<sub>3</sub>, and Ga<sub>2</sub>O<sub>3</sub> on the viscosity of vitreous silica. *Sov. J. Glass*

202 *Phys. Chem.* 3, 204-210.

203 Lee, S.K. and J.F. Stebbins, (2003) Nature of cationmixing and ordering in Na-Ca silicate glasses and

204 melts, *J. Phys. Chem. B* 107 3141–3148, <http://dx.doi.org/10.1021/jp027489y>.

205 Lee S.K., Stebbins J. (2009) Effects of the degree of polymerization on the structure of sodium silicate

206 and aluminosilicate glasses and melts: An <sup>17</sup>O NMR study, *Geochim. Cosmochim. Acta* 73, 1109–

207 1119

208 Lee S. K. (2005) Structure and the extent of disorder in quaternary (Ca-Mg and Ca-Na) aluminosilicate

209 glasses and melts. *Am. Mineral.* 90, 1393–1401.

210 Lee S. K. and Stebbins J. F. (1999) The degree of aluminum avoidance in aluminosilicate glasses. *Am.*

211 *Mineral.* 84, 937–945.

212 Lee, S.K. and Stebbins, J.F. (2000) Al-O-Al and Si-O-Si sites in framework aluminosilicate glasses with

213 Si/Al=1: quantification of framework disorder. *Journal of Non-Crystalline Solids*, 270, 260-264.

214 Lee S.K. and Stebbins J.F. (2002) The extent of inter-mixing among framework units in silicate glasses

215 and melts. *Geochimica et Cosmochimica Acta*, 66, 303–309.

- 216 Lee S. K., Mysen B. O. and Cody G. D. (2003) Chemical order in mixed-cation silicate glasses and melts.  
217 Phys. Rev. B 68, 214206.
- 218 Lee S.K. and Kim E. J. (2015) Probing Metal-Bridging Oxygen and Configurational Disorder in  
219 Amorphous Lead Silicates: Insights from  $^{17}\text{O}$  Solid-State Nuclear Magnetic Resonance. The Journal  
220 of Physical Chemistry C, 119, 1, 748–756.
- 221 Lee S. K., Kim H.-I., Kim E. J., Mun K. Y. and Ryu S. (2016) Extent of Disorder in Magnesium  
222 Aluminosilicate Glasses: Insights from  $^{27}\text{Al}$  and  $^{17}\text{O}$  NMR. J. Phys. Chem. C 120, 737–749.
- 223 Léger, A., Rouan, D., Schneider, J., Barge, P., Fridlund, M., Samuel, B., Ollivier, M., Guenther, E.,  
224 Deleuil, M., Deeg, H.J., Auvergne, M., Alonso, R., Aigrain, S., Alapini, A., Almenara, J.M., Baglin,  
225 A., Barbieri, M., Bruntt, H., Bordé, P., Bouchy, F., Cabrera, J., Catala, C., Carone, L., Carpano, S.,  
226 Csizmadia, S., Dvorak, R., Erikson, A., Ferraz-Mello, S., Foing, B., Fressin, F., Gandolfi, D., Gillon,  
227 M., Gondoin, P., Grasset, O., Guillot, T., Hatzes, A., Hébrard, G., Jorda, L., Lammer, H., Llebaria,  
228 A., Loeillet, B., Mayor, M., Mazeh, T., Moutou, C., Pätzold, M., Pont, F., Queloz, D., Rauer, H.,  
229 Renner, S., Samadi, R., Shporer, A., Sotin, C., Tingley, B., Wuchterl, G., Adda, M., Agogu, P.,  
230 Appourchaux, T., Ballans, H., Baron, P., Beaufort, T., Bellenger, R., Berlin, R., Bernardi, P., Blouin,  
231 D., Baudin, F., Bodin, P., Boissard, L., Boit, L., Bonneau, F., Borzeix, S., Briet, R., Buey, J.-T., Butler,  
232 B., Cailleau, D., Cautain, R., Chabaud, P.-Y., Chaintreuil, S., Chiavassa, F., Costes, V., Parrho, V.C.,  
233 Fialho, F.D.O., Decaudin, M., Defise, J.-M., Djalal, S., Epstein, G., Exil, G.-E., Fauré, C., Fenouillet,  
234 T., Gaboriaud, A., Gallic, A., Gamet, P., Gavalda, P., Grolleau, E., Gruneisen, R., Gueguen, L., Guis,  
235 V., Guivarc'h, V., Guterman, P., Hallouard, D., Hasiba, J., Heuripeau, F., Huntzinger, G., Hustaix,  
236 H., Imad, C., Imbert, C., Johlander, B., Jouret, M., Journoud, P., Karioty, F., Kerjean, L., Lafaille, V.,  
237 Lafond, L., Lam-Trong, T., Landiech, P., Lapeyrere, V., Larqué, T., Laudet, P., Lautier, N., Lecann,  
238 H., Lefevre, L., Leruyet, B., Levacher, P., Magnan, A., Mazy, E., Mertens, F., Mesnager, J.-M.,  
239 Meunier, J.-C., Michel, J.-P., Monjoin, W., Naudet, D., Nguyen-Kim, K., Orcesi, J.-L., Ottacher, H.,  
240 Perez, R., Peter, G., Plasson, P., Plessier, J.-Y., Pontet, B., Pradines, A., Quentin, C., Reynaud, J.-L.,  
241 Rolland, G., Rollenhagen, F., Romagnan, R., Russ, N., Schmidt, R., Schwartz, N., Sebbag, I., Sedes,  
242 G., Smit, H., Steller, M.B., Sunter, W., Surace, C., Tello, M., Tiphène, D., Toulouse, P., Ulmer, B.,  
243 Vandermarcq, O., Vergnault, E., Vuillemin, A., Zanatta, P., 2009. Transiting exoplanets from the  
244 CoRoT space mission - VIII. CoRoT-7b: the first super-Earth with measured radius. Astron.  
245 Astrophys. 506, 287–302. <https://doi.org/10.1051/0004-6361/200911933>
- 246 Levin E.M., Robbins C.R. and Mc Murdie H.F. (1964) Phase diagram for ceramist, 2nd ed Amer Ceram  
247 Soc. Columbus, Ohio 601pp.
- 248 Losq C. and Neuville D.R. (2013) Effect of K/Na mixing on the structure and rheology of tectosilicate  
249 silica-rich melts. Chemical Geology, 346, 57-71.

250 Le Losq Ch., Neuville D.R., Florian P., G.S. Henderson and Massiot D. (2014) Role of Al<sup>3+</sup> on rheology  
251 and nano-structural changes of sodium silicate and aluminosilicate glasses and melts. *Geochimica*  
252 *Cosmochimica Acta*, 126, 495-517.

253 Le Losq C, Neuville D.R., Florian P., Massiot D., Zhou Z., Chen W., Greaves N. (2017) Percolation  
254 channels: a universal idea to describe the atomic structure of glasses and melts. *Scientific Reports*, 7,  
255 Article number: 16490, doi:10.1038/s41598-017-16741-3

256 Le Losq Ch., Neuville D.R. (2017) Molecular structure, configurational entropy and viscosity of silicate  
257 melts: link through the Adam and Gibbs theory of viscous flow. *Journal of Non-Crystalline Solids*.  
258 463, 175-188.

259 Le Losq C., Cicconi M.R., Greaves G.N. and Neuville D.R. (2019) Silicate glasses. *Springer Handbook*  
260 *of Glass*. 441-488 – DOI 10.1007/978-3-319-93728-1

261 Le Losq C., Valentine A., Mysen B.O., Neuville D.R. (2021) Deep learning model to predict the structure  
262 and properties of aluminosilicate glasses and melts. *Geochimica and Cosmochimica Acta*. DOI:  
263 <https://doi.org/10.1016/j.gca.2021.08.023>

264 de Ligny and Westrum E.F. (1996) Entropy of calcium and magnesium aluminosilicate glasses. *Chemical*  
265 *Geology* 128 113-128

266 Licheron M., Montouillout V., Millot F., Neuville D.R. (2011) Raman and <sup>27</sup>Al NMR structure  
267 investigations of aluminate glasses: (1-x)Al<sub>2</sub>O<sub>3</sub>- x MO, with M=Ca, Sr, Ba and 0.5<x<0.75). *Journal*  
268 *of Non Crystalline Solids*. 257, 2796-2801.

269 Lines, M. E., MacChesney, J. B., Lyons, K. B., Bruce, A. J., Miller, A. E., Nassau K., 1989. Calcium  
270 aluminate glasses as potential ultralow-loss optical materials at 1.5–1.9 μm. *J. Non-Cryst. Solids*  
271 107, 251-260.

272 Lockyer M.W.G., Holland D. and Dupree R., 1995. NMR investigation of the structure of some bioactive  
273 and related glasses. *J. Non-Crystal. Sol.* 188, 207-219.

274 Loewenstein, W., 1954. The distribution of aluminum in the tetrahedra of silicates and aluminates. *Am.*  
275 *Mineral.* 39, 92-96.

276 Macedo P.B and Litovitz P.B. (1965), On the relative roles of free volume and activation energy in the  
277 viscosity of liquids. *J. Chem. Phys.* 42, 24. <https://doi.org/10.1063/1.1695683>

278 McMillan, P., Piriou, B., 1983. Raman spectroscopy of calcium aluminate glasses and crystals. *J. Non-*  
279 *Cryst. Solids* 55, 221-242.

280 McMillan, P.F. and Kirkpatrick, R.J. (1992) Al coordination in magnesium aluminosilicate glasses.  
281 *American Mineralogist* 77, 898-900.

282 McMillan, P., Piriou, B., and Navrotsky, A. (1982) A Raman spectroscopic study of glasses along the  
283 joins silica-calcium aluminate, silica-sodium aluminate, and silica-potassium aluminate. *Geochimica*

284 and *Cosmochimica Acta*, 46, 2021-2037.

285 McMillan P. F. (1984) Structural studies of silicate glasses and melts - Applications and limitations of  
286 Raman spectroscopy. *Am. Mineral.* 69, 622–644.

287 Maekawa H., Maekawa T., Kawamura K. and Yokokawa T., 1991. The structural group of alkali silicate  
288 glasses determined from <sup>29</sup>Si MAS-NMR. *J. Non-Cryst. Solids* 127, 53-64.

289 Magnien V., Neuville D.R., Cormier L., Mysen B.O. and Richet P. (2004) Kinetics of iron oxidation in  
290 silicate melts: A preliminary XANES study. *Chem. Geol.*, 213, 253-263.

291 Magnien V, Neuville D.R., Cormier L., Roux J., Hazemann J-L., de Ligny D., Pascarelli S., Vickridge  
292 I., Pinet O. and Richet P. (2008) Kinetics and mechanisms of iron redox reactions in silicate melts:  
293 The effects of temperature and alkali cations. *Geochim. Cosmochim. Acta.*, 72, 2157-2168.

294 Malfait W. J. (2009) Quantitative Raman spectroscopy: speciation of cesium silicate glasses. *J. Raman  
295 Spectrosc.* 40, 1895–1901.

296 Malfait W. J., Zakaznova-Herzog V. P. and Halter W. E. (2007) Quantitative Raman spectroscopy: high-  
297 temperature speciation of potassium silicate melts. *J. Non-Cryst. Solids* 353, 4029–4042.

298 Massiot D., Fayon F., Montouillout V., Pellerin N., Hiet J., Roiland C., Florian P., Coutures J-P. , Cormier  
299 L. and Neuville D.R. (2008) Structure and dynamics of oxide melts and glasses: a view from  
300 multinuclear and high temperature NMR. *J. Non-Crystal Solids.* 354, 249-254.

301 Mastelaro V, Zanotto E., Lequeux N., Cortes R. (2000) Relationship between short-range order and ease  
302 of nucleation in Na<sub>2</sub>Ca<sub>2</sub>Si<sub>3</sub>O<sub>9</sub>, CaSiO<sub>3</sub> and PbSiO<sub>3</sub> glasses. *Journal of Non-Crystalline Solids* 262,  
303 191-199

304 Mauro J. (2011) Through a Glass, Darkly: Dispelling Three Common Misconceptions in Glass Science.  
305 *International Journal of Applied Glass Science* 2 [4] 245–261

306 Mauro J. , Y. Yue, A.J. Ellison, P.K. Gupta, D.C. Allan, (2009) Viscosity of glass-forming liquids, *Proc.  
307 Natl. Acad. Sci.* 106 (2009) 19780–19784.

308 Méducin F., Redfern S.A.T., Le Godec Y., Stone H.J., Tucker M.G., Dove M.T. and Marshall W.G.  
309 (2004) Study of cation order-disorder in MgAl<sub>2</sub>O<sub>4</sub> spinel by in situ neutron diffraction up to 1600K  
310 and 3.2GPa. *Americ Mineral.*, 89, 981-986.

311 Meiling G.S. and Uhlmann D.R., 1977. Crystallisation and melting kinetics of soda disilicate. *Phys.  
312 Chem. Glas.* 8, 62-68.

313 Merzbacher, C.I., Sheriff, B.L., Hartman, J.S., White, W.B., 1990. A high-resolution <sup>29</sup>Si and <sup>27</sup>Al NMR  
314 study of alkaline-earth aluminosilicate glasses. *J. Non-Cryst. Solids* 124, 194-206.

315 Merzbacher, C.I., McGrath, K.J., Highby, P.L., 1991. <sup>29</sup>Si NMR and infrared reflectance spectroscopy  
316 of low-silica calcium aluminosilicate glasses. *J. Non-Cryst. Solids* 136, 249-259.

317 Merzbacher C. I. and White W. B. (1991) The structure of alkaline-earth aluminosilicate glasses as

determined by vibrational spectroscopy. *J. Non-Cryst. Solids* 130, 18–34.

Moore and Carey (1951) Limiting Compositions of Binary Glasses of the Type  $xR_2O \cdot SiO_2$  and of Ternary Glasses of Types  $yR_2O \cdot yR_2O_3 \cdot SiO_2$  in Relation to Glass Structure. *Trans. Soc. Glass Technol.*,

Morey G. W. and Bowen N.L., 1925. The melting relations of the soda-lime-silica glasses. *J. Soc. Glass. Tech.* 9, 226-264.

Moretti R. (2005). Polymerisation, basicity, oxidation state and their role in ionic modelling of silicate melts. *Annals of Geophysics*, 48, 4/5, 583-608.

Morey G. (1930) The devitrification of soda-lime-silica glasses. *Journal of the American Ceramic Society*. 683-714.

Morikawa, H., Takagi, Y., Ohno, H., 1982. Structural analysis of  $2PbO \cdot SiO_2$  glass. *J. Non-Cryst. Solids* 53, 173–182.

Mossa S., La Nave E., Stanley H. E., Donati C., Sciortino F. and Tartaglia P. (2002) Dynamics and Configurational Entropy in the LW Model for Supercooled Orthoterphenyl. *Condensed Matter*. arXiv:cond-mat/0111519v2

Moulton B. and Henderson G.S. (2021) Glasses: Alkali and Alkaline-Earth Silicates. *Encyclopedia of Materials: Technical Ceramics and Glasses*, vol. 2, pp. 462–482. Oxford: Elsevier. <http://dx.doi.org/10.1016/B978-0-12-818542-1.00050-3>.

Moynihan C.T. Easteal A.J. Wilder J. (1974) Dependence of the glass transition temperature on heating and cooling rate. *The Journal of Physical Chemistry*. 78, 2873-2879.

Moynihan C.T., Sasabe J. Tucker (1976) Kinetics of the Glass Transition in a Calcium-Potassium Nitrate Melt. *Proceedings of The Electrochemical Society*, 6, 182-194

Moynihan C.T., Gupta P.K. (1978) The order parameter model for structural relaxation in glass. *J. Non-Cryst. Solids.*, 29, 143

Moynihan C.T., Easteal A.J., Tran D.C., Wilder J.A. and Donovan E.P. (1976a) Heat capacity and structural relaxation of mixed-alkali glasses. *J. Phys. Chem.*, 78, 2673

Moynihan C.T., Macedo P.B., Montrose C.J., Gupta P.K., De Bolt M.A., Dill J.F., Dom B.E., Drake P.W., Easteal A.J., Elterman P.B., Moeller R.P., Sasabe M. and Wilder J.A. (1976b) Structural relaxation in vitreous materials. *Ann. New-York Acad. Sci.*, 279, 15

Musgraves J.D., J. Hu, L. Calvez (Eds.), *Springer Handbook of Glass*, Springer Handbooks, [https://doi.org/10.1007/978-3-319-93728-1\\_1](https://doi.org/10.1007/978-3-319-93728-1_1)

Murdoch, J.B., Stebbins, J.F., and Carmichael, I.S.E. (1985) High-resolution  $^{29}Si$  NMR study of silicate and aluminosilicate glasses: the effect of network modifying cations. *American Mineralogist*, 70, 332-343.

352 Mysen B.O. (1990) Role of Al in depolymerized, peralkaline aluminosilicate melts in the systems  $\text{Li}_2\text{O}-$   
353  $\text{Al}_2\text{O}_3-\text{SiO}_2$ ,  $\text{Na}_2\text{O}-\text{Al}_2\text{O}_3-\text{SiO}_2$ , and  $\text{K}_2\text{O}-\text{Al}_2\text{O}_3-\text{SiO}_2$ , *Am. Mineral.* 75,120–134.

354 Mysen, B.O. (1999). Structure and properties of magmatic liquids: From haplobasalt to haploandesite.  
355 *Geochimica and Cosmochimica Acta* 63: 95-112.

356 Mysen B. O. (1995) Experimental, in situ, high-temperature studies of properties and structure of silicate  
357 melts relevant to magmatic processes. *Eur. J. Mineral.* 7, 745–766.

358 Mysen B. O. (1990) Role of Al in depolymerized, peralkaline aluminosilicate melts in the systems  $\text{Li}_2\text{O}-$   
359  $\text{Al}_2\text{O}_3-\text{SiO}_2$ ,  $\text{Na}_2\text{O}-\text{Al}_2\text{O}_3-\text{SiO}_2$ , and  $\text{K}_2\text{O}-\text{Al}_2\text{O}_3-\text{SiO}_2$ . *Am. Mineral.* 75, 120–134.

360 Mysen B.O. J.D. Frantz (1993) Structure of silicatemelts at high temperature: in-situ measurements in  
361 the system  $\text{BaO}-\text{SiO}_2$ , *Am. Mineral.* 78, 699–709.

362 Mysen, B.O. J.D. Frantz, Structure of haplobasaltic liquids at magmatic temperatures: in situ, high-  
363 temperature study of melts on the join  $\text{Na}_2\text{Si}_2\text{O}_5-\text{Na}_2(\text{NaAl})_2\text{O}_5$ , *Geochim. Cosmochim. Acta* 58  
364 (1994) 1711–1733.

365 Mysen B. O., Lucier A. and Cody G. D. (2003) The structural behavior of  $\text{Al}^{3+}$  in peralkaline melts and  
366 glasses in the system  $\text{Na}_2\text{O}-\text{Al}_2\text{O}_3-\text{SiO}_2$ . *Am. Mineral.* 88, 1668–1678.

367 Mysen B. O., Virgo D. and Seifert F. A. (1982) The structure of silicate melts: Implications for chemical  
368 and physical properties of natural magma. *Rev. Geophys.* 20, 353–383.

369 Mysen, B.O., Virgo, D., and Kushiro, I. (1981) The structural role of aluminum in silicate melts -A  
370 Raman spectroscopic study at 1 atmosphere. *American Mineralogist*, 66, 678-701.

371 Nakamura K., Takahashi Y., Osada M. and Fujiwara T. (2013) Low-frequency Raman scattering in  
372 binary silicate glass: Boson peak frequency and its general expression. *J. Ceram. Soc. Japan* 121,  
373 1012–1014.

374 Napolitano A.n Macedo P.B. and Hawkins E.G. (1965). Viscosity and Density of Boron Trioxide. *Journal*  
375 *of the American Ceramic Society.* <https://doi.org/10.1111/j.1151-2916.1965.tb14690.x>

376 Navrotsky, A., Perandeanu, P., McMillan, P.F., and Coutures, J.P. (1982) A thermochemical study of  
377 glasses and crystals along the joins silica-calcium aluminate and silica-sodium aluminate. *Geochimica*  
378 *and Cosmochimica Acta*, 46, 2039-2049.

379 Navrotsky A., Geisinger K., P., Gibbs G.V. (1985) The tetrahedral framework in glasses and melts —  
380 inferences from molecular orbital calculations and implications for structure, thermodynamics, and  
381 physical properties. *Physics and Chemistry of Minerals* volume 11, pages284–298

382 Natrup F.V., Bracht H, Murugavel S. and Roling B. (2005) Cation diffusion and ionic conductivity in  
383 soda-lime silicate glasses. *Phys. Chem. Chem. Phys.* 7, 2279 – 2286

384 Nernst W. (1911) *Theoretical Chemistry*,” London, 810p.

385 Nesbitt H.W, O’Shaughnessy C., Bancroft G.M., Henderson G.S., and Neuville D.R. (2018) Factors



386 affecting line shapes and intensities of Q3 and Q4 Raman bands of Cs silicate glasses. *Chemical*  
387 *Geology*. 10.1016/j.chemgeo.2018.12.009

388 Nesbitt, H.W., Henderson, G.S., Bancroft, G.M., Neuville D.R., (2021) Spectral resolution and Raman  
389 Q and Q cross sections. *Chemical Geology*. DOI : 10.1016/j.chemgeo.2020.120040

390 Neuville D.R. (1992) Etude des Propriétés Thermodynamiques et Rhéologiques des Silicates Fondus.  
391 Thèse de l'Université de Paris VII, spécialité Géochimie Fondamentale.

392 Neuville D.R., (2005) Structure and properties in (Sr, Na) silicate glasses and melts. *Phys Chem Glasses*,  
393 46, 112-119.

394 Neuville D.R. (2006) Viscosity, structure and mixing in (Ca, Na) silicate melts. *Chem. Geol.*, 229, 28-  
395 42. Neuville D.R. et Richet P. (1990) Viscosité et entropie des silicates fondus. *Rivista del la Staz.*  
396 *Sper. Vetro*, 6, 213-221.

397 Neuville D.R. and Richet P. (1991) Viscosity and mixing in molten (Ca,Mg) pyroxenes and garnets.  
398 *Geochim. Cosmochim. Acta.*, 55, 1011-1021.

399 Neuville D.R. and Mysen B.O (1996) Role of aluminium in the silicate network: in situ, high-temperature  
400 study of glasses and melts on the join SiO<sub>2</sub>-NaAlO<sub>2</sub>. *Geochimica Cosmochimica Acta.*, 60, 1727-  
401 1737.

402 Neuville D.R., Cormier L, R., Flank A.M., Prado R.J. and Lagarde P. (2004) Na K-edge XANES spectra  
403 of minerals and glasses. *Eur. J Mineral*, 16, 809-816.

404 Neuville D.R., Cormier L, Flank A.M. and Lagarde P. Massiot D. (2004) Aluminum X-ray absorption  
405 near edges structure in minerals and glasses. *Chem Geol.*, 213, 153-163.

406 Neuville D.R., Cormier L. and Massiot D. (2004) Role of aluminium in peraluminous region in the CAS  
407 system. *Geochim. Cosmochim. Acta.*, 68, 5071-5079.

408 Neuville D.R., Cormier L, Flank A.M, Lagarde P. (2005) A XANES study at the Na and Al K-edge of  
409 soda-lime aluminosilicate glasses. *Phys. Scripta.*, 115, 316-318.

410 Neuville D.R., Cormier L., Massiot D. (2006) Al speciation in calcium aluminosilicate glasses: A NMR  
411 and Raman spectroscopie. *Chem Geol.*, 229, 173-185

412 Neuville D.R., Courtial P., Dingwell D.B. and Richet P. (1993) Thermodynamic and rheological  
413 properties of rhyolite and andesite melts. *Contrib. Mineral. Petrol.*, 113, 571-581.

414 Neuville D.R. Cormier L., Montouillout V., Massiot D. (2007) Local environment of Al in  
415 aluminosilicate glasses: a NMR point of view. *J. Non Crystal Solid*, 353, 180-185.

416 Neuville D.R., Cormier L., Montouillout V., Florian P., Millot F., Rifflet J.C. and Massiot D. (2008a)  
417 Structure of Mg- and Mg/Ca aluminosilicate glasses: <sup>27</sup>Al NMR and Raman spectroscopy  
418 investigations. *American Mineralogist* 83, 1721-1731.

419 Neuville D.R. Cormier L., Flank AM, de Ligny D., Roux J. and Lagarde P. (2008b) Environment around

420 Al, Si and Ca in aluminate and aluminosilicate melts by X-ray absorption spectroscopy at high  
421 temperature. *American Mineralogist*, 93, 228-234.

422 Neuville D.R., de Ligny D., Cormier L., Henderson G.S., Roux J., Flank AM, and Lagarde P. (2009) The  
423 crystal and melt structure of spinel and alumina at high temperature: an in-situ XANES study at the  
424 Al and Mg K-edge. *Geochimica Cosmochimica Acta*, 73, 3410-3422.

425 Neuville D.R., Henderson G.S., Cormier L., Massiot D. (2010) Structure of CaO-Al<sub>2</sub>O<sub>3</sub> crystal, glasses  
426 and liquids, using X-ray absorption at Al L and K edges and NMR spectroscopy. *American*  
427 *Mineralogist*, 95, 1580-1589.

428 Neuville D.R., Henderson G.S and de Ligny D. (2014) Advances in Raman Spectroscopy Applied to  
429 Earth and Material Sciences. In Henderson G.S, Neuville D.R., Down B. (2014) "Spectroscopic  
430 methods in Mineralogy and Material Sciences" *Review in Mineralogy and Geochemistry*, Vol 78,  
431 509-541.

432 Neuville D.R., Hennet L., Florian P., de Ligny D. (2014) In situ high temperature experiment. In  
433 Henderson G.S, Neuville D.R., Down B. (2014) "Spectroscopic methods in Mineralogy and Material  
434 Sciences" *Review in Mineralogy and Geochemistry*, Vol 78, 779-800.

435 Novikov A., Neuville D.R., Hennet L., Thiaudière D., Gueguen Y., Florian P. (2017) Al and Sr  
436 environment in tectosilicate glasses and melts: viscosity, Raman and NMR investigation. *Chemical*  
437 *Geology*, 461, 115-127.

438 Alexey Novikov (2017) Structure et propriétés des aluminosilicates de Sr, Ba et Zn, Université d'Orléans

439 Ohtani E., Taulelle F., Angell C.A. (1985) Al<sup>3+</sup> coordination changes in aluminosilicates under pressure.  
440 *Nature*, 314, 78-82.

441 O'Shaughnessy C., Henderson G.S., Nesbitt H.W., Bancroft G.M., Neuville D.R. (2017) The structure of  
442 caesium silicate glasses and melts: implications for the interpretation of Raman spectra. *Chemical*  
443 *Geology*, 461, 82-95.

444 O'Shaughnessy C., Henderson G. S., Nesbitt H.W, Bancroft G.M., Neuville D.R. (2020) The behaviour  
445 of modifier cations in alkali silicate glasses. *Journal of the American Ceramic Society*. DOI:  
446 10.1111/jace.17081

447 Parks G.S. and Huffman H.M. (1926) Glass as a fourth state of matter. *Science*, 64, 364 (1926).

448 Parks G.S. and Huffman H.M. (1927) Studies on glass. I. The transition between the glassy and liquid  
449 states in the case of some simple organic compound. *J. Phys. Chem.*, 31, 1842

450 Pena R.B., Sampaio D.V., Lancelotti R.F., Cunha T.R., Zanotto E.D., Pizani P.S. (2020) In-situ Raman  
451 spectroscopy unveils metastable crystallization in lead metasilicate glass. *Journal of Non-Crystalline*  
452 *Solids*. Volume 546, 120254

453 Persikov E. S. (1991) The viscosity of magmatic liquids : experiment, generalized patterns. A model for

454 calculation and prediction. Applications. *Adv. Phys. Geochem.* 9, 1–40.

455 Petit A. T. and Dulong P. L. (1819) Recherches sur quelques points importants de la théorie de la chaleur,  
456 dans *Annales de chimie et de physique*, 10, 395–413

457 Poe B.T., Romano C., Zotov N., Cinin G., Marcelli A. (2001) Compression mechanism in aluminosilicate  
458 melts : Raman and XANES spectroscopy of glasses quenched from pressures up to 10Gpa. *Chem*  
459 *Geol.*, 174, 21-31.

460 Poe, B.T., McMillan, P.F., Angell, C.A., and Sato, R.K. (1992) Al and Si coordination in SiO<sub>2</sub>-Al<sub>2</sub>O<sub>3</sub>  
461 glasses and liquids: a study by NMR and IR spectroscopy and MD simulations. *Chemical Geology*,  
462 96, 333-349.

463 Poole J.P., 1948. Viscosité à basse température des verres alcalino-silicatés. *Verres Réfrac.* 2, 222-230.

464 Popov A.I. (2018) What is glass? *Journ. Non-Cryst. Solids* **502**, 249–250.

465 Poulain M. and Lucas J. (1970) NEW TRANSITION METAL FLUOROZIRCONATES. *Comptes*  
466 *Rendus de Seances de l'Academie des Sciences.* 281, 2345-2349.

467 Poulain M. (1983) Halide glasses. *Journal of Non-Crystalline Solids*, 56, 1-14

468 Putnis, A. (1992) An introduction to mineral sciences. Cambridge press, ISBN 0521 419220

469 Rankin G. A., (1915) The ternary system CaO-Al<sub>2</sub>O<sub>3</sub>-SiO<sub>2</sub>. *Amer. J. Sci.*, 39, 1-79.

470 Rekhson S.M. (1989) Computer modeling of glass behavior. Congress on glass in Leningrad, U.S.S.R.

471 Rekhson S.M. (1975) Relaxation of Glass, *Sov. J. Glass Phys. Chem.*, 1 (1975) 417.

472 Rekhson S.L. (1980) Viscosity and stress relaxation in commercial glasses in the glass transition region.  
473 *Journal of Non-Crystalline Solids*, 38-39; 457-462

474 Richet P. (1984) Viscosity and configurational entropy of silicate melts. *Geochim. Cosmochim. Acta* 48,  
475 471–483.

476 Richet, P. and Bottinga, Y. (1985) Heat capacity of aluminum-free liquid silicates. *Geochimica et*  
477 *Cosmochimica Acta*, 49, 471–486.

478 Richet P. (1987) Heat capacity of silicate glasses. *Chem. Geol.* 62, 111–124.

479 Richet P. (2009) Residual and configurational entropy: Quantitative checks through applications of  
480 Adam-Gibbs theory to the viscosity of silicate melts. *Journal of Non-Crystalline Solids* **355**, 628–635.

481 Richet P. and Bottinga Y. (1984) Glass transitions and thermodynamic properties of amorphous SiO<sub>2</sub>,  
482 NaAlSi<sub>3</sub>O<sub>8</sub> and KAlSi<sub>3</sub>O<sub>8</sub>. *Geochim. Cosmochim. Acta* 48, 453–470.

483 Richet P. and Neuville D.R. (1992) Thermodynamics of silicates melts: Configurational properties. *Adv.*  
484 *Phys. Geochim.*, 10, 132-161. [https://doi.org/10.1007/978-1-4612-2842-4\\_5](https://doi.org/10.1007/978-1-4612-2842-4_5)

485 Richet P., Robie R. A. and Hemingway B. S. (1986) Lowtemperature heat capacity of diopside glass  
486 (CaMgSi<sub>2</sub>O<sub>6</sub>): a calorimetric test of the configurational entropy theory applied to the viscosity of  
487 liquid silicates. *Geochim. Cosmochim. Acta* 50, 1521–1533.

488 Richet P., Nidaira A., Neuville D.R. and Atake T. (2009a) Aluminum speciation, vibrational entropy and  
489 short-range order in calcium aluminosilicate glasses *Geochimica Cosmochimica Acta*, 73, 3894-3904.

490 Richet P., Nidaira A., Neuville D.R., Atake T. (2009b) Low-temperature heat capacity and short-range  
491 order in alkaline-earth metasilicates. *American Mineralogist*, 94, 1591-1596.

492 Riebling E. F. (1966) Structure of sodium aluminosilicate melts containing at least 50 mol% SiO<sub>2</sub> at  
493 1500°C. *J. Chem. Phys.* 44, 2857–2865.

494 Risbud, S.H., Kirkpatrick, R.J., Tagliavere, A.P., Montez, B. (1987) Solid-state NMR evidence of 4-,  
495 5- and 6-fold aluminum site in roller-quenched SiO<sub>2</sub>-Al<sub>2</sub>O<sub>3</sub> glasses. *Journal of the American*  
496 *Ceramics Society*, 70, C10-C12.

497 Ritland H.N. (1954) Density phenomena in the transformation range of a borosilicate crown glass. *J. Am.*  
498 *Ceram. Soc.*, 37, 370

499 Robert G., Smith R. A. and Whittington A. G. (2019) Viscosity of melts in the NaAlSiO<sub>4</sub>-KAlSiO<sub>4</sub>-  
500 SiO<sub>2</sub> system: Configurational entropy modelling. *J. Non-Cryst. Solids* 524, 119635.

501 Rosenhauer M., Scarfe C.M. and Virgo D. (1979) Pressure dependence of the glass transition temperature  
502 in glasses of diopside, albite, and sodium trisilicate composition. *Carnegie Inst. Wash. Yearb.*, 78, 547

503 Robie R.A, Hemingway B.S. and Fisher J.R. (1979) Thermodynamic Properties of Mineral and related  
504 substance at 298,15K and 1 bar Pressure and at higher temperature. *USGS Bulletin* 1432.

505 Roling, B., Ingram, M.D., 2000. Mixed alkaline-earth effects in ion conducting glasses. *J. Non-Cryst.*  
506 *Solids* 265, 113–119.

507 Roy, B.N. and Navrotsky, A. (1984) Thermochemistry of charge-coupled substitution in silicate glasses:  
508 the system M<sub>1</sub>/nn+AlO<sub>2</sub>-SiO<sub>2</sub> (M=Li, Na, K, Rb, Cs, Mg, Ca, Sr, Ba, Pb) *Journal of the American*  
509 *Ceramic Society*, 67, 606-610.

510 Russell, J.K. D. Giordano, (2005) A model for silicate melt viscosity in the system CaMgSi<sub>2</sub>O<sub>6</sub>-  
511 CaAl<sub>2</sub>Si<sub>2</sub>O<sub>8</sub>-NaAlSi<sub>3</sub>O<sub>8</sub>, *Geochim. Cosmochim. Acta* 69 5333–5349,  
512 <http://dx.doi.org/10.1016/j.gca.2005.06.019>.

513 Russell J. K. and Giordano D. (2017) Modelling configurational entropy of silicate melts. *Chem. Geol.*  
514 461, 140–151.

515 Ryan M. and Blevins S., 1987. Viscosity of silicate melts and glasses. U.S.G.S. 1764. 1080pp

516 Sampaio D.V., Picinin A., Moulton B.J., Rino J.P., Pizani P.S., Zanutto E.D. (2018) Raman scattering  
517 and molecular dynamics investigation of lead metasilicate glass and supercooled liquid structures.  
518 *Journal of Non-Crystalline Solids* 499, 300–308

519 Sato, R. K., McMillan, P. F., Dennison, P., Dupree, R., 1991. High-resolution <sup>27</sup>Al and <sup>29</sup>Si MAS NMR  
520 investigation of SiO<sub>2</sub>-Al<sub>2</sub>O<sub>3</sub> glasses. *J. Phys. Chem.* 95, 4483-4489.

521 Schreiber, H.D. (1986) REDOX PROCESSES IN GLASS-FORMING MELTS. *Journal of Non-*  
522 *Crystalline Solids* 84, 129-141

523 Schmelzer J. and Tropin T. (2018) Glass Transition, Crystallization of Glass-Forming Melts, and  
524 Entropy. *Entropy* 20, 103.

525 Schmelzer J.W.P., Abyzov A.S and Fokin W.M. (2016) Thermodynamic Aspects of Pressure-Induced  
526 Crystallization: Kauzmann Pressure International Journal of Applied Glass Science, 7, 474-486.

527 Sakamaki and Ohtani (2021) High pressure melts. *Review in Mineralogy and Geochemistry*. (this issues)

528 Sasabe H., De Bolt M.A., Macedo P.B., Moynihan C.T. (1977) Structural relaxation in an alkali-lime-  
529 silicate glass. *Proc. XIth International Congress on Glass*, 1, 339

530 Sharma S.K., Virgo D. and Mysen B.O. (1978) Structural of glasses and melts of  $\text{Na}_2\text{O} \cdot x\text{SiO}_2$  ( $x = 1,2,3$ )  
531 composition from Raman spectroscopy. *Carnegie Inst. Wash. Yearb.*, 77, 649

532 Sharma S.K., J.A. Philpotts, D.W. Matson (1985) Ring distributions in alkali- and alkaline-earth  
533 aluminosilicate framework glasses – A Raman spectroscopic study, *J. Non-Cryst. Solids* 71, 403–410

534 Shaw, H.R. (1972) Viscosities of magmatic silicate liquids: an empirical method of prediction, *Am. J.*  
535 *Sci.* 272 870–893.

536 Shi C., Alderman O., Berman D., Du J., Neufeind J., Tamalonis A., Weber R., You J., Benmore C.  
537 (2019) The structure of amorphous and deeply supercooled liquid alumina. *Front. Mater.*, 19 March  
538 2019 | <https://doi.org/10.3389/fmats.2019.00038>

539 Schneider, V.R. Mastelaro, E.D. Zanotto, B.A. Shakhmatkin, N.M. Vedishcheva, A.C. Wright, H.  
540 Panepucci: (2003) Qn distribution in stoichiometric silicate glasses: thermodynamic calculations and  
541  $^{29}\text{Si}$  high resolution NMR measurements, *J. Non- Cryst. Solids* 325, 164–178

542 Schuller S. (2017) Phase separation processes in glass in Neuville et al., 2017 EDP Sciences. 665pp.  
543 ISBN 978-2-7598-1783-2

544 Shevyakov A.M., Trofinenko A.V., Sizonzko A.P., Burkov V.P. and Zhuravlev G.I. (1978) Study of  
545 the structure and crystallisation of melts of the system  $\text{Li}_2\text{O}-\text{SiO}_2$  by high temperature infrared  
546 spectroscopy. *Zh. Priklad. Khim.*, 51, 2612

547 Schairer J. F. and Bowen N. L. (1956) The system  $\text{Na}_2\text{O}-\text{Al}_2\text{O}_3-\text{SiO}_2$ . *Am. J. Sci.* 254, 129–195.

548 Scherer G. W. (1984) Use of the Adam-Gibbs Equation in the Analysis of Structural Relaxation. *J. Am.*  
549 *Ceram. Soc.* 67, 504–511.

550 Seifert, F. A., Mysen, B. O., & Virgo, D. (1982). Three-dimensional network structure in the systems  
551  $\text{SiO}_2-\text{NaAlO}_2$ ,  $\text{SiO}_2-\text{CaAl}_2\text{O}_2$  and  $\text{SiO}_2-\text{MgAl}_2\text{O}_2$ . *Amer. Mineral.*, 67, 696-711.

552 Sen S., George A.M., Stebbins J.F. (1996) Ionic conduction and mixed cation effect in silicate glasses  
553 and liquids:  $^{23}\text{Na}$  and  $^7\text{Li}$  NMR spin-lattice relaxation and a multiple-barrier model of percolation.  
554 *Journal of non-crystalline solids*, 197, 53-59.

555 Sen S., R.E. Youngman, (2003) NMR study of Q-speciation and connectivity in  $\text{K}_2\text{O}-\text{SiO}_2$  glasses with  
556 high silica content. *Journal of Non-Crystalline Solids*, 331, 100–107,  
557 <http://dx.doi.org/10.1016/j.jnoncrysol.2003.08.071>.

558 Sen S., Maekawa H. and G. Papatheodorou. (2009) Short-Range Structure of Invert Glasses along the  
559 Pseudo-Binary Join  $\text{MgSiO}_3\text{-Mg}_2\text{SiO}_4$ : Results from  $^{29}\text{Si}$  and  $^{25}\text{Mg}$  MAS NMR Spectroscopy. *J.*  
560 *Phys. Chem. B* 2009, 113, 46,

561 Shan Z., Liu S., Tao H. and Yue Y. (2018) Mixed alkaline-earth effects on several mechanical and  
562 thermophysical properties of aluminate glasses and melts. *Journal of the American Ceramic Society.*  
563 102, 1128–1136. DOI: 10.1111/jace.15975.

564 Shimoda, K., Tobu, Y., Shimoikeda, Y., Nemoto, T., and Saito K. (2007a) Multiple  $\text{Ca}^{2+}$  environments  
565 in silicate glasses by high-resolution  $^{43}\text{Ca}$  MQMAS NMR technique at high and ultra-high (21.8 T)  
566 magnetic fields. *Journal of Magnetic Resonance*, 186, 114–117.

567 Shimoda, K., Tobu, Y., Hatakeyma, M., Nemoto, T., and Saito K. (2007b) Structural investigation of Mg  
568 local environments in silicate glasses by ultra-high field  $^{25}\text{Mg}$  3QMAS NMR spectroscopy. *American*  
569 *Mineralogist*, 92, 695-698.

570 Schirmacher W. and Ruocco G. (2020) Heterogeneous Elasticity: The tale of the boson peak. *Condensed*  
571 *Matter.* arXiv:2009.05970

572 Schirmacher W., Ruocco G. Mazzone V. (2015) Heterogeneous viscoelasticity: a combined theory of  
573 dynamic and elastic heterogeneity. *Phys. Rev. Lett.* 115, 015901

574 Simmons J.H., S.A. Mills and A. Napolitano, (1974) Viscous flow in glass during phase separation *J.*  
575 *Am. Ceram. Soc.* 57 109.

576 Simmons J.H., A. Napolitano and P.B. Macedo, (1970) Supercritical viscosity anomaly in oxide mixtures  
577 *J. Chem. Phys.* 53 1170.

578 Sipp A., Neuville D.R. and Richet P. (1997) Viscosity and configurational entropy of borosilicate melts.  
579 *J. Non-Crystal. Solids.*, 211, 281-293.

580 Sossman, (1933) The “Physical Chemistry” of a System of Refractory Components. *Journal of the*  
581 *American Ceramic Society.* <https://doi.org/10.1111/j.1151-2916.1933.tb17098.x>

582 Sreenivasan H. Kinnunen P., Adesanya E., Patanen M., Kantola A., (2020) Field Strength of Network-  
583 Modifying Cation Dictates the Structure of (Na-Mg) Aluminosilicate Glasses. *Frontier in Material.*  
584 doi: 10.3389/fmats.2020.00267

585 Starodub K., Wu G., Yazhenskikh E., Müller M., Khvan A. and Kondratiev A. (2019) An Avramov-  
586 based viscosity model for the  $\text{SiO}_2\text{-Al}_2\text{O}_3\text{-Na}_2\text{O-K}_2\text{O}$  system in a wide temperature range. *Ceram.*  
587 *Int.* 45, 12169–12181.

588 Stebbins, J. F., 1991. NMR evidence for five-coordinated silicon in silicate glass at atmospheric pressure.  
589 *Nature* 351, 638-639.

590 Stebbins, J.F. and Farnan, I. (1992) Effects of high temperature on silicate liquid structure: a multinuclear  
591 NMR study. *Science*, 255, 586-589.

592 Stebbins J.F., I. Farnan, X. Xue, (1992) The structure and dynamics of alkali silicate liquids: a view from  
593 NMR spectroscopy, *Chem. Geol.* 96, 371–385, [http://dx.doi.org/10.1016/0009-2541\(92\)90066-E](http://dx.doi.org/10.1016/0009-2541(92)90066-E).

594 Stebbins J. F., Carmichael I. S. E. and Moret L. K. (1984) Heat capacities and entropies of silicate liquids  
595 and glasses. *Contrib. Mineral. Petrol.* 86, 131–148.

596 Stebbins J. F., Dubinsky E. V., Kanehashi K. and Kelsey K. E. (2008) Temperature effects on non-  
597 bridging oxygen and aluminum coordination number in calcium aluminosilicate glasses and melts.  
598 *Geochim. Cosmochim. Acta* 72, 910–925.

599 Stebbins J. F., Kroeker S., Lee S. K. and Kiczinski T. J. (2000) Quantification of five- and six-  
600 coordinated aluminum ions in aluminosilicate and fluoride-containing glasses by high-field, high-  
601 resolution  $^{27}\text{Al}$  NMR. *J. Non-Cryst. Solids* 275, 1–6.

602 Stebbins J. F., Lee S. K. and Oglesby J. V. (1999) Al-O-Al oxygen sites in crystalline aluminates and  
603 aluminosilicate glasses; high-resolution oxygen-17 NMR results. *Am. Mineral.* 84, 983–986.

604 Stebbins J. F. and Xu Z. (1997) NMR evidence for excess non-bridging oxygen in an aluminosilicate  
605 glass. *Nature* 390, 60–62.

606 Stebbins J.F. (2008) Temperature effects on the network structure of oxide melts and their consequences  
607 for configurational heat capacity. *Chemical Geology* 256, 80–91

608 Strukelj, E. (2008) Propriété des verres d'aluminosilicate de lithium. M2, Université Paris 6

609 Sugawara T. Seto M., Kato M., Yoshida S., Matsuoka J., Miura Y. (2013)  $\text{Na}_2\text{O}$  activity and  
610 thermodynamic mixing properties of  $\text{SiO}_2\text{--Na}_2\text{O--CaO}$  melt. *Journal of Non-Crystalline Solids* 371–  
611 372 (2013) 58–65

612 Suzuki A., Ohtani E., Funakoshi K., Terasuki H., Kubo T. (2002) Viscosity of albite melt at High-  
613 pressure and High-temperature. *Phys. Chem. Mineral.*, 29, 159-165.

614 Takahashi S., Neuville D.R., Takebe H. (2015) Thermal Properties, Density and Structure of Peralcic  
615 and Peraluminous  $\text{CaO--Al}_2\text{O}_3\text{--SiO}_2$  Glasses. *Journal of Non-Crystalline Solids.* 411, 5-12.

616 Tamman, G. 1925. *States of Aggregation*, Edited by: Mehl, R. New York: Van Nostrand.

617 Tammann G., and Hesse W. (1926) Die Abhängigkeit der Viskosität von der Temperatur bei unterkühlten  
618 Flüssigkeiten. *Z. Anorg. Allg. Chem.*, 156, 245

619 Tangemann, J and R.A. Lange, The effect of  $\text{Al}^{3+}$ ,  $\text{Fe}^{3+}$ , and  $\text{Ti}^{4+}$  on the configurational heat capacities  
620 of sodium silicate liquids, *Phys. Chem. Miner.* 26 (1998) 83–99.

621 Taylor T. D. and Rindone G. E. (1970) Properties of Soda Aluminosilicate Glasses: V, Low-Temperature  
622 Viscosities. *J. Am. Ceram. Soc.* 53, 692–695.

623 Téqui C., Robie R.A., Hemingway B.S., Neuville D.R. and Richet P. (1991) Melting and thermodynamic  
624 properties of pyrope ( $\text{Mg}_3\text{Al}_2\text{Si}_3\text{O}_{12}$ ). *Geochim. Cosmochim. Acta.*, 55, 1005-1011.

625 Thompson L. M. and Stebbins J. F. (2011) Non-bridging oxygen and high-coordinated aluminum in

626 metaluminous and peraluminous calcium and potassium aluminosilicate glasses: High-resolution  $^{27}\text{Al}$  MAS NMR results. *Am. Mineral.* 96, 841–853.

627

628 Thompson L. M. and Stebbins J. F. (2012) Non-stoichiometric non-bridging oxygens and five-  
629 coordinated aluminum in alkaline-earth aluminosilicate glasses: Effect of modifier cation size. *J. Non-  
630 Cryst. Solids* 358, 1783–1789.

631 Thompson L. M. and Stebbins J. F. (2013) Interaction between composition and temperature effects on  
632 non-bridging oxygen and high-coordinated aluminum in calcium aluminosilicate glasses. *Am.  
633 Mineral.* 98, 1980–1987.

634 Tomozawa M. (1978) “Compositional changes as evidence for spinodal decomposition in glass.” *J. Am.  
635 Ceram. Soc.*, 61, 444-447.

636 Tomozawa M. (1999) “A source of the immiscibility controversy of borate and borosilicate glass  
637 systems.” *J. Am. Ceram. Soc.*, 82, 206-209.

638 Toplis M. and Dingwell D.B., (2004) Shear viscosities of  $\text{CaO-Al}_2\text{O}_3\text{-SiO}_2$  and  $\text{MgO-Al}_2\text{O}_3\text{-  
639 SiO}_2$  liquids: Implications for the structural role of aluminium and the degree of polymerisation of  
640 synthetic and natural aluminosilicate melts. *Geochimica et Cosmochimica Acta*, 68, 5169-5188

641 Tool A.Q., and Eichlin C.G. (1931) Variations caused in the heating curves of glass by heat treatment. *J.  
642 Amer. Ceram. Soc.*, 14, 276

643 Trcera N., Cabaret D., Rossano S., Farges F., Flank A-M, Lagarde P. (2009) Experimental and theoretical  
644 study of the structural environment of magnesium in minerals and silicate glasses using X-ray  
645 absorption near-edge structure. *Phys Chem Minerals* 36:241–257

646 Urbain G. (1972) Etude expérimentale de la viscosité de silicoalumineux liquides et essai d'interprétation  
647 structurale. Thèse de Doctorat d'Etat es Sciences Physiques, Université Paris VI.

648 Urbain, G., Y. Bottinga, P. Richet, Viscosity of liquid silica, silicates and alumino-silicates, *Geochim.  
649 Cosmochim. Acta* 46 (1982) 1061–1072.

650 Urbain, G. (1983) Viscosités de liquide du système  $\text{CaO-Al}_2\text{O}_3$ . *Revue Internationale des Hautes  
651 Températures et Réfractaires*, 20, 135–139.

652 Villeneuve N, Neuville D.R. Boivin P., Bachelery P. and Richet P. (2008) Magma crystallization and  
653 viscosity: A study of molten basalts from the Piton de la Fournaise volcano (La Réunion island)  
654 *Chemical Geology*, 256, 242-251.

655 Vogel H (1921) Das Temperaturabhängigkeitsgesetz der Viskosität von Flüssigkeiten. *Phys. Z.*, 22, 645

656 Voigt U. Lammert H., Eckert H, and Heuer A. (2005) Cation clustering in lithium silicate glasses:  
657 Quantitative description by solid-state NMR and molecular dynamics simulations. *PHYSICAL  
658 REVIEW B* 72, 064207

659 Wallenberger, F. T. , Hicks, R. J. , Bierhals, A. T. , 2004. Design of environmentally friendly fiberglass



660 compositions: ternary eutectic SiO<sub>2</sub>-Al<sub>2</sub>O<sub>3</sub>-CaO compositions, structures and properties, *J. Non-*  
661 *Cryst. Solids* 349, 377-387

662 Wang, T. Sakamaki, L.B. Skinner, Z. Jing, T. Yu, Y. Kono, C. Park, G. Shen, M.L. Rivers, S.R. Sutton,  
663 Atomistic insight into viscosity and density of silicate melts under pressure, *Nat. Commun.* 5  
664 (2014)<http://dx.doi.org/10.1038/ncomms4241>.

665 Wang Y., Wei S., *Cicconi M.R.*, Tsuji Y., Shimizu M., Shimotsuma Y., Miura K., Peng G.D., Neuville  
666 D.R., Poumellec B. and Lancry M. (2020) Femtosecond laser direct writing in SiO<sub>2</sub>-Al<sub>2</sub>O<sub>3</sub> binary  
667 glasses and thermal stability of Type II permanent modifications. *Journal of the American Ceramic*  
668 *Society*. DOI: 10.1111/jace.17164

669 Whittaker and Muntus (1970) Ionic radii for use in geochemistry. *Geochimica et Cosmochimica Acta*,  
670 23, 945-956

671 Woelffel, W., Claireaux, C., Toplis, M.J., Burov, E., Barthel, É., Shukla, A., Biscaras, J., Chopinet, M.-  
672 H., and Gouillart, E. (2015) Analysis of soda-lime glasses using non-negative matrix factor  
673 deconvolution of Raman spectra. *Journal of Non-Crystalline Solids*, 428, 121–131.

674 Worrell C.A. and Henshall T. (1978) Vibrational spectroscopic studies of some lead silicate glasses.  
675 *Journal of Non-Crystalline Solids* 29, 283-299.

676 Wright A. (1990) Diffraction studies of glass structure. *Journal of Non-Crystalline Solids* 123 (1990)  
677 129-148

678 Winter A. (1943) Transformation region of the glass. *J. Am. Ceram. Soc.*, 26, 189 Wright 1990,

679 Wong J. and Angell A.C. (1976) *Glass Structure*. Marcel Dekker. New-York, 864pp.

680 Wu J. and Stebbins J.F., (2009) Effects of cation field strength on the structure of aluminoborosilicate  
681 glasses: high-resolution <sup>11</sup>B, <sup>27</sup>Al and <sup>23</sup>Na MAS NMR. *Journal of Non-Crystalline Solids*, 556-562

682 Zakaznova-Herzog V. P., Malfait W. J., Herzog F. and Halter W. E. (2007) Quantitative Raman  
683 spectroscopy: Principles and application to potassium silicate glasses. *J. Non-Cryst. Solids* 353, 4015–  
684 4028.

685 Zanutto E. D. and Mauro J. C. (2017) The glassy state of matter: Its definition and ultimate fate. *J. Non-*  
686 *Cryst. Solids* 471, 490–495.

687 Zachariasen W.H. (1932) The atomic arrangement in glass. *J. Am. Chem. Soc.* 54, 10, 3841–3851

688 Zhang, P.; Dunlap, C.; Florian, P.; Grandinetti, P. J.; Farnan, I.; Stebbins, J. F. (1996) Silicon site  
689 distributions in an alkali silicate glass derived by two-dimensional <sup>29</sup>Si nuclear magnetic resonance.  
690 *J. Non.-Cryst. Solids* 204, 294-300.

691 Zhang P., Grandinetti P. and Stebbins J.F. (1997) Anionic Species Determination in CaSiO<sub>3</sub> Glass Using  
692 Two-Dimensional <sup>29</sup>Si NMR. *J. Phys. Chem. B* 101, 4004-4008

693

694  
695  
696  
697  
698  
699  
700  
701  
702  
703  
704  
705  
706  
707  
708  
709  
710  
711  
712  
713  
714  
715  
716  
717  
718  
719  
720  
721